Modification and characterization of the interface in polymer/inorganic composites

Madsen, Nils Berg

Publication date:
1999

Document Version
Publisher's PDF, also known as Version of record

Modification and characterization of the interface in polymer/inorganic composites

Nils Berg Madsen

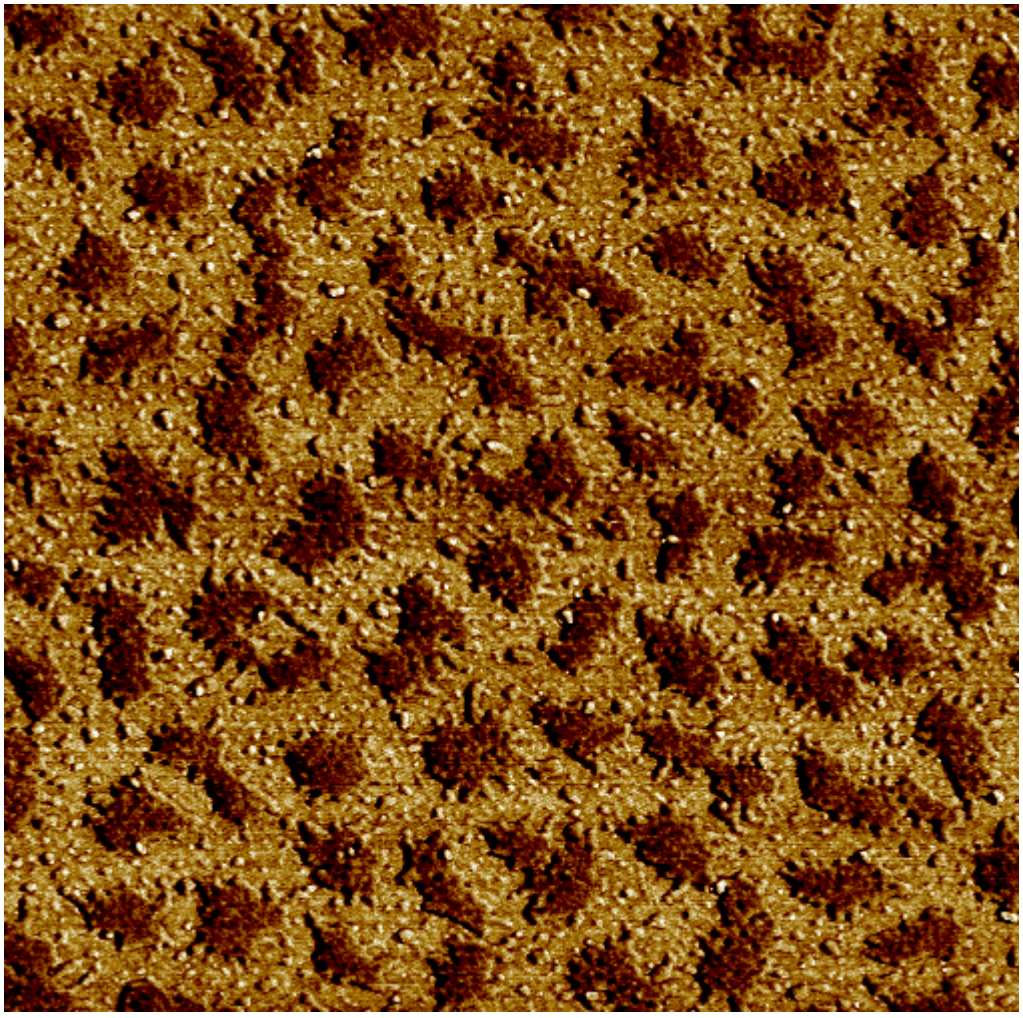

Risø National Laboratory, Roskilde, Denmark
March 1999

ISBN 87-550-2540-4; 87-550-2541-2 (Internet)
ISSN 0106-2840

Information Service Department · Risø · 1999

Preface

This dissertation was prepared to fulfill the requirements for receiving the Ph.D. degree at the Technical University of Denmark. This work was carried out at the Institute of Chemistry, Technical University of Denmark and Department of Condensed Matter Physics and Chemistry, Risø National Laboratory form July 1995 to July 1998. The work included a two months visit at the Department of Chemical Engineering and Materials Science, University of Minnesota, Minneapolis from January to March 1997. The project was financially supported by the Danish Materials Development Program 2 (MUP2 j.nr. 1994-503/0926-67 and 1994-503/0926-49) which is acknowledged.

I would like to thank my two advisors at Risø Walther Batsberg Pedersen and Ib Johannsen for their direction and support throughout the project. I also want to thank my supervisor professor Jakob W. Høj for his full understanding throughout the project.
I would like to thank all my colleagues at Risø especially Lene Hubert, Kristoffer Almdal, Niels B. Larsen and Peter Sommer-Larsen for useful discussions and technical support.

Professor Mathew Tirrell and the members of his group at Department of Chemical Engineering and Materials Science are all thanked for sharing their knowledge on JKR and ellipsometry measurements.

Bent Hall Jensen (Danfoss A/S) and Truels Sterm Larsen (former Grundfos A/S) are thanked for their good collaboration in the work on hydrothermal aging of glassfiber composites.

Finally I like to thank Walther Batsberg Pedersen and Jacob Hooker for valuable help by carefully reading and commenting the manuscripts for this thesis.

14/8-1998.

_____

Nils Berg Madsen

Ph.d.nr: 950148RIS

Content

Modification and Characterization of the interface in polymer/inorganic composites

Abstract

New types of diblock copolymer silane coupling agents have been investigated as interface modifiers in polymer/inorganic composites. Diblock copolymers composed of polybutadiene-polystyrene (PB-PS) and polybutadiene-polydimethylsiloxane (PB-PDMS) have been synthesized with varying molecular mass of the PS and PDMS blocks by living anionic polymerization. The target molecular masses were chosen to be below, around and above the critical molecular mass for formation of entanglements. These polymers have been catalyticly hydrosilylated with triethoxysilane to form diblock copolymer silane coupling agents. The investigation has involved a number of surface analytical techniques such as wet chemical analysis, Fourier transformed infrared spectroscopy with different sampling techniques, X-ray photoelectron spectroscopy, ellipsometry, atomic force microscopy and contact angle measurements. These analyses showed that the average layer thickness of PDMS block copolymer silanes vary with the molecular mass of the PDMS block when applied to an oxidized silicon wafer from toluene. This variation was not observed for the PS block copolymer silanes. Furthermore atomic force microcopy showed that the PS block copolymer silanes segregate into an island structure on oxidized silicon. Investigations of the interfacial adhesion have been done by JKR-measurements and single fiber microdebond experiments. The investigations showed that the synthesized diblock copolymer silanes perform well as adhesion promoters between SiO_2 and a polymer matrix equal to end block of the silane. The measurements showed no increase in interfacial adhesion by increasing the molecular mass of the end block up to 100 kg/mol which could be below the critical mass for formation of entanglement at the interface. Furthermore microdebond experiments showed that the interfacial adhesion was significantly reduced by exposing glassfiber micro composites to boiling water for 100 hours.
This work also included a study of hydrothermal stability of *state of the art* glassfiber reinforced polyphenylensulfide (PPS) and Poly(Hexamethylene adipamide) (PA66) composites. The materials were exposed in water at different temperature and pH values up to more than one year. Measurement of various mechanical properties in combination with electron microscopy showed the primary mechanism for reduction of mechanical properties was hydrolysis of the interfacial region. Furthermore gel permeation chromatography showed extensive reduction of the molecular mass of PA66 as a result of exposure in hot water. The drastic decrease in mechanical properties of the PA66 composites is related to hydrolysis of both the interface region and the PA66 matrix.
Hydrolysis of the interface region is still the main problem in thermoplastic glassfiber composites. Diblock copolymer silanes show potential as coupling agents for such systems but they must be optimized for hydrolytic stability. This work presents the tools for such an optimization.

Dansk resumé

Modificering og karakterisering af grænsefladen i polymer/uorganiske kompositter

Dette arbejde omhandler bindingen mellem polymerer og uorganiske fyldstoffer. Hovedformålet er at undersøge en ny type af grænseflade modificerende stoffer. Denne nye type grænseflade modificerende stoffer er baseret på diblok copolymerer. Traditionelle grænseflade modificerende stoffer til polymer/uorganiske kompositter er baseret på lavmolekylære specier, som er i stand til at danne kovalente bindinger med både den uorganiske overfalde og polymer matrisen. Af disse er silaner blandt de mest anvendte i polymer kompositter. Virkemåden af sådanne lav-molekylære silaner afhænger af om polymer matrisen indeholder reaktive grupper, således at der kan dannes en binding mellem silan og polymer.

En stor gruppe termoplastiske polymerer som anvendes til kompositmaterialer indeholder ingen reaktive grupper, hvortil man kan binde lavmolekylære silaner. Derfor er hovedideen i dette arbejde at modificere specifikke polymerer med silan-grupper, således silan-grupperne kan binde til den uorganiske overfalde, og bindingen til matrix sker ved diffusion af de fast ankrede kæder ind i matrisen, som er fuldt kompatible. Erfaringen har vist at polymerer modificeret således, at de kan binde til den uorganiske overfalde, virker godt som grænseflade additiver, men det er nødvendigt med mere end én binding pr kæde for at opnå gode egenskaber (Pluddemann 1982). Ideen er at fremstille diblock copolymerer, hvor den ene blok har samme sammensætning som matrix og den anden er polybutadiene (PB). Polybutadiene indeholder en dobbeltbinding pr mer-enhed, som kan katalytisk hydrosilyleres. Ved katalytisk hydrosilylering af polybutadiene opnås en struktur, hvor en række funktionelle silaner er bundet sammen af en polymerkæde. Den teoretiske fordel ved en sådan kæde er at mange bindinger skal brydes samtidigt for at fjerne den fra en overflade.
En anden teoretisk fordel ved blok copolymer silaner er, hvis den matrix-kompatible blok bliver tilstrækkelig lang, er der mulighed for dannelse af kæde-sammenvikling (*entanglements*). Kæde-sammenvikling er meget vigtig for de mekaniske egenskaber af rene amorfe polymerer. Disse materialer opnår egenskaber som et krydsbundet polymer netværk når molekylvægten overstiger en vis værdi på grund af dannelsen af kæde-sammenviklinger. Ideen i dette arbejde er at variere molekylvægten af den kompatible blok på begge sider af den kritiske molekylvægt for dannelse af kæde-sammenvikling for den rene polymer. Dette gøres for at undersøge om dannelse af kæde-sammenvikling kan forøge grænseflade adhæsionen.

Dette arbejde omfatter syntese og strukturel karakterisering af to nye typer blok copolymer baserede grænseflade modifikatorer. Derudover udvælgelse og afprøvning af en række analyse metoder til undersøgelse af grænseflade modfikatorer generelt og specifikt blok copopolymer baserede silaner.

Syntese og strukturel karakterisering af diblok copolymer silaner er beskrevet i kapitel 2. Der er fremstillet seks forskellige diblok copolymerer ved levende anionisk polymerisation i tetrahydrofuran: Polybutadien-polystyren (PB-PS) og polybutadien-poly(dimethylsilioxane) (PS-PDMS med molekylvægt af PS og PDMS blokkene på 10,30 og 100 kg/mol. Dette er for begge systemer under, omkring og over den kritiske molekylvægt for dannelse af kæde-sammenviklinger. De fremstillede diblok copolymerer blev katalytisk hydrosilyleret med triethoxysilan i tilstedeværelse af hexaklorplatinsyre i toluen. Produktet blev seks forskellige diblok copolymer silaner.

Til undersøgelse af disse blok copolymer silaner og andre lav molekylære silaner på uorganiske overflader er der udført eksperimenter ved anvendelse af en række forskellige analyseteknikker. Af disse kan nævnes: kemisk identifikation af silan-baserede grænseflade additiver, Fourier transformeret infrarød spektroskopi med anvendelse af forskellige metoder, Røntgen induceret fotoelektron spectroskopi, ellipsometry, *atomic force* mikroskopi samt kontakt vinkel målinger. Resultaterne viste at blok copolymer silanerne kobler til uorganiske overflader som $Mg(OH)_2$ og SiO_2 fra toluen opløsninger ved stuetemperatur. Resultaterne fra disse undersøgelser viste endvidere specifikke forskelle mellem blok copolymerene afhængig af om de indeholdt PS eller PDMS ende-blokke. Behandling af kemisk oxideret silicium med toluen opløsninger af PDMS blok copolymer silaner resulterede i gennemsnitlige lagtykkelser, som voksede med voksende molekyle vægt af PDMS blokken. For PS blok copolymerene var lagtykkelsen konstant. Dette relateres til at PDMS ikke har tendens til at absorbere på SiO_2 fra en toluen opløsning mens PS har. Endvidere blev det fundet at PS blok copolymer silanerne danner en domæne struktur på overfladen af oxideret silicum som resultat af segregering af PS blokkene. Dette fænomen blev ikke observeret for PDMS blok copolymer silaner.

For at undersøge indflydelsen af blok copolymer silaner på grænseflade-vedhæftningen mellem uorganiske overflader og polymerer med samme sammensætning som ende-blokken, er der anvendt to forskellige teknikker: JKR-metoden og enkelt fiber mikro-vedhæftnings metode. JKR-metoden er en metode til bestemmelse af adhæsions arbejde. Med denne metode er man i stand til både at måle det termodynamiske adhæsions arbejde samt måle forøgelse af grænseflade adhæsionen som følge af rearrangering af grænsefladen ved kontakt. Resultaterne viste en forøget grænsefladeadhæsion mellem oxideret silicium behandlet med PDMS copolymer silan og krydsbundet PDMS. Der blev dog ikke fundet forøgelse af adhæsionen med voksende molekylevægt af PDMS ende-blokkene.
Enkeltfiber mikro-vedhæftning er en metode til bestemmelse af tilsyneladende grænsefladestyrke af små polymer kugler, som omslutter en glasfiber. Resultaterne fra denne metode viste, at blok copolymer silaner giver forøget vedhæftning mellem glasfibre og en polymer med samme sammensætning som ende-blokken af silanen. Der blev heller ikke her observeret forøget grænseflade adhæsion ved forøgelse af molekylvægten af ende-blokken. Undersøgelser foretaget af Creton et al. (1994) og andre tyder på at den kritiske molekylvægt for kæde-sammenviklinger

ved grænsefladen er langt højere end inde i materialet. Det er derfor muligt at den manglende effekt af molekylevægten skyldes at selv de største molekyler anvendt her, ikke er tilstrækkeligt store til at danne kæde-sammenviklinger. Målinger af tilsyneladende grænseflade styrke på emner kogt i vand i 100 timer viste en kraftig reduktion. Dette viser at trods den teoretiske fordel ved blok copolymer silaner, kan de ikke fuldstændigt beskytte grænsefladen mod hydrolyse. Dette henføres til at den anvendte triethoxysilan indholder et overskud af ethoxy eller silanol grupper som ikke kan binde til overfladen. Tilstedeværelsen af sådanne grupper kan forøge fremfor at forhindre hydrolyse af grænsefladen. Undersøgelser af Kirkland & Henderson (1994) har vist at anvendelsen at di(t-butyl)methoxysilaner forbedrer hydrolyse-stabiliteten betydeligt i forhold til trimethoxysilaner, derfor foreslås det at anvende sådanne mono-funktionelle silaner med beskyttelses sidegrupper til fremtidige forsøg med blok copolymer silaner.

Sideløbende med arbejdet med blok copolymer silaner er der i samarbejde med Danfoss A/S og Grundfos A/S foretaget undersøgelser af hydrothermal ældning af udvalgte glasfiber fyldte polyphenylensulfid (PPS) og poly(hexamethylene adipamide) (PA66) kompositter. Hovedformålet med dette arbejde var at undersøge mekanismerne bag hydrotermisk ældning af disse glasfiber fyldte termoplastiske komposit materialer, samt at undersøge status i udviklingen af kommercielle glasfiber kompositter. Dette arbejde er beskrevet i kapitel 5 i denne afhandling og i to tekniske rapporter på dansk vedlagt som bilag. Sprøjte støbte emner blev eksponeret i varmt vand ved forskellige temperaturer og pH værdier i op til 9000 timer. De mekaniske egenskaber blev målt som funktion af ældnings tiden og sammenholdt med elektron mikroskopi analyser. Endvidere blev der foretaget størrelses kromatografi analyser af molekylevægts nedbrydningen af PA66. Undersøgelserne af PPS kompositter viste at reduktionen i de mekaniske egenskaber primært skyldes hydrolyse af grænsefladen mellem glasfiber og PPS. Undersøgelserne af PA66 kompositter viste, at de drastiske fald i mekaniske egenskaber skyldes hydrolyse af grænsefladen og hydrolyse af selve polymeren. Konklusionen af dette arbejde er at selv for helt nyudviklede kommercielle thermoplastiske kompositmaterialer er nedbrydningen af grænsefladen den vigtigste grund til fald i de mekaniske egenskaber. Dette viser at forskning og udvikling indenfor grænseflade modificering af termoplastiske komposit materialer er vigtig for forbedring af disse.

Hovedkonklusionen på dette arbejde er at blok copolymer silaner viser potentielle muligheder som grænseflade modificatorer, men disse bør optimeres på en række områder. Områder som: molekylvægt af ende-blokken, den kemiske natur af silan-grupperne samt valg af solvent i forbindelse med behandling af overflader. Dette arbejde giver forskellige værktøjer til at foretage sådanne optimeringer.

1 Coupling agents for polymer/inorganic composites

1.1 Introduction

The use of polymer matrix composites continues to grow as these materials find new uses and increasingly replace metals in various applications. Composites with high strength fillers such as glass fibers usually have strength to weight ratios that exceed values for metals and their alloys. This property makes polymer matrix composites ideal for structural applications. Most of the research in the area has concentrated on thermosetting matrices such as epoxy and unsaturated polyesters. The research in thermoplastic composites is a still growing area because of the processing advantages. No matter what kind of polymer matrix is used in combination with inorganic fillers, the single most important property is the state of the matrix-filler interface.

1.2 Historic perspective

The first synthetic plastics were the phenol-formaldehyde resins introduced by Baekeland in 1907. Melamine and urea also react with formaldehyde to form intermediate methylol compounds, which condense to cross-linked polymers much like phenol-formaldehyde resins. Cellulose products are still used as reinforcement for these methylol-functional polymers. Methylol groups react with pendant hydroxyl groups on the surface of the cellulose to form stable ether bonds between polymer and filler. The other reason of success for these early polymer composites is that cellulose has a thermal expansion coefficient that is very close to that of the matrix polymers. This illustrates that good composites relay on compatibility between filler and matrix.

The introduction of glass fibers in the early 1940's opened new possibilities for polymer reinforcement. The high strength and modulus of the glass fibers seemed very promising for polymer reinforcements. It was found however that glass fibers had very unsatisfying reinforcement properties for methylol-functional polymers and the newly developed unsaturated polyester resins. Although the resins bonded well to dry glass, the formed alkoxysilane bonds were easily hydrolyzed by water. The specific dry strength and modulus of fiberglass reinforced plastics were better than aluminum and steel, but properties decreased dramatically under exposure to ambient humid conditions. It was found that glass fibers and many other inorganic fillers were incompatible with these polymer matrices.

This problem resulted in a joint research effort in 1943 by Dow Corning Corporation and the United States military. Organosilicon compounds of structure $RSiX_3$ were obvious choices in searching for "coupling agents" to make fiberglass compatible with organic polymers since they are hybrids of organic molecules and minerals. An organofunctional R-group bonded to silicon

by a stable C-Si bond would provide compatibility with the polymer, while the SiX_3 part of the molecule could form typical inorganic bonds with the mineral surface.
A Coupling agent may be defined as a material that acts at the interface of dissimilar materials in a composite to provide a stable bond resulting in improved composite properties and retention of these properties under corrosive conditions.
Unsaturated polyesters were originally the preferred resins for fiberglass-reinforced composites, since they could be cured rapidly at low pressure. Therefore the development of coupling agents is closely related to unsaturated polyesters.
Robert Steinman of Owens-Corning Fiberglas described the use of allylsilanes as sizings on glass. (Steinman 1951).
In 1947 Witt et al. observed that allyltriethoxysilane gave polyester composites with twice the strength of those where the glass was treated with ethyltrichlorosilane.
In 1949 the Bjorksten organization was given a contract by the U.S. Air force to explore the effect of fiberglass treatment on the wet strength of polyester laminates. A total of 2000 compounds were screened. The best of these was a solvent treatment named BJY, based on equimolar adduct of vinyltrichlorosilane and 2-chloroallylalcohol (Bjorksten and Yaeger 1952).
In 1951 DuPont introduced the methacrylato-chrome complex Volan A. For the next 10 years this became the standard coupling agent for the polyester/glassfiber industry. The typical green color of the chrome complex became associated with high quality polyester laminates.
During the 1950's the group of John Speier at Dow Corning developed a number of synthesis methods for new silane coupling agents. The discovery of the catalytic effect of hexa-chloroplatinum acid on hydrosilylation was a very important event in silane coupling agent chemistry. Speier synthesized the first amino-functional silane in 1951. Aminosilanes have since become a major type of coupling agent in commercial use.
In 1957 Dr. Edwin Plueddemann of Dow Corning began his life long work on silane coupling agents resulting in 2 books, 55 scientific publications and 94 US. patents. He developed a wide variety of organofunctional silanes, many of which are still standards of the industry. The silane functionalities include; epoxy (Plueddemann 1960), methacrylate (Plueddemann 1962), styrene (Plueddemann 1963) and cationic vinylbenzyl (Plueddemann 1974). Figure 1.1. illustrates the historic progress for polyester-glassfiber composites.

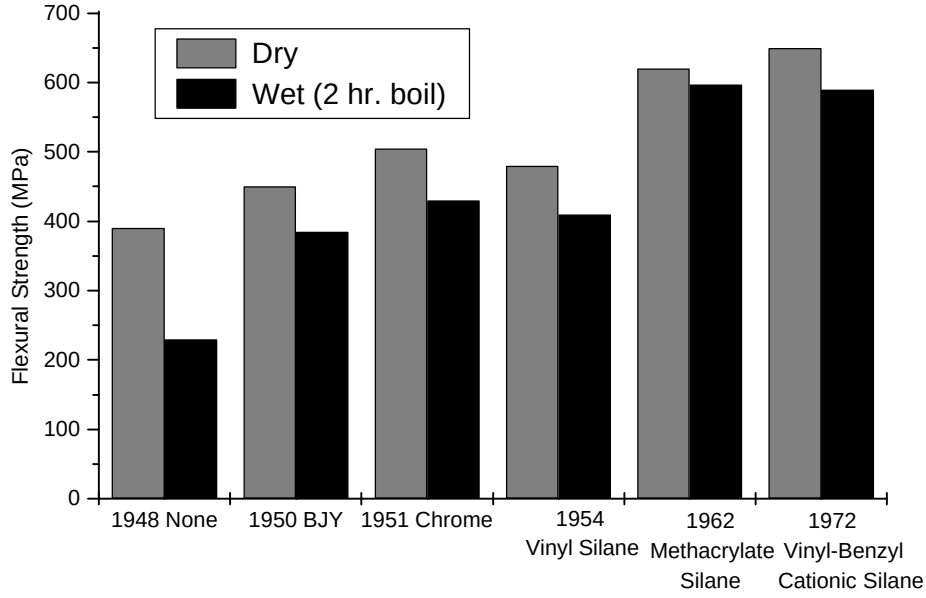

Figure 1.1. Progress of coupling agent improvement in fiberglass-polyester composites. Data from (Pape & Plueddemann 1986).

1.3 Silane coupling agents.

The most common type of coupling agents used are alkoxysilanes. According to Plueddemann (1982) alkoxysilanes bond to a glass surface by the following reaction (1):

$$R' Si(OR)_3 + HOSi \equiv \rightarrow R' Si(OR)_2 OSi \equiv + ROH \qquad (1)$$

R is typically a methyl or ethyl group, and *R′* contains a functionality that can react readily with the polymer. A selection of functionalities and silane structures is given in Table 1.1. HOSi≡ can be either an isolated surface silanol or a hydrogen-bonded hydroxyl group. The coupling of silanes to an inorganic surface is usually done by prehydrolysis. The water reacts with the methoxy- or ethoxygroup to form silanol and free methanol/ethanol (2).

$$R' Si(OR)_3 + H_2O \rightarrow R' Si(OR)_2 OH + ROH \qquad (2)$$

Then the formed silanol can react with surface silanols (3) to give the total reaction (1).

$$R' Si(OR)_2 OH + HOSi \equiv \rightarrow R' Si(OR)_2 OSi \equiv + H_2O \qquad (3)$$

Until recently, it was thought that reactive hydroxyl groups were necessary for the bonding to take place. But, recent publications Debois & Zagarski (1993) and Blümel (1995) indicate that alkoxysilanes can react directly on the Si-O-Si Sites. These observations were made using FTIR and solid state ^{29}Si NMR respectively. In this case the reaction will be the following:

$$R' Si(OR)_3 + Si - O - Si \rightarrow R' Si(OR)_2 O - Si \cdots Si - OR \qquad (4)$$

where $Si \cdots Si$ means two adjacent silicon atoms.

Table 1.1. Selection of commercial silane coupling agents.

Organofunctional group	**Chemical structure**
Vinyl	CH_2=CHSi$(OCH_3)_3$
Chloropropyl	Cl$CH_2CH_2CH_2$Si$(OCH_3)_3$
Epoxy	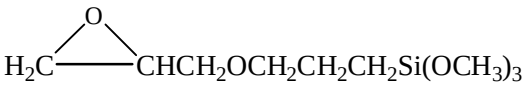
Methacrylate	
Primary amine	$H_2NCH_2CH_2CH_2$Si$(OCH_3)_3$
Diamine	$H_2NCH_2CH_2NHCH_2CH_2CH_2Si(OCH_3)_3$
Mercapto	$HSCH_2CH_2CH_2$Si$(OCH_3)_3$
Cationic styryl	CH_2=CH$C_6H_4CH_2NHCH_2CH_2NH(CH_2)_3Si(OCH_3)_3$ ·HCl

The structure and properties of the silane layer on an inorganic filler depend on the functionality attached to the silane, but also on the method used to apply the silane to the surface. The ideal case would be to form a monolayer of coupling agent to the surface where all silanol groups have reacted either with surface hydroxyl groups or silanol groups on neighboring silanes. The ideal reaction is sketched in Figure 1.2. In practice this is very seldom the case. Usually a silane coupling layer consists of several monolayers depending on the method of application.
There are basically four different methods of applying silane coupling agents:

1. *Aqueous solutions*. From dilute solutions in pure water or in blends of water and polar solvents like alcohols. This method is used in large-scale industrial processes for environmental reasons. The method often results in multilayer structures where outer layers can be removed by solvents.

2. *Organic solutions*. From dilute solutions in dry organic solvents. Tends to form more monolayer like structures than from aqueous solutions due to lack of condensation in the solution.

3. *Integral blend*. Particulate fillers in liquid resins are readily modified with coupling agents by adding silanes as integral blends to the mixture. Particulate fillers may also be treated in-situ when milled with elastomers by integral blending. The structure of the silane layer is unknown because of the difficulties in studying the layer in the matrix.

4. *Vapor phase*. Volatile silanes can be applied to inorganic surfaces from vapor phase under reduced pressure. Experiments show that silanes applied using this method form near perfect monolayer structures.

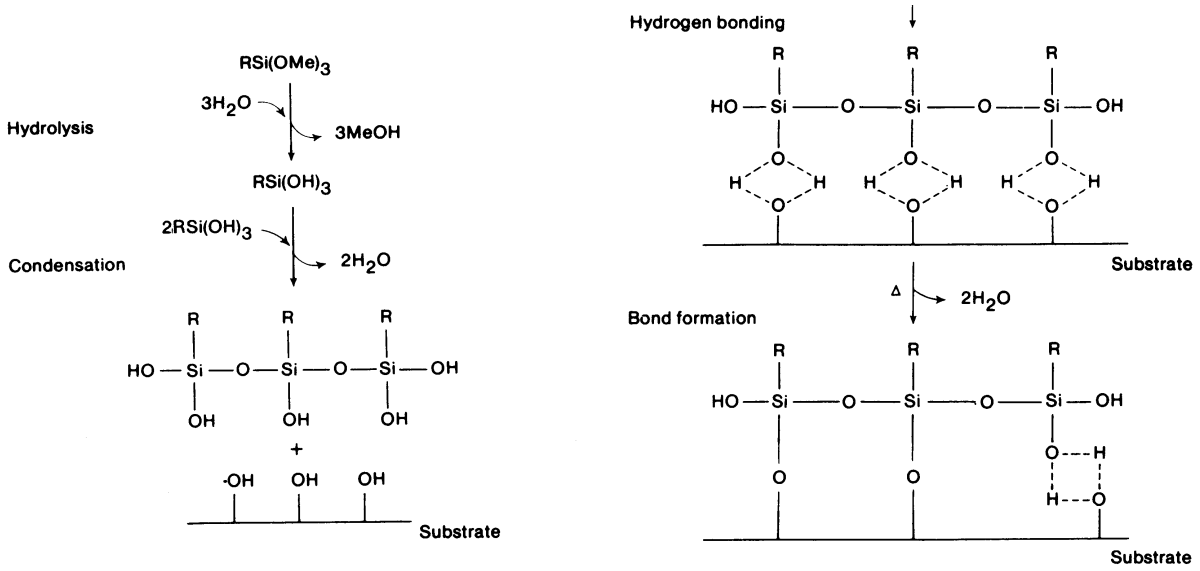

Figure 1.2. Ideal reaction of silane coupling agents to an inorganic surface.

It is fairly well established that silane coupling agents form oxane bonds (M-O-Si) with mineral surfaces where M = Si, Ti, Mg, Al, Fe etc. It is not obvious that such bonds should contribute outstanding water resistance to the interface, since oxane bonds between silicon and iron or aluminum, are not resistant to hydrolysis. Even covalent siloxane bonds are hydrolyzed to silanols by water with an activation energy of 98.8 kJ/mol. Hydrolysis catalyzed by benzoic acid or potassium hydroxide has an activation energy around 25 kJ/mol., which is comparable to the strength of a hydrogen bond. The hydrolysis reaction of an oxane bond (5) is believed to be a true equilibrium with bond breaking and reforming at the interface in the presence of water.

$$\text{M-O-Si-} + H_2O \Leftrightarrow \text{M-O-H} + \text{H-O-Si-} \qquad (5)$$

This equilibrium reaction is of major importance for the performance of silane modified inorganic fillers in the presence of water. Plueddemann (1982) states three conditions for maintaining bonding in the presence of water:

1. A maximum initial formation of M-O-Si bonds.

2. A minimum penetration of water to the interface.

3. Polymer structures that hold silanols at the interface.

For low molecular weight silanes the fist condition can be achieved by using acid or base catalyst in the application of silanes. Acid or base catalysts lower the activation energy of the condensation reaction. The second condition can be met by applying hydrophobic spacer groups on the silanes in order to hinder the penetration of water to the interface. The third condition is met by using tri functional silanes capable of forming a network structure on the filler surface (as shown in Figure 1.2). It should be considered that the siloxane network structure itself is sensitive to hydrolysis especially in the presence of acids or bases.

1.4 Theories of bonding through coupling agents

All experiments show that coupling agents have profound effects on the performance of composites. A clarification of the coupling mechanism will be useful in the understanding the fundamental nature of adhesion of organic polymers to inorganic surfaces. There are different theories on the coupling mechanism reviewed by Plueddemann (1982):

The chemical bonding theory: This theory is the oldest and still best known theory for coupling agents. The coupling must contain chemical functional groups that can react with silanol groups on the glass surface. In addition the coupling agents contain at least one reactive group that can form a covalent bond to the polymer matrix. This theory successfully explains the active coupling agents for curable thermosetting resins.

The wetting theory: Zisman (1963) concluded that good wetting of a filler was of prime importance in preparations of composites. Physical absorption of the polymer on high energy surfaces would provide adhesive strength far in excess of cohesive strength of the polymer matrix.
In order to achieve complete wetting of a surface the polymer must have low viscosity and a surface tension lower than the critical surface tension (γ_c) of the surface. All clean solid mineral surfaces have γ_c values much higher than surface tensions of polymers, but many hydrophilic mineral surfaces are covered with a layer of water in equilibrium with atmospheric moisture. This results in poor wetting and spreading of nonpolar polymers on the mineral surface. The wetting theory is especially important in the choice of coupling agents for relative high surface tension polymers, because surface treatments producing low surface tension will result in poor wetting.

The compatibility theory: In polymer systems where no reaction occur between the polymer and the coupling agent the definite maximum laminate properties are obtained with silanes that have optimum compatibility with the polymer. The compatibility can be calculated form solubility parameters (d) of the coupling agents and polymer matrix. The ultimate in compatibility is obtained with a silane modified polymer as coupling agent for a similar polymer. According to Plueddeman (1982) coupling through solution compatibility is most successful with glassy polymers like polystyrene, but less effective with polymers like polyethylene or polypropylene.

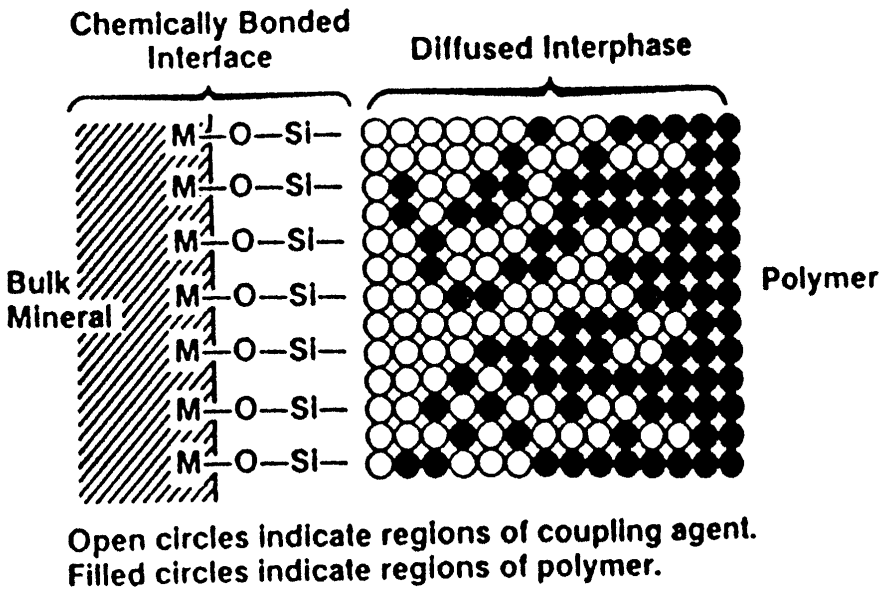

Figure 1.3. Interdiffusion model for composites. From Plueddemann (1988)

Interpenetrating network theory: Certain reactive silanes with amine, methacrylate, or cationic vinylbenzyl functions often perform very well as coupling agents in thermoplastic composites even though there is no obvious reaction or preferred solubility of the silane and the polymer. The theory is that the siloxane network produced by silane coupling agents is partly soluble in the polymer at melting temperatures and form an interpenetrating network structure by cooling. The concept of interpenetration is illustrated in Figure 1.3.

1.5 Coupling agents for thermoplastics

Silane coupling agents were developed for use in thermosetting resins utilizing the reactivity of the thermosetting monomers. Although thermoplastics do not undergo chemical reactions during molding and forming, thermoplastics may be divided into broad classifications of reactive and nonreactive polymers. Reactive polymers contain functional groups such as amide ester carboxyl, hydroxyl or halide that could react with organofunctional groups at molding temperatures.

For nonreactive polymers where no reaction is possible between the polymer and the silane the maximum laminate properties are obtained using silanes with optimal compatibility with the polymer according to Plueddemann (1982).

Paul (1969) patented one of the fist systems using a modified polymer as coupling agent for a similar polymer. The system was based on a combination of amino silane treated glass fibers and

maleic anhydride modified polypropylene as coupling agent to polypropylene. This system proved to give excellent coupling between polypropylene and glass fillers. This successful coupling system prompted many chemists to investigate other systems to achieve the same. Instead of using a master batch of maleic anhydride modified polypropylene a number of patents were granted on reacting unsaturated acids to polypropylene using a peroxide initiator during extrusion (Plank (1974), Steinkamp & Grail (1975) and McConnell (1975)).

A study by Plueddemann (1982) showed that trimethoxysilane modified polystyrene is a good adhesion promoter for polystyrene. A systematic variation of the number of trimethoxysilyl groups in a silane-styrene copolymer with a molecular mass of 10 kg/mole showed that one trimethoxysilyl group was not sufficient for bonding. It was observed that five to ten trimethoxysilyl groups were necessary in a copolymer of the molecular mass of 10 kg/mole for optimum performance. Unfortunately it has not been possible to disclose the exact chemistry behind these results.

Strålin & Hjertberg (1993) studied the adhesion of ethylene copolymers to aluminium. The polymers were ordinary LDPE, copolymers with butyl acrylate (EBA), copolymers with vinyltrimethoxysilane (EVS) and copolymers with both comonomers. Peel experiments were conducted with these copolymers on untreated or hydrated aluminium. Peel strengths were compared with SEM and FTIR analysis of the interfaces. The experiments showed that hydration of the aluminium surface increased the adhesion to all tested polymers due to morphology changes, but the copolymers containing methoxysilane groups showed significantly better adhesion caused by covalent bonding to the hydrated aluminium. These results indicate the possible use of silane containing ethylene copolymers as coupling agents for polyethylene/ inorganic composites.

Landry et al. (1996) studied random, block and graft copolymers of polystyrene and poly(4-vinylphenol) as compatibilizers for in situ produced titanium- and zirconium oxide/ polystyrene composites. The copolymers proved to be excellent compatibilizers reducing the domain size of the dispersed oxide phase and improving the mechanical properties of the organic-inorganic composite materials.

Yamamoto & Ohata (1996) have recently patented new types of macromolecular silane coupling agents, which are end-triethoxysilylated polystyrene. The synthesis is based on living anionic copolymerization of styrene and p-triethoxysilyl-α-methylstyrene. Silica particles treated with these copolymers showed significantly better dispersion in polystyrene-toluene solutions than untreated silica. The focus of attention of the work by Yamamoto & Ohata has been better dispersion of inorganic pigments in paint systems, so these new macromolecular silane coupling agents have not yet been tested as coupling agents for styrene based composites.

Around the same time Feller et al. (1996) published a study of silane modified polypropylene. Using a Zieger-Natta polymerization technique they synthesized copolymers based on propene and two different types of dienes. The copolymers were hydrosilylated with trichloro- or triethoxysilane using a platinum acid catalyst. The copolymer silanes showed grafting to glass as

well as co-crystallization with blends of pure polypropylene. The copolymer silanes were tested as coupling agents using a microdebond method.

In analogy to the pioneering work by Paul (1969), Gonon et al. (1997) studied the use of carboxy-functionalized polyphenylenesulfide (PPS) and γ-aminopropyltriethoxysilane (γ-APS) as a coupling system for PPS to glass fibers. Microdebond experiments showed that the use of carboxy-functionalized PPS, in addition to γ-APS, improved the interfacial shear strength. The same trend was observed on the mechanical properties of short glass fiber reinforced PPS in comparison with commercially treated glass fibers.

Common for all these studies is that polymers functionalized in such a way that they can form covalent bonds to inorganic surfaces perform well as coupling agents between similar polymers and inorganic fillers.

Souheng Wu (1982) expressed this in the following way in his splendid monograph on polymer adhesion: “The extent of molecular or local segmental diffusion across the interface determines the structure of the interfacial zone, which critically effects the mechanical strength of an adhesive bond. Negligible diffusion will give a sharp interface. For a sharp interface, high adhesive strength can be obtained only when strong polar interactions or chemical bonds exist across the interface. On the other hand, if the interface is sufficiently diffuse as a result of extensive diffusion, dispersion force alone will give high adhesive strength.”

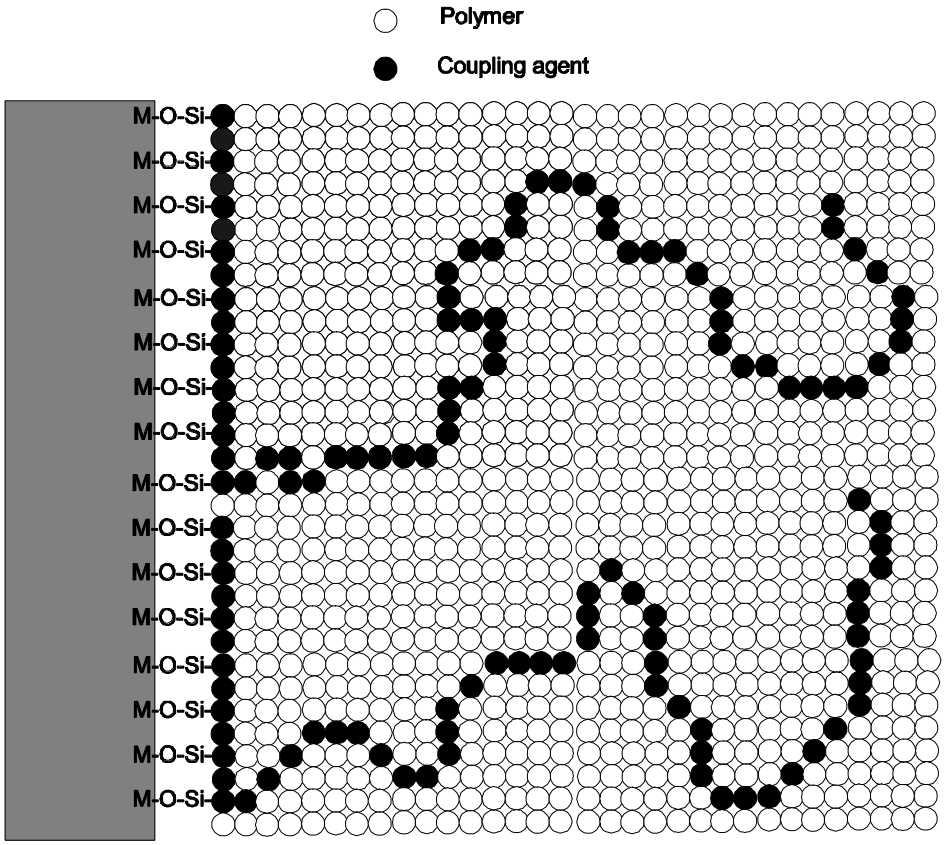

Figure 1.4. Concept of Block copolymer silane coupling agents.

1.6 This work

The main focus of this Ph.D. work is to investigate new kinds of silane coupling agents based on block copolymers where one block is capable of forming multiple covalent bonds to the surface and the other block is fully compatible with the polymer matrix. The concept of using block copolymer coupling agents is illustrated in Figure 1.4. As a concept, block copolymer silane coupling agents possess two separate advantages over conventional low molecular mass silanes. The first advantage is that the separate silanes groups are connected by a polymer backbone and not depending on a network formation through silanol condensation. This means that in order to detach the block copolymer coupling agent from the inorganic surface by hydrolysis, multiple bond sites have to be hydrolysed simultaneously or subsequently without reforming through condensation. The second advantage is the total compatibility between the coupling agent tail end and the polymer matrix. This compatibility insures good interdiffusion of the coupling agent in the matrix polymer at temperatures higher than the glass transition temperature. This gives the possibility of chain entanglements between the coupling agent on the polymer matrix. Entanglements are very important for the mechanical properties of uncrosslinked polymers.

When the molecular mass of glassy polymers exceeds a certain molecular mass a rubber plateau appears in the relaxation spectrum in spite of the fact that no chemical crosslinking exists. This plateau is caused by chain entanglement. From the shear modulus of this plateau it is possible to calculate a molecular mass between entanglements M_e. The critical molecular mass necessary to enter the plateau region is denoted M_c. It has been argued that $M_c = 2M_e$ (Matsuoka 1992). The idea is to vary the molecular mass of the tail end of block copolymer with respect to the critical molecular mass of entanglements in order to study the molecular mass effect on interfacial adhesion.

The initial idea is to synthesize block copolymers by living anionic polymerization containing unsaturated hydrocarbons capable of undergoing catalytic hydrosilylation.
Synthesizing the block copolymers using living anionic polymerization gives the possibility to control the molecular mass of the blocks and usually results in very narrow molecular mass distributions. Synthesizing block copolymers with controlled molecular mass gives the possibility to study the effect of the molecular mass of the tail end on the adhesion to a polymer matrix similar to the tail end of the block copolymer. If chain entanglement is a possible way of increasing interfacial adhesion, then increasing the molecular mass of the tail end of the block copolymer above the molecular mass between entanglements for bulk (M_e) should effect the interfacial adhesion.

This work involves living anionic polymerization of block copolymers of polybutadiene-polystyrene (PB-PS) and polybutadiene-polydimethylsiloxane (PB-PDMS) with varying molecular mass of the PS and PDMS blocks. The target molecular masses of the PS and PDMS end blocks are varied to have block copolymer silanes with molecular masses below, around and above the critical molecular mass of entanglement (M_c) for bulk polymer. The average molecular masses between entanglements (M_e) for polystyrene and polydimethysiloxane calculated on the basic of dynamic mechanic analyses are tabulated in Table 1.2. On the basis of the average values of M_e the target molecular masses of the tail block were chosen to be 10, 30 and 100 kg/mol for both PB-PS and PB-PDMS block copolymers.

Table 1.2. Molecular masses of entanglement M_e for polystyrene and polydimethylsiloxane as reported by different authors.

Polymer	Temp. °C	M_e (g/mole)	Ref.
Polystyrene	140	17.300	a
	140	13.000	b
	183	16.500	c
Polydimethylsiloxane	25	12.300	a
	25	9.600	b
	25	12.300	c
	140	12.000	b

a) Ferry (1980), b) Mark (1996), c) Matsuoka(1992)

By catalytic hydrosilylation of the double bonds in polybutadiene with triethoxysilane it is possible to modify the PB-PS and PB-PDMS block copolymer to form block copolymer silane coupling agents. The hydrosilylated block copolymers denoted sPB-PS and sPB-PDMS can then by applied to various inorganic surfaces such as oxidized silicon, glass fiber or $Mg(OH)_2$ to investigate their structure and influence on interfacial adhesion.

The other part of this work is to explore different analytical methods for investigation of coupling agents on inorganic surfaces, and methods to investigate the influence of such coupling agents on the interfacial adhesion. This part is primarily concentrated on investigations on the synthesized block copolymer silane coupling agents, but other silane coupling agents have also been investigated.

The following paragraphs give an outline of the content of this thesis:

Chapter 2 is a description of living anionic polymerization of PB-PS and PB-PDMS block copolymers with varying molecular mass of the PS and PDMS blocks. The catalytic hydrosilylation of these block copolymers is described and the structural analysis of these block copolymers using FTIR, ^{1}H-NMR and GPC.

Chapter 3 concerns different analytical techniques used to investigate silane coupling agents on inorganic surfaces. Special emphasis is laid on the analysis of block copolymer silane coupling agents on inorganic surfaces. Other silane coupling agents have also been investigated where it has been relevant. The surface analytical techniques include: wet chemical analyses, different

FTIR sampling techniques, X-ray photoelectron spectroscopy (XPS), Ellipsometry, Atomic force microscopy (AFM) and contact angle measurements.

Chapter 4 concerns investigation of interfacial adhesion. Two separate methods have been applied to investigate the influence of block copolymer silane coupling agents on the interfacial adhesion between an inorganic surface and a polymer matrix similar to the tail end of the block copolymer. The methods are the JKR-method and a microdebond method. The JKR-method is a technique to measure the thermodynamic work of adhesion between different materials and to determine adhesion hysteresis caused by rearrangement of the interface region during contact. The microdebond technique is a method to determine the debonding force between a glass fiber and a microdrop of polymer embedding the fiber.

Chapter 5 is a brief description of a separate project concerning hydrothermal aging of glass fiber filled polyphenylensulfide (PPS) and polyamide (PA 6,6) composites. This project has been running parallel to the work on block copolymer silane coupling agent and is fully described in two technical reports in Danish. This project is relevant in connection with research in new silane coupling agents because it concerns hydrothermal aging of state of the art short fiber composites. The project shows that state of the art materials still are very sensitive to exposure in hot water.

Chapter 6 is an attempt to draw together a conclusion based on the observations made by the various analytical methods applied in this Ph.D. project.

Chapter 7 is suggestions for further work in the area of block copolymer silane coupling agents.

2 Synthesis of block copolymer silane coupling agents

2.1 Introduction

To investigate the conceptual idea of using block copolymers with multiple silane sites to react with an inorganic surface and long polymer chains to interact with the polymer matrix, it is necessary to synthesize new block copolymers.

A review of the literature shows that introduction of silanes on a polymer backbone can be done by catalytic hydrosilylation of unsaturated polymers. In particular, butadiene polymers are suitable for hydrosilylation (Cameron & Qureshi (1981) , Guo *et al*. (90&92), Iraqi *et al.* (92), Marciniec *et al*. (97)).

Polybutadienes can be synthesized using various polymerization methods resulting in a large variety of structures and properties (Richard 1977). Butadiene has the ability to form stable carbanions through resonance. As a result, polybutadienes can be synthesized using living anionic polymerization. “Living” refers to the absence of termination during propagation. As a result, all initiated chains grow equally and are still active after consumption of all monomers. Anionic refers to the initiation reaction that can either be addition of a negative ion to a monomer or an electron transfer reaction. A variety of anionic initiators has been investigated, but the organic alkali metal salts like butyl-lithium are perhaps the most common. The advantage in using the living anionic polymerization technique is the outstanding control of the polymerization process. Firstly, the initiator / monomer ratio determines the molecular mass, and the living nature of the polymerization results in very narrow and well controlled molecular mass distributions. Secondly, by the choice of initiator, solvent and reaction temperature it is possible to control the structure of the polymer. Thirdly, anionic polymerization gives the possibility to form block copolymers directly by adding a second monomer. The procedure, mechanisms and kinetics for anionic polymerization of polybutadiene is given by Morton *et al*. (1963 a&b).

Hydrosilylation is the subject of many publications, i.e. Speier (1979) and Marciniec (1992), although there are only a few papers published on hydrosilylation of polymers. Catalytic hydrosilylation of polybutadienes is a well-described reaction type in the literature. Guo and Rempel (1990) report successful hydrosilylation of pendant double bonds in polybutadiene with R_3SiH (R = Me, Et, n-Bu or OEt) using a chloro-tris(triphenylphosphine)rhodium(I) ($RhCl(PPh_3)_3$) catalyst. Analyzing the products with a combination of IR and (^1H,^{13}C and ^{29}Si)-NMR spectroscopy reveal the addition is strictly anti-Markovnikov. From quantitative treatment of the ^1H-NMR data the highest degree of silylation is found to be 85.0%.

In 1992,Guo and Rempel published a paper concerning hydrosilylation of styrene-butadiene and nitrile-butadiene copolymers catalyzed by $RhCl(PPh_3)_3$. The results of the studies suggest that $RhCl(PPh_3)_3$ is highly selective toward hydrosilylating the pendant double bonds. In

the presence of styrene functional groups, this addition is anti-Markovnikov while the presence of nitrile functional groups effects the reaction to occur via a Markovnikov addition.

Iraqi *et al*. (1992) describe in detail the hydrosilylation of a variety of polybutadiene types using $HsiMe_xCl_{3-x}$ (x = 0-2) in the presence of $H_2[PtCl_6]$. ^1H and ^{13}C NMR spectroscopy analysis indicate complete anti-Markovnikov funtionalization of the pendant double bonds when polybutadiene is reacted in toluene at 80°C in presence of $H_2[PtCl_6]$ (10^{-4} mole per mole of double bonds in the starting polymer). The results also show some reactivity of the double bonds in the backbone of the polymer especially in polymers containing high amounts of cis-units. Furthermore, the analysis shows that changing silane from $HSiMe_2Cl$ to $HSiMeCl_2$ or $HSiCl_3$ results in a decreasing reactivity towards backbone double bonds (and isomerization). Iraqi et al. also show that chlorosilane functionalized polybutadiene can be fully converted to ethoxysilane functionalized polybutadiene by addition of ethanol in excess in presence of triethylamine.

2.2 Experimental

The initial strategy for the experimental work has been to investigate the addition of ethoxysilane to commercial polybutadiene before engaging in polymerization of butadiene containing block copolymers

2.2.1 Preliminary study: Hydrosilylation of polybutadiene

On the basis of the literature the reaction between $HSi(OC_2H_5)_3$ and a sample of polybutadiene was investigated. This polybutadiene is predominantly 1,2-units (~86 % determined by ^1H NMR). The reaction was carried out in presence of $H_2[PtCl_6]$ (10^{-4} mole per mole of double bonds in the starting polymer). The reaction is shown in Figure 4.1. 10 g of polybutadiene was reacted with 1,9 g of ethoxysilane in 100 ml toluene. The reaction was carried out by refluxing under argon for 24 hours at 80°C. The solvent and reactants were used as received in order to investigate the influence of water contamination on the reaction.

After the reaction, the solvent was removed by evaporation under vacuum and small samples were taken for NMR and FTIR studies. The product was then dissolved in pentane and kept under dry nitrogen. Samples were taken out for GPC analysis.

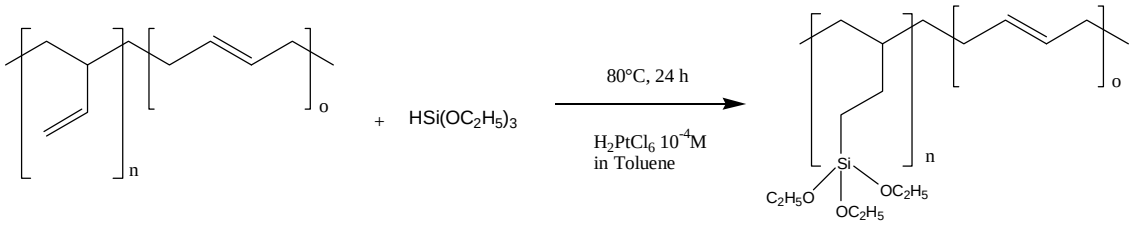

Figure 2.1 Catalytic hydrosilylation of pendent double bonds in polybutadiene.

2.2.2 Polymerization

Based on the preliminary study, 6 different diblock copolymers were chosen as synthetic targets. These included polymers containing a polybutadiene block with a molecular mass of ~3 kg/mol with the other blocks being polystyrene (PS) and polydimethylsiloxane (PDMS) with target molecular masss of 10, 30 and 100 kg/mole. The reaction schemes are given in Figure 2.2 and 2.3.

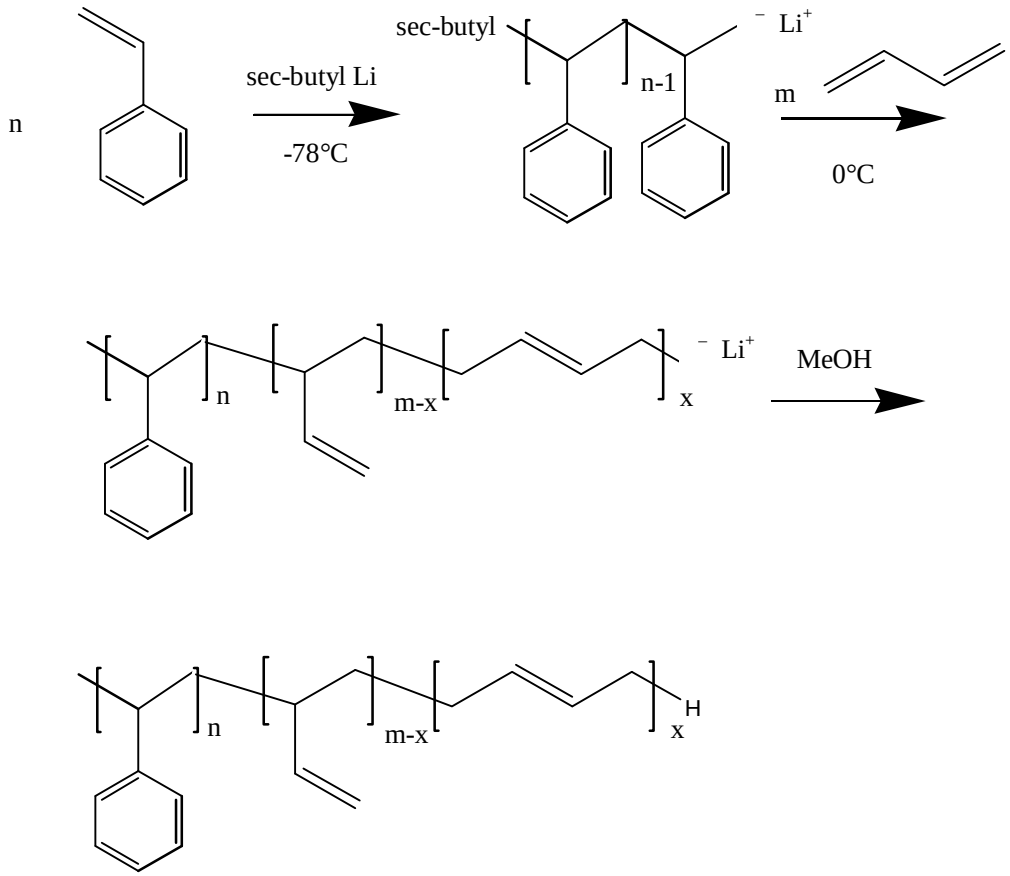

Figure 2.2. Living anionic polymerization of polybutadiene-polystyrene (PB-PS) block copolymers.

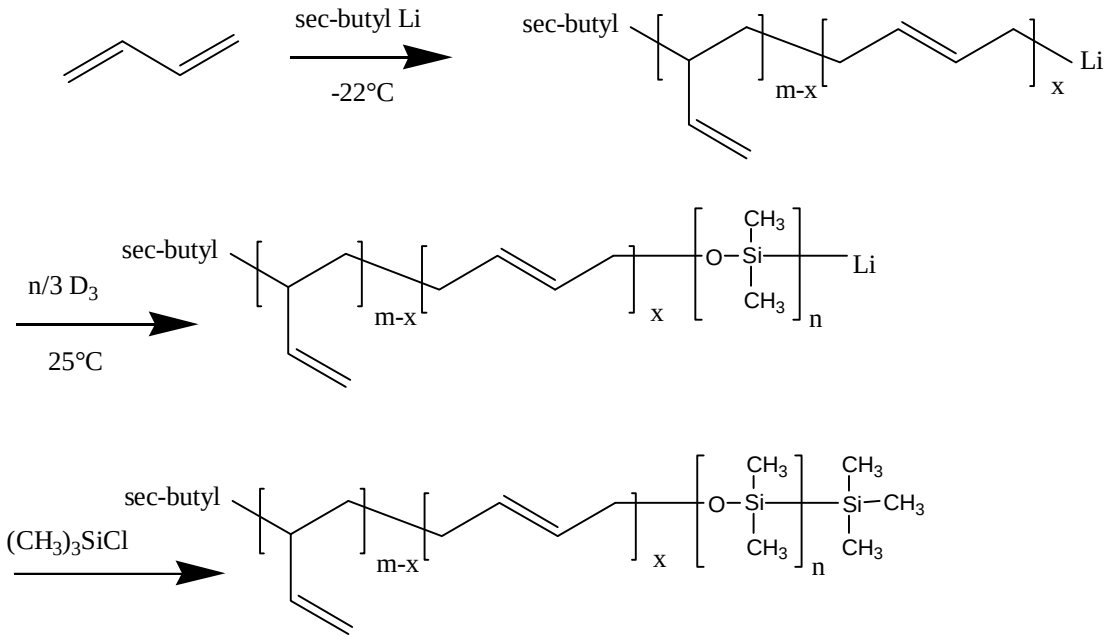

Figure 2.3. Living anionic polymerization of polybutadiene-polydimethylsiloxane (PB-PDMS) block copolymers.

The solvent used for the reaction influences the distribution of 1,4- and 1,2-units in polybutadiene prepared by living anionic polymerization. The solvent used for all polymerization reactions in this work is tetrahydrofuran (THF). Polybutadiene from THF polymerization contains ~90% 1,2-units. THF was chosen as the solvent because all three polymerization reactions PB, PS and PDMS are possible without using polarity modifiers or co-solvents.

Anionic polymerization is very sensitive to oxygen and water contamination. Because of this all reactant preparation and reactions were carried out under vacuum or highly purified argon. The polymerization was carried out in a special laboratory at Risø built by Kristoffer Almdal (Ndoni *et al.* 1995). The chemicals for the polymerizations are given in Table 2.1.

Table 2.1. List of chemicals used for anionic polymerization of PB-PS and PB-PDMS block-copolymers

Function	Chemical name	Description
Monomers	Butadiene	13 Butadiene N25, Hede Nielsen
	Styrene	Zür syntesen Merck Art 807679
	Hexamethylcyclo trisiloxane (D_3)	>98% Aldrich 23,568-7
Solvent	Tetrahydrofuran	HPLC grade Rathburn UN2056
Initiator	Sec-butyllithium	1,3 M lsg in cyclohexane Aldrich 19,559-6
Terminators	Methanol	Super pure Rohmil 205
	Trimethyl-chlorosilane	>99% Fluka 92360
Purification agents	Aluminum oxide (Al_2O_3)	90 Aktiv basisch (Activitätsstufe I) 70-230 mesh Merck # 1076
	Calcium hydride	95% -4, +40 Mesh Aldrich 20,802-7
	Dibutyl magnisium	1,0 M sol. In heptane Aldrich 34,511-3
	Benzophenon	Purum >99% Fluka
	Sodium	50 wt% dispersion in paraffin Aldrich 24,468-8

Careful preparation of the reactants for anionic polymerization is essential for the resulting polymers. The living anions of dienes and styrene formed during polymerization will react with almost any impurity in the reactor resulting in termination of the polymerization.

The procedure is as follows:
Solvent: 2 liter Tetrahydrofuran (THF) was passed through a glass filter containing 50g of alkaline Al_2O_3 into a 3 l three neck flask containing 15 g Na paraffin dispersion. The THF was refluxed in a closed system under argon overnight then cooled to room temperature at which time a benzophenone crystal is added. The solution turns royal blue. By refluxing the color changes from royal blue to dark violet indicating that the THF is sufficiently dry for living anionic polymerization. The determined volume was distilled into a solvent flask under argon.

Butadiene: 7 ml dibutyl magnesium was placed in a 2-neck flask with a stirring magnet. The flask was cooled in liquid N_2 and evacuated and the butadiene gas was added from a pressure vessel through a special valve. The solution was then stirred in an ice bath for 2 hours. The butadiene was stored at –78°C in solid CO_2/isopropanol bath. The calculated volume is distilled to a graded monomer flask under vacuum at 0°C. *It is important to note that the handling of 1,3-butadiene requires great care. It boils at –4.41°C and is toxic and very flammable. It is therefore very important to keep the temperature below 0°C at all times.*
Styrene: 100 g styrene was transferred to a 500 ml 2-neck flask containing 10 g CaH_2. The flask was cooled in liquid N_2 and evacuated. The solution was stirred at room temperature for 4 hours, then distilled in to a 250 ml 2-neck flask containing 7 ml dibutyl magnesium, stirred 1 hour at room temperature, then cooled in liquid N_2 and evacuated. The calculated volume was distilled to a graded monomer flask under vacuum at 25°C. The flask was filled with purified THF to prevent styrene form freezing when added to the reactor at –78°C.
Hexamethyl cyclotrisiloxane (D_3): 100 g D_3 was transferred to a 500 ml 2-neck flask containing 10 g CaH_2. The flask was cooled in liquid N_2 and evacuated, then stirred at for 4 hours at 75°C, distilled in to a 250 ml 2-neck flask containing 7 ml dibutyl magnesium at 85°C. Stirred 1 hour at 75°C, then cooled in liquid N_2 and evacuated. The calculated volume was distilled to a graded monomer flask under vacuum at 85°C. The flask was filled with purified THF to dissolve D_3.
Initiator (sec-butyl lithium) was used directly. The concentration is determined prior to polymerization by Gillmans double titration.
The preparation steps are sketched in Figure 2.4.

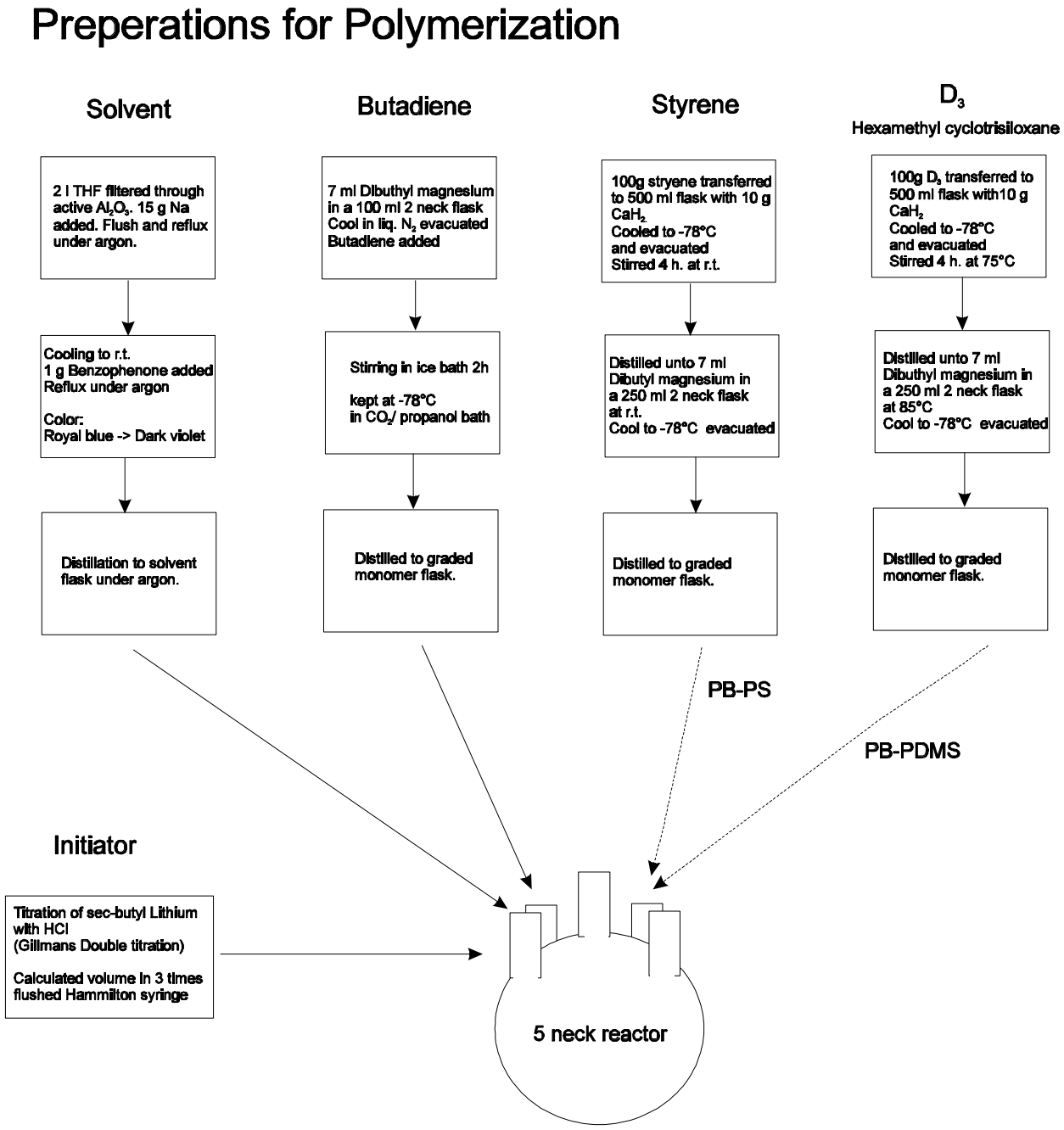

Figure 2.4. Preparation steps for living anionic polymerization of Polybutadiene-Polystyrene (PB-PS) and Polybutadiene-Polydimethylsiloxane (PB-PDMS) diblock copolymers.

Polymerization:

PB-PS: The solvent flask and the two monomer flasks were fitted on a 1 liter (5+1)-neck reactor. The other necks were fitted to a vacuum/argon line with a separate pressure sensor, thermocouple and a septum separately connected to the vacuum/ argon line. A stirring magnet was placed in the top of the reactor held by an outside magnet. The reactor was evacuated and baked overnight at 260°C then cooled to room temperature and flushed 3 times with argon. The solvent was added and cooled to –78°C in solid CO_2/isopropanol bath. The calculated volume of initiator was injected from a Hamilton syringe which had been previously flushed 3 times with argon. The solution was slightly yellow after adding sec-butyl lithium. Adding styrene drop by drop started the polymerization. Adding the styrene took around 1 hour. It is important to add styrene very slowly to avoid a sudden raise of temperature due to the reaction heat and at the same time prevent the styrene from freezing on top of the solvent. The solution turned red after adding styrene. After adding the last styrene, all the butadiene is added and the temperature is raised to 0°C in an ice bath. The reaction turns slightly yellow after adding butadiene. Termination by 1 ml purified methanol was done after waiting the calculated time from kinetic data. The solution was transferred to 1 l cold methanol at which time the polymer precipitates. The polymer was washed two times in methanol, dried under vacuum and stored in freezer at –18°C. 25 g of each block copolymer was synthesized with an overall yield of ~98%

PB-PDMS: The reactor set-up was the same as for PB-PS polymerization. The THF is added and cooled to 0°C in ice bath. The calculated volume of initiator was injected from a Hamilton syringe which had been previously flushed 3 times with argon. All butadiene was added and reacted the calculated time. Then, all D_3 is added and allowed to polymerize the calculated time. Adding purified trimethyl chlorosilane in cyclohexane terminates the polymerization. The polymer is isolated by adding 200 ml n-hexane and extracting tree times with 1 liter distilled water. Most n-hexane is removed in rotation evaporation and the rest by stirring under high vacuum.
The procedures of the polymerizations are given in Figure 2.5. There were synthesized ~25 g of each block copolymer was synthesized with an overall yield from 63-84%

Polymerization

PB-PS

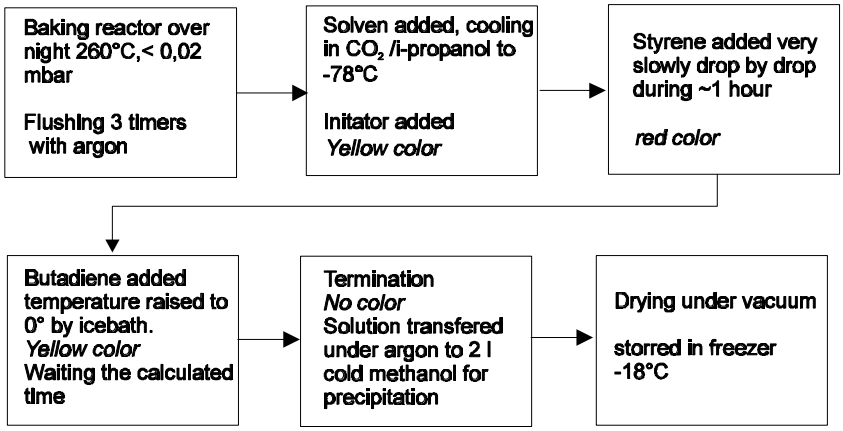

PB-PDMS

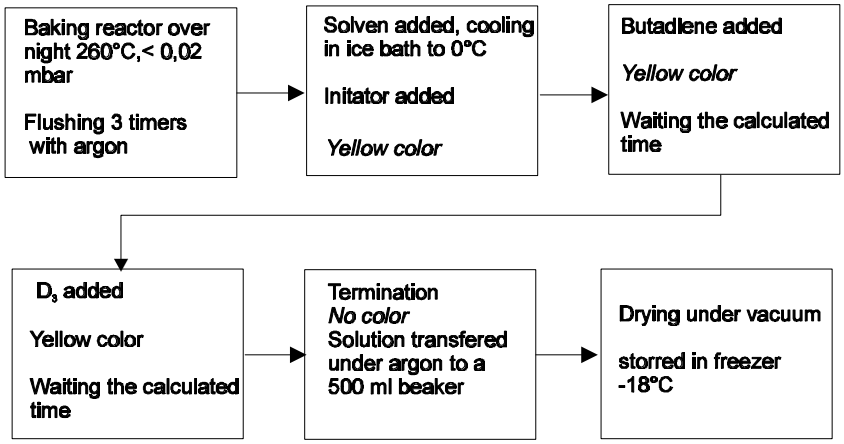

Figure 2.5. Procedure for living anionic polymerization of Polybutadiene-Polystyrene (PB-PS) and Polybutadiene-Polydimethylsiloxane (PB-PDMS) diblock copolymers.

2.2.3 Kinetic calculations

To be able to estimate reaction times for the living polymerisation reactions, it is necessary to investigate the kinetics. Investigations by Morton et al. (1963 a&b) showed that living anionic propagation reaction of polystyrene and polybutadiene in THF is first order both in monomer and initiator concentration as expressed in (2.1):

$$(2.1) \quad -\frac{d[M]}{dt} = k_p [I]_0 [M] \ ,$$

where [M] is the monomer concentration $[I]_0$ is the initial initiator concentration and k_p is the propagation rate constant at the reaction temperature. The kinetics of living anionic polymerisation in THF is different from the kinetics in hydrocarbon solvents. Propagation in hydrocarbon solvents is normally ½-order in respect to the initiator or living chain concentration. This is due to self-association of the living chains, which is blocking the chains from reaction with monomers. The solvating effect of polar solvents like THF blocks the self-association as shown in reaction scheme below:

$$\left(\mathrm{RM_jLi}\right)_2 + 2\mathrm{THF} \Leftrightarrow 2(\mathrm{RM_jLi.THF})$$

Reaction times can then be calculated by integration of the rate expression (2.1) resulting in:

$$(2.2) \quad t = \log\left(\frac{[M]_0}{[M]}\right) / k_p [I]_0$$

The remaining is then to find reliable values of the propagation rate constant at the reaction temperature.
Morton et al. have, on basis of polymerisation experiments, calculated the Arrhenius parameters for the propagation rate constant for butyl-lithium initiated polymerization of butadiene in THF. Using the Arrhenius equation (2.3), it is possible to find the propagation rate constant for a given temperature.

$$(2.3) \quad k_p = Ae^{-\frac{E_a}{RT}} \ ,$$

where A is the frequency factor and E_a is the activation energy for the propagation reaction. Morton found for butadiene a frequency factor of $4.3 \cdot 10^4$ l/(mole·s) and an activation energy of 25.5 kJ/mole. At 0°C this corresponds to a propagation rate constant of 0.56 l/(mole·s). For the

block copolymer PB-PS block copolymer with highest PS molecular mass (~100kg/mole) the initiator concentration is $3.7 \cdot 10^{-4}$ M.
The reaction time to 99% monomer conversion then calculates to 6,2 hours.
For polystyrene the frequency factor is $1.1 \cdot 10^{9}$ l/(mole·s) and the activation energy is 24.7 kJ/mole. Although the activation energy is almost equal to that of butadiene the frequency factor is almost 5 orders of magnitude higher. Calculating the propagation rate constant for styrene in THF at –78°C gives a value of 270 l/(mole·s). Using the same initiator concentration as for the butadiene, the reaction time to 99% monomer conversion calculates to 45 seconds.
It has not been possible to find reliable kinetic data for anionic polymerisation of PDMS in pure THF although the monomer conversion rate is believed to be first order in both monomer and intiator concentration. On the basis of this assumption, the reaction times to equal monomer conversions at the same reaction temperatures can be calculated using (2.4).

(2.4) $$\frac{t_1}{t_2} = \frac{[I]_2}{[I]_1}$$

The first PDMS polymerizations were followed using GPC (see Fig 2.11) and the reaction times to equal monomer conversion were calculated using (2.4).

2.2.4 Hydrosilylation

The hydrosilylation of polybutadiene (Figure 2.1.) in the block copolymers is carried out using the same precautions to water contamination as for the polymerization reactions, because ethoxysilane is very sensitive to water resulting in coupling of the polymer chains.

2 l toluene (HPLC grade Romil) is refluxed in a closed system under argon with 10g CaH_2. 200 ml is distilled in to a solvent flask under argon. Triethoxy silane is used as received. The amount of triethoxy silane used is calculated as the total molar amount of double bond in the polymer (both 1,2 and 1,4 units). The H_2PtCl_6 is used as a 0.02 M solution in n-propanol. All reactions are carried out using 10 g polymer in 200 ml toluene with 10^{-4} M H_2PtCl_6 and equamolar triethoxy silane at 80°C for 24 hours. The reaction is carried out in a one liter 5 neck reactor sealed under super dry argon. The reactor is fitted with a temperature controller and a pressure sensor. After the reaction, the solution is stored under argon at –18°C.

2.2.5 Characterization methods

Block copolymers were characterised using Fourier transformed infrared spectroscopy (FTIR), nuclear magnetic resonance (NMR) and gel permeation chromatography (GPC).

FTIR: The Infrared spectroscopy was carried out using a Perkin Elmer FT 1600 fitted with a PC for data processing. The samples for FTIR are prepared by coating a KBr disc with a thin film of the polymer either directly or by solvent casting from CH_2Cl_2. Measurements are made by adding 32 transmission scans. Difference spectra were made by normalizing the recorded spectra before subtracting.

NMR: Conventional ^{1}H-NMR experiment was carried out using a Bruker Advance DPX 250 spectrometer. Samples for NMR were prepared by diluting the polymers in $CDCl_3$ in approx. 15 mg/ml solutions.

GPC: Molecular mass distribution of the polymers is measured using a VISCOTEK 200 Differential Refractometer/Viscometer connected to a TriSEC Data Acquisition system used to record the reflective index and the pressure drop signal as a function of elution volume. The column system used for the block copolymers is three Nucleosil columns (500Å + 100Å + 50Å surface modified by C_4,C_8 and C_3 respectfully). The eluent used is THF stabilized with BHT. The samples are made by diluting the polymers in THF enriched with BHT (for internal calibration) to 1 mg/ml solutions.

2.3 Results and discussion

2.3.1 Preliminary study

The preliminary experiments on hydrosilylation of commercial polybutadiene from anionic polymerisation with a molecular mass of approx. 3000 g/mole were carried out to determine if direct reaction with ethoxy silane was possible. Figure 2.6. shows the infrared spectra of this polybutadiene before and after catalytic hydrosilylation with ethoxy silane. The infrared spectra show that the wanted reaction (Figure 2.1) is carried out successfully under the given conditions. The assignment of selected IR absorbence peeks is given in Table 2.2. The absorbancy peeks originating form C=C double bonds almost disappear after hydrosilylation, but there are remaining double bonds indicating less than 100% conversion.

Table 2.2. Assignment of selected IR absorbence peeks.
Data from Ying *et al.*. (1993) and Laumer (1987).

Wave number (cm^{-1})	Assignment
Butadiene	
674	1,2-cis out of plane bending
910	1,2 – out of plane bend
965	1,4-trans out of plane bending
995	1,2-Out of plane twist
1419	1,2- in-plane deformation
1641	1,2 vinyl stretch
1828	Overtone to 910 cm^{-1}
2843	CH_2 symmetric stretch
2917	CH_2 anti-symmetric stretch
2972	$=CH_2$ symmetric stretch
3075	$=CH_2$ anti-symmetric stretch
Ethoxy silane	
800	Si-O-C symmetric stretch
940-970	Si-O stretch
1170	Si-O-C anti-symmetric stretch
1100 and 1075	Si-O-C anti-symmetric stretch strong doublet

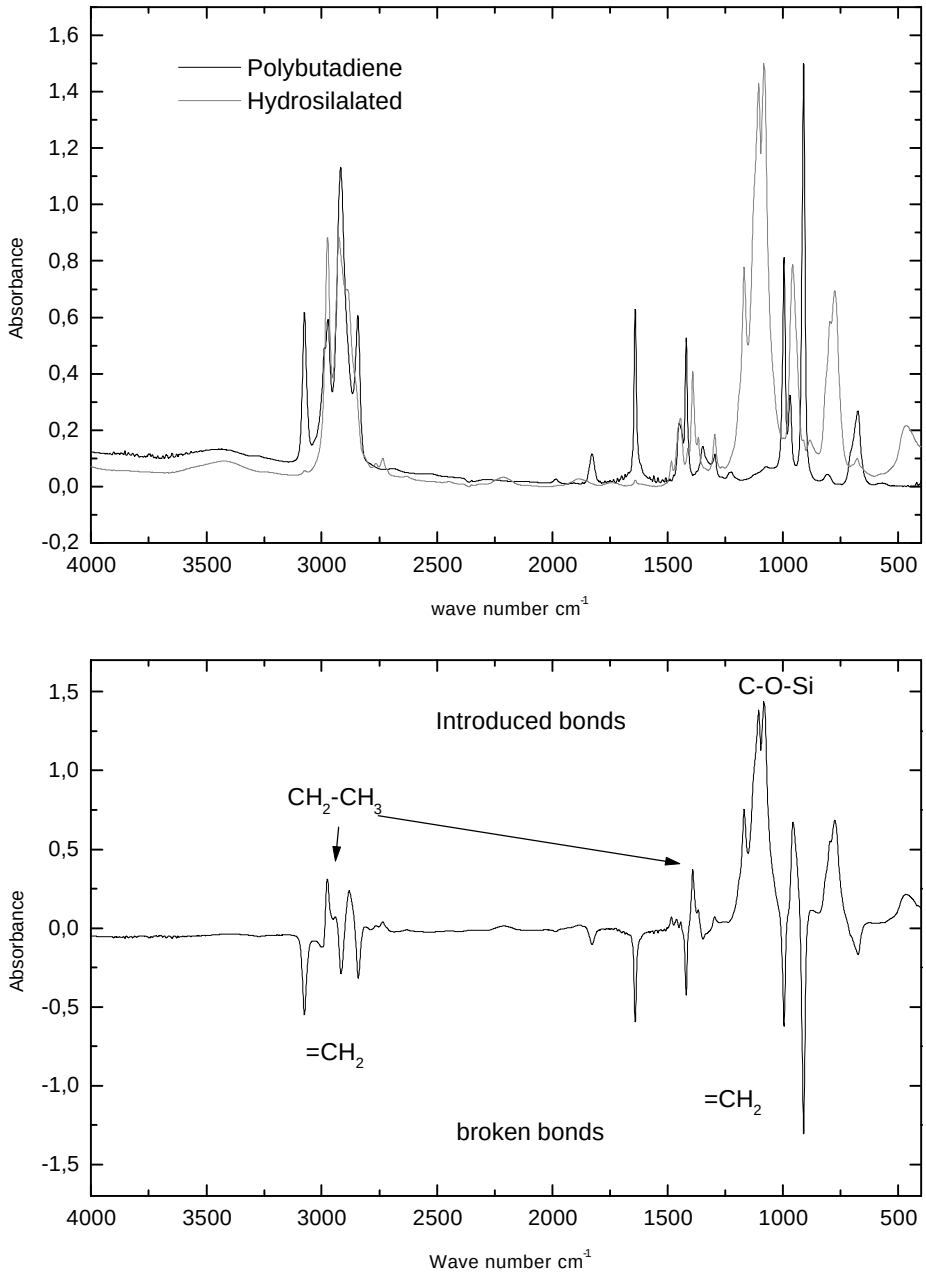

Figure 2.6. Infrared spectra of polybutadiene before and after catalytic hydrosilylation with ethoxysilane. The lower is the difference spectrum.

By subtraction of the two infrared spectra it is possible to get a picture of which bonds are broken and which are introduced by the catalytic hydrosilylation. The difference spectrum shows that all the broken bonds can by assigned to 1,2-polybutadiene units.

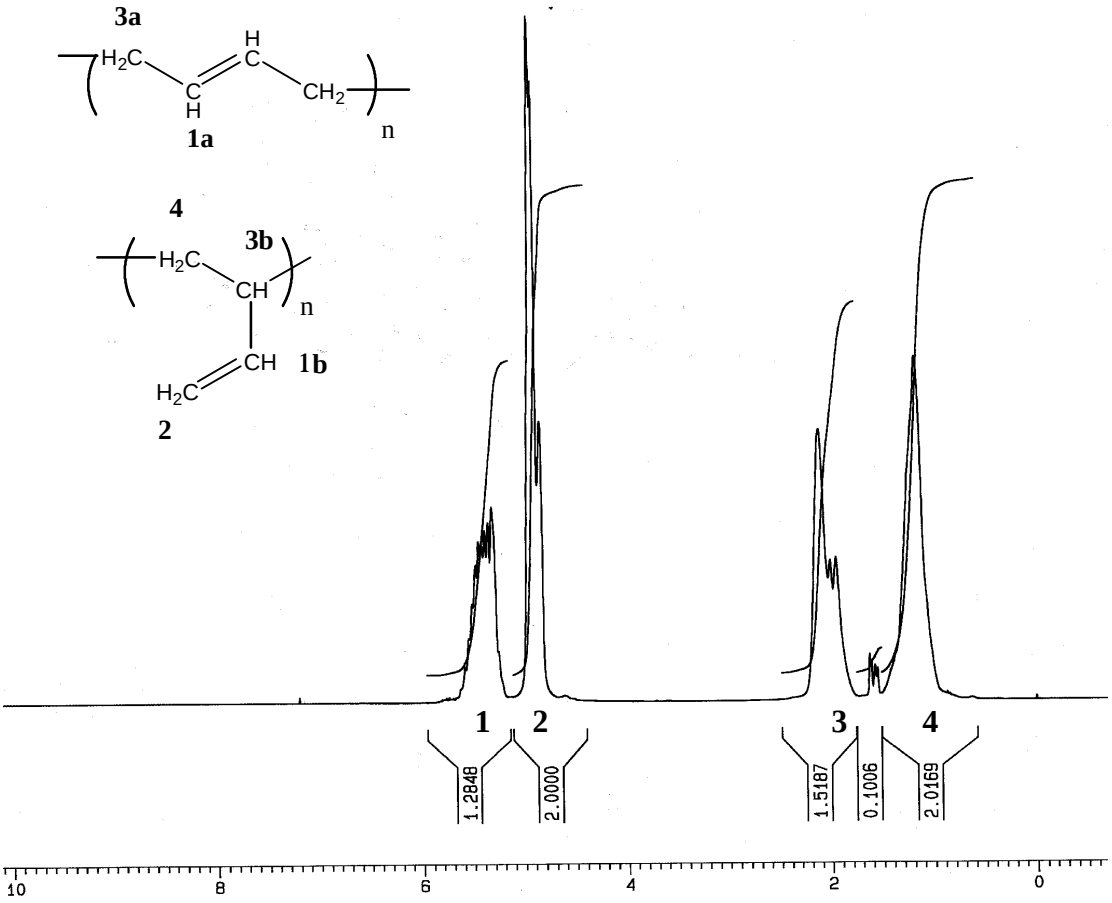

Figure 2.7. [1]H-NMR of a commercial polybutadiene used for hydrosilylation experiments.

[1]H NMR on polybutadiene reveals the distributions of 1,2- and 1,4-units in the polymer. The two hydrogens on the pendant vinyl carbon in the 1,2-units have a chemical shift of 5,0 ppm. The other hydrogen in the double bond has a chemical shift of 5,3 ppm which is equal to the shift of the hydrogens on the unsaturated carbons in the 1,4-units. The ratio of 1,4-units can then be calculated on the basis of peek **1** and **2** in Figure 2.7. The [1]H-NMR of the starting polymer shows that it contains approx. 12,5 mole % 1,4 units and it contains traces of tetrahydrofuran from the polymerization. These information fit very well together because anionic polymerization of butadiene in THF results in polybutadienes with 8-15% 1,4-units.

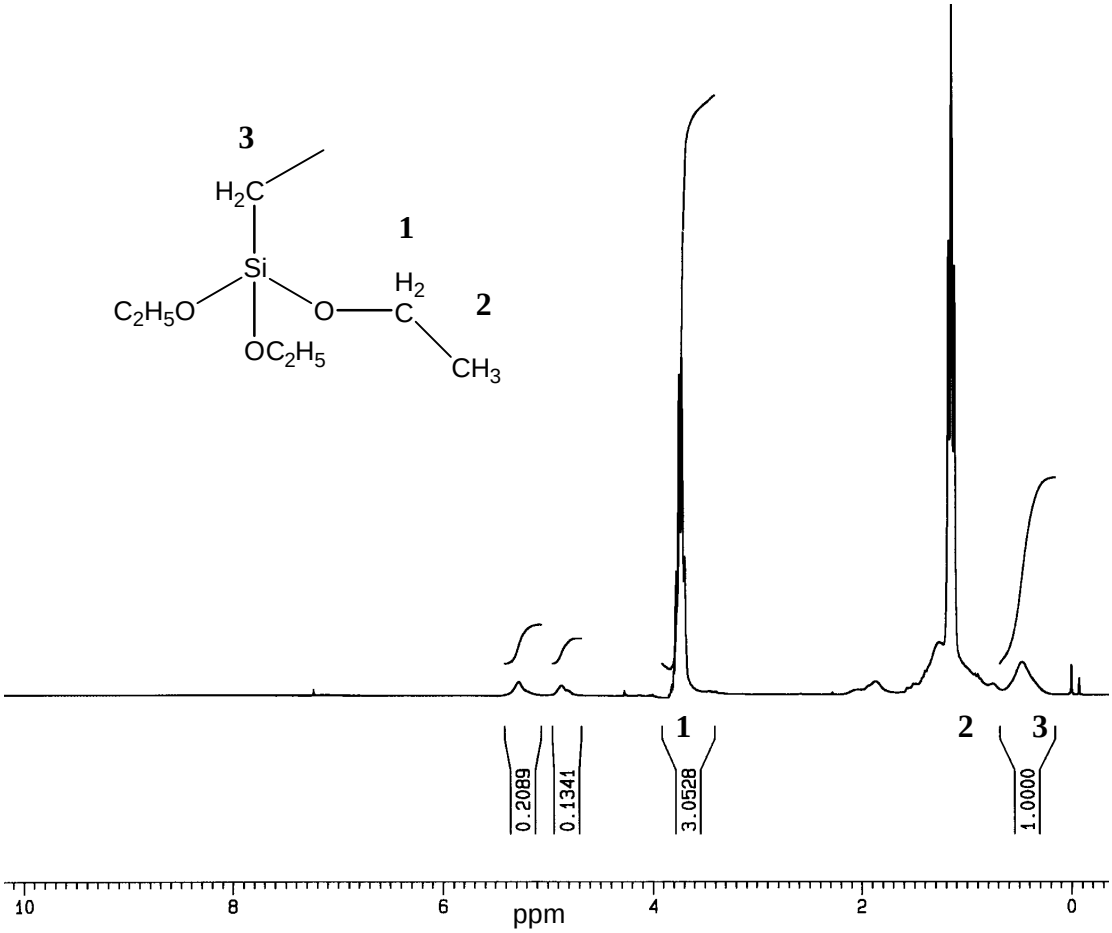

Figure 2.8. ^{1}H-NMR of commercial polybutadiene after catalytic hydrosilylation.

^{1}H-NMR of polybutadiene after catalytic hydrosilylation shows remaining double bonds like the FTIR results. The conversion of double bonds can be calculated on the base of the integral of peek **1** or peek **3** in Figure 2.8. These calculations both give a conversion of approx. 79 %. Of the remaining double bonds approx. 50% originate from 1,4-units. This shows that ethoxysilane reacts predominately with the 1,2- units in the presence of platinum acid catalyst. This was also found for a variety of other hydrosilanes by Iraqi *et al.*. (1992).

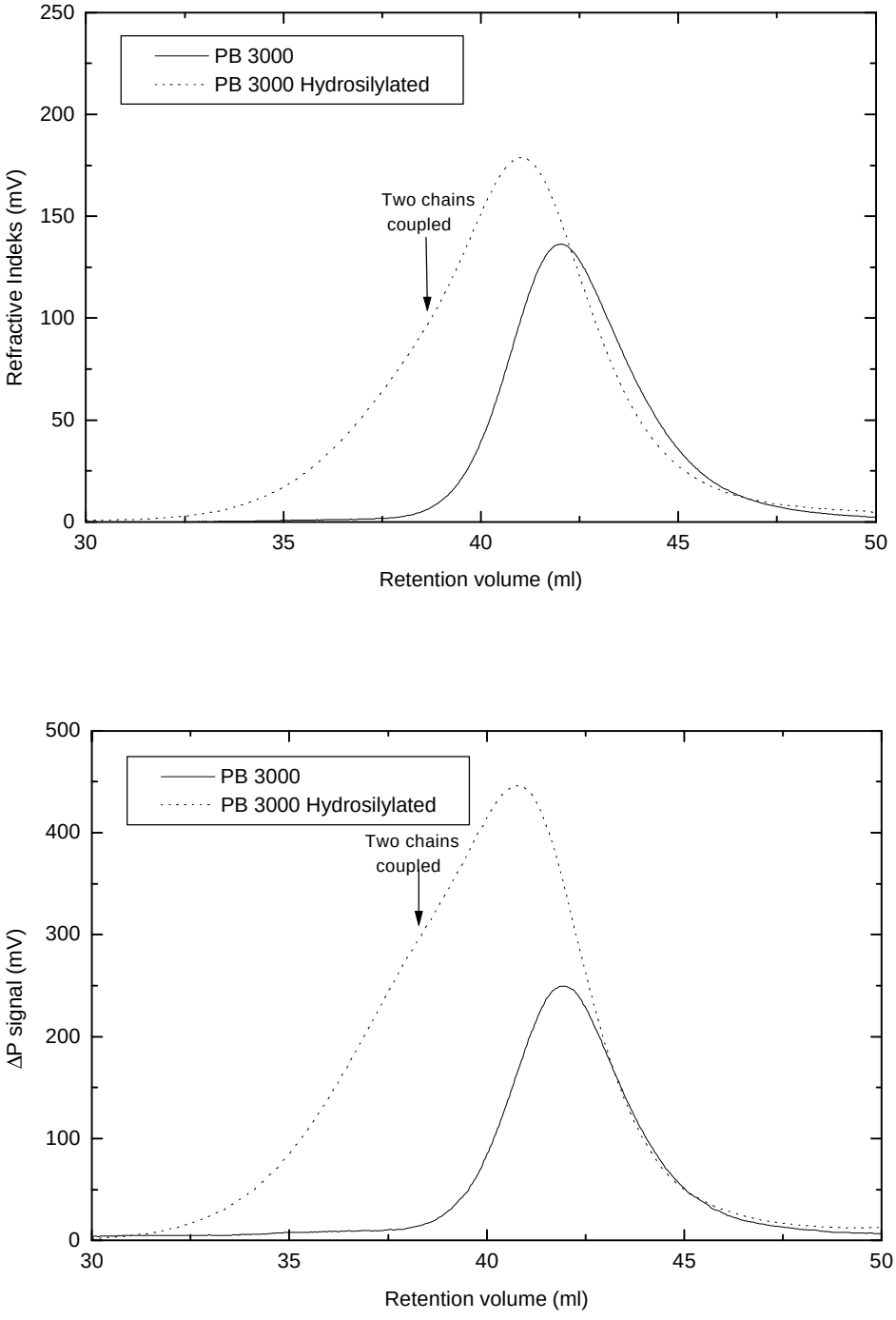

Figure 2.9 GPC analysis of commercial polybutadiene before and after catalytic hydrosilylation. *Upper*: Refractive index signal. *Lowe*r: Differential pressure signal.

Table 2.3. Molecular masses and polydispersity index form GPC based on polystyrene calibration curve.

Sample	M_n	M_w	Polydispersity index
PB 3000	4150	6250	1,506
PB 3000 hydrosilylated	5700	13000	2,333

The GPC results (Figure 2.9. and Table 2.3.) show the expected rise in molecular mass as a result of hydrosilylation, but furthermore they show that coupling of the chains occur as a result of the hydrosilylation. This is shown most clearly on the viscosity signal because of the enhanced signal of higher molecular mass species. The coupling of polymer chains due to silanol condensation in the presence of water also has a large effect on the polydispersity index of the polymers.
The results from the preliminary studies of hydrosilylation of polybutadiene show that it is possible to make ethoxysilane functional polymers by platinum acid catalyzation. GPC indicates that the reaction and afterwards handling should be done in completely water free environment.

2.3.2 Polymerization and hydrosilylation

All prepared polymers were characterised using ^{1}H-NMR before and after hydrosilylation with ethoxysilane. On the basis of this, the molar ratio of polybutadiene was calculated to compare with the target ratio for each polymerization. The results are given in Table 2.4. The molar ratios measured by ^{1}H-NMR are with one exception, the same as the predicted within the experimental uncertainty. PB-PDMS30 has higher content of butadiene units than expected from experimental data. This indicates that the PDMS polymerization was not carried out to full conversion of the D_3 monomers.

Table 2.4. Molecular ratio of polybutadiene (PB) from H^1-NMR Data

Polymer	Target M_w PB (kg/mole)	Target M_w PS/PDMS	Molar ratio of PB	Molar ratio of PB (^{1}H-NMR)
PB-PS10	3	10	0,366	0,364
PB-PS30	3	30	0,161	0,157
PB-PS100	3	100	0,055	0,051
PB-PDMS10	3	10	0,327	0,348
PB-PDMS30	4	30	0,148	0,189
PB-PDMS100	6	100	0,076	0,075

All prepared block copolymers were characterized using GPC to determine the molecular mass distributions. The recorded chromatograms were data processed using standard polystyrene

calibrations to determine the number- (M_n) and weight- (M_w) average molecular masses and calculate the molecular mass distributions. The average molecular masses are defined in terms of the specific molecular mass M_i and the number of moles n_i or the weight w_i of molecules with this specific molecular mass.

Number average molecular mass

$$(2.5) \quad M_n = \frac{\sum n_i M_i}{\sum n_i} = \frac{\sum w_i}{\sum w_i / M_i}$$

Weight average molecular mass

$$(2.6) \quad M_w = \frac{\sum w_i M_i}{\sum w_i} = \frac{\sum n_i M_i^2}{\sum n_i M_i}$$

The polydispersity Q is defined as:

$$(2.7) \quad Q = M_w / M_n = 1 + U \,,$$

where U is the molecular inhomogeneity.
Very narrow molecular distributions of polymers made by living anionic polymerization are believed to be Poisson distributed. The polydispersity derived from the Poisson distribution was found by Flory (1940) are shown in (2.8).

$$(2.8) \quad Q = M_w / M_n = 1 + 1/DP - (1/DP)^2 \,,$$

where DP is the degree of polymerization. This results in lower polydispersity the higher the molecular mass.

Figure 2.10 shows the calculated molecular mass distributions from the GPC measurements of polybutadiene-polystyrene block copolymers with varying lengths of the polystyrene block. The molecular distributions are defined in a way that the integral of each distribution equals 1. This means that the higher the peak the more narrow is the distribution. Figure 2.10 shows that the higher the molecular mass of the polystyrene blocks the more narrow the distribution becomes. This is in agreement with (2.8) even though the measured values of the polydispersity are much higher than the values calculated using (2.8).
Figure 2.10 also reveals that coupling between polymer chains have occurred during polymerization or termination for the high molecular mass polystyrene block. This kind of

coupling is typical of oxygen impurities. Then the coupling can either originate from a small leak in the reactor set-up or oxygen impurities in the methanol used as terminator.

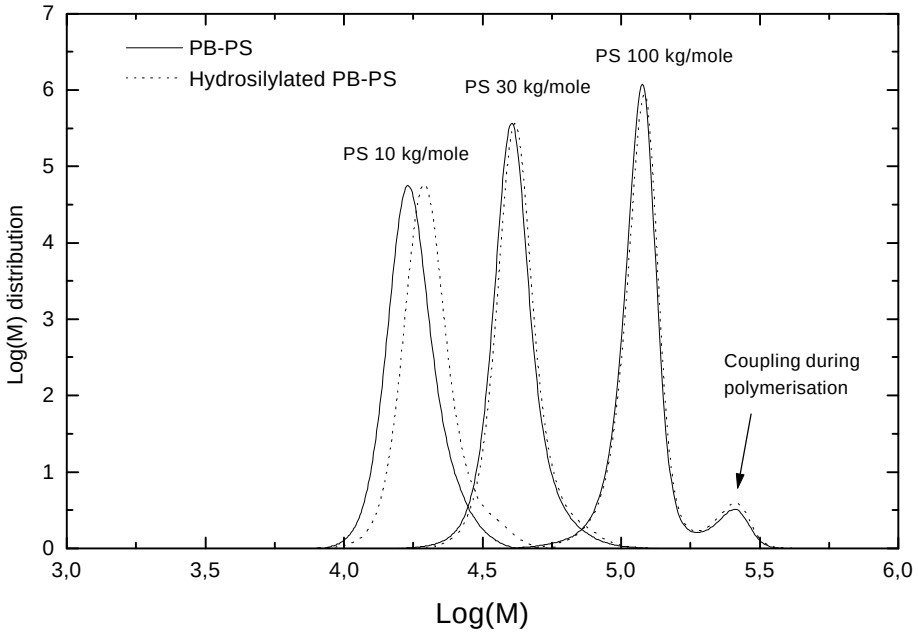

Figure 2.10 Molecular mass distributions from GPC of PB-PS block copolymers before and after catalytic hydrosilylation. Calculation based on standard polystyrene calibration.

Table 2.5. Average molecular masses and polydispersity calculated from GPC measurements using standard polystyrene calibration. sPB refers to polybutadiene after hydrosilylation with ethoxysilane.

Polymer	M_n kg/mole	M_w kg/mole	Q polydispersity
PB3-PS 10	17,3	18,1	1,046
sPB3-PS 10	19,7	20,8	1,056
PB3-PS 30	40,3	42,1	1,045
sPB3-PS 30	41,6	43,4	1,043
PB3-PS 100	117,8	126,5	1,074
sPB3-PS 100	120,7	130,1	1,078

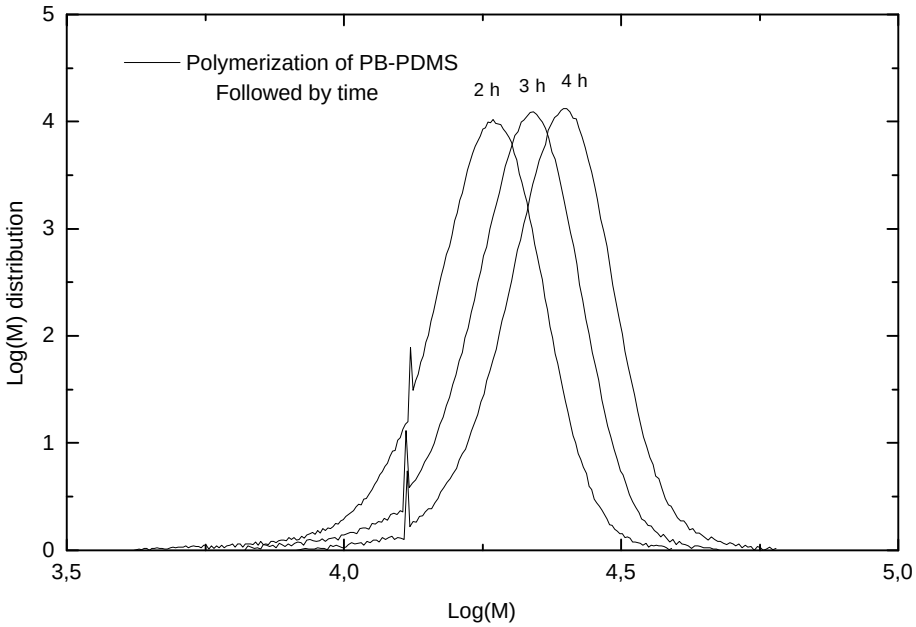

Figure 2.11. Molecular mass distributions form GPC of PB-PDMS taken out at different times during polymerisation. Calculation based on standard Polystyrene calibration. The sharp peeks origins from internal volume calibration.

Table 2.6. Average molecular masses and polydispersity calculated from GPC measurements using standard polystyrene calibration.

Sample	M_n kg/mole	M_W kg/mole	Q polydispersity
PB-PDMS 2h	17,0	18,2	1,071
PB-PDMS 3h	20,1	21,3	1,060
PB-PDMS 4h	23,4	24,7	1,056

Figure 2.11 shows the molecular mass distributions of polybutadiene-polydimethylsiloxane block copolymer taken from the reactor at different time during polymerization. This monitoring of the polymerization shows that the polymerisation runs as intended. Figure 2.11 shows the same narrowing of molecular mass distributions with growing molecular mass as shown in (2.8). A known problem with living anionic polymerisation of PDMS is reaction of growing silanolate-ends with Si-O bonds of already formed polymer chains causing redistribution (Hölle and Lehnen 1975). This effect becomes more important as the conversion increases. Table 2.7. shows increasing polydispersity of the PDMS containing block copolymer with increasing molecular mass of the PDMS block. This is interpreted as redistribution.

Table 2.7. Average molecular masses and polydispersity calculated from GPC measurements using standard polystyrene calibration.

Sample	M_n kg/mole	M_W kg/mole	Q polydispersity
PB3-PDMS10 silane	22,5	23,1	1,071
PB4-PDMS30 silane	77,6	92,9	1,197
PB6-PDMS100 silane	87,9	128	1,461

To synthesize PDMS containing block copolymers with narrow molecular mass distributions in THF it would be recommended to add an excess of D_3 monomer and control the molecular mass by reduced reaction time. By using this polymerization strategy it is possible to have sufficient high monomer concentration at all times to suppress redistribution. (Hammouch *et al*. 1995) The catalytic hydrosilylation of the polybutadiene blocks Figure 2.1. was found to be very sensitive to water contamination in the preliminary study. Figure 2.8. shows that coupling by siloxane bridging can be avoided by carrying out the reaction in a water free environment. The conversion of double bonds in polybutadiene can be calculated for H^1-NMR data. Comparing the content of 1,2-units in the polybutadiene before and after hydrosilylation shows that addition of ethoxysilane is predominantly to the pendant double bonds in the 1,2-units. Higher conversion of butadiene in PS-PB block copolymers than in PDMS-PB block copolymers using the same conditions is observed.

Table 2.8. Conversion of polybutadiene double bonds in block copolymers compared with content of 1,2 butadiene units before and after hydrosilylation with ethoxysilane in toluene at 80° for 24 hours (10^{-4}M H_2PtCl_6). Calculated for ^{1}H-NMR data.

Block copolymer	Conversion of C=C (%) By ethoxysilane	Mole % 1,2 units
PB3-PS10		89
PB3-PS10 silane	80	47
PB3-PS30		90
PB3-PS30 silane	88	57
PB3-PS100		94
PB3-PS100 silane	75	81
PB3-PDMS10		88
PB3-PDMS10 silane	55	63
PB4-PDMS30		89
PB3-PDMS30 silane	56	60
PB6-PDMS100		88
PB6-PDMS100 silane	69	58

2.4 Summary

PB-PS and PB-PDMS block copolymers have been synthesized with varying molecular mass by living anionic polymerisation in THF. The structures and molecular mass distributions have been examined using FTIR, ^{1}H-NMR and GPC. The living anionic polymerisation of PB-PS block copolymers resulted in well-defined block copolymers with narrow molecular mass distributions: polydispersity indexes 1,04-1,08. The polymerization of PB-PDMS showed broadening of the molecular mass distribution with increased molecular mass of the PDMS block resulting in polydispersity indexes ranging from 1.07 for PDMS 10 kg/mole to 1.46 for PDMS 100 kg/mole. These block copolymers have successfully been catalytically hydrosilylated with ethoxysilane in presence of chloro-platinum acid to form a new type of macromolecular coupling agents. The conversion of double bonds in the PB block ranges from 75-88% for the PB-PS block copolymer and from 55-69% for the PB-PDMS block copolymers. The catalytic hydrosilylation of the double bonds is found to be preferential anti-Markovnikov addition to the pendant double bonds in the 1,2 units in polybutadiene.

3 Characterization of interface modifiers on surfaces

3.1 Introduction

This chapter is a review of some of the analytical methods used to investigate surface modifiers on inorganic surfaces during this study. Investigations of interface modifiers on filler materials for polymer composite are a difficult task because of the low concentrations. The typical concentration of surface modifiers ranges from 0.1-2% wt. depending on the specific surface area of the filler material.
These low concentrations demand the use of specialized analytical techniques. The analytical techniques to investigate interface modifiers in this work include wet chemical identification methods for silane coupling agents of which one has been extended to quantitative analysis for amino-silanes. Another method used is Fourier transformed infrared spectroscopy (FTIR) where three different sampling techniques have been investigated as an analytical tool for silane coupling agents and other interface modifiers. For chemical analysis of the top surface layers of surface modified inorganic filler and flat model surfaces, x-ray induced photoelectron spectroscopy (XPS) has been used. The determination of layer thickness of silane coupling agents on flat model surfaces has been done using ellipsometry. To investigate the surface properties of silane layers on inorganic surfaces, an apparatus was built to measure contact angles using the sessile drop method. Finally, the lateral placement of the block copolymer based silane coupling agent were investigated using atomic force microscopy.

3.2 Chemical methods

Identification of an unknown coupling agent on a filler system can be necessary to understand the behavior of a given composite system. Wiedemann et al. (1978) have developed a number of wet chemical tests for identifying the most commonly used coupling agents/sizing systems. These tests are organized in an identification scheme that should be carried out in the order indicated (Table 3.1). This scheme is a powerful tool in investigating and understanding of the behavior of commercial composites, because the materials suppliers usually keep information of the used sizing system as internal know how.

Table 3.1. Chemical identification of primers on fillers.
The tests should be carried out in the order indicated. If there is a positive reaction, the color indicated is produced. The results can be confirmed by complementary tests (*a*). In case of a negative result, the next test is carried out.

Test No.	Reagent	Colour	Nature of Coating
1	ninhydrin	violet:	aninosilane
1*a*	Green GW:	violet: grey:	primary amino group primary or secondary amino groups
2	iodine/ potassium iodine	dark blue/ violet: orange-yellow:	Starch-oil Size paraffin emulsion size
2*a*	bromocresol green	blue:	paraffin emulsion size
3	diphenylcarbazide	Violet	methacrylic acid-chromium complex
4	Rhodamine B	Red	methacrylic silane or vinyl silane
4*a*	$KMnO_4$ solution	Discolouration	methacrylic silane or vinyl silane
5	sodium thiosulphate and bromothymol blue	Blue	epoxysilane (also aminosilane)

3.2.1 Quantitative test for aminosilanes

The quantitative Kaiser test is used in the determination of amino groups in various polypeptides (Sarin et al. 1981). An analogue qualitative test has been used for identification of primers on glass cloth (Wiedemann et al. 1978). The principle in both tests is the reaction of ninhydrin with a primary amine with a free proton on the carbon next to the amine to form Ruhemann’s purple, which is highly conjugated with a strong absorption around 570 nm (blue color). The reaction scheme is shown in Figure 3.1.
The quantitative Kaiser test has here been used to determine the number of aminosilanes attached to the surface of inorganic fillers used in polymer composites. The test is identical with the test for polypeptides, but is calibrated for aminosilanes.
The measurement is done by measuring the absorbancy of Ruhemann's purple (Fig. 1) at the wavelength of 570 nm. Calibration using solutions with a known concentration of aminosilane makes it possible to determine the concentration of free amine on filler surface. With knowledge of the specific surface area of the sample, it is possible to determine the average surface coverage of aminosilanes.

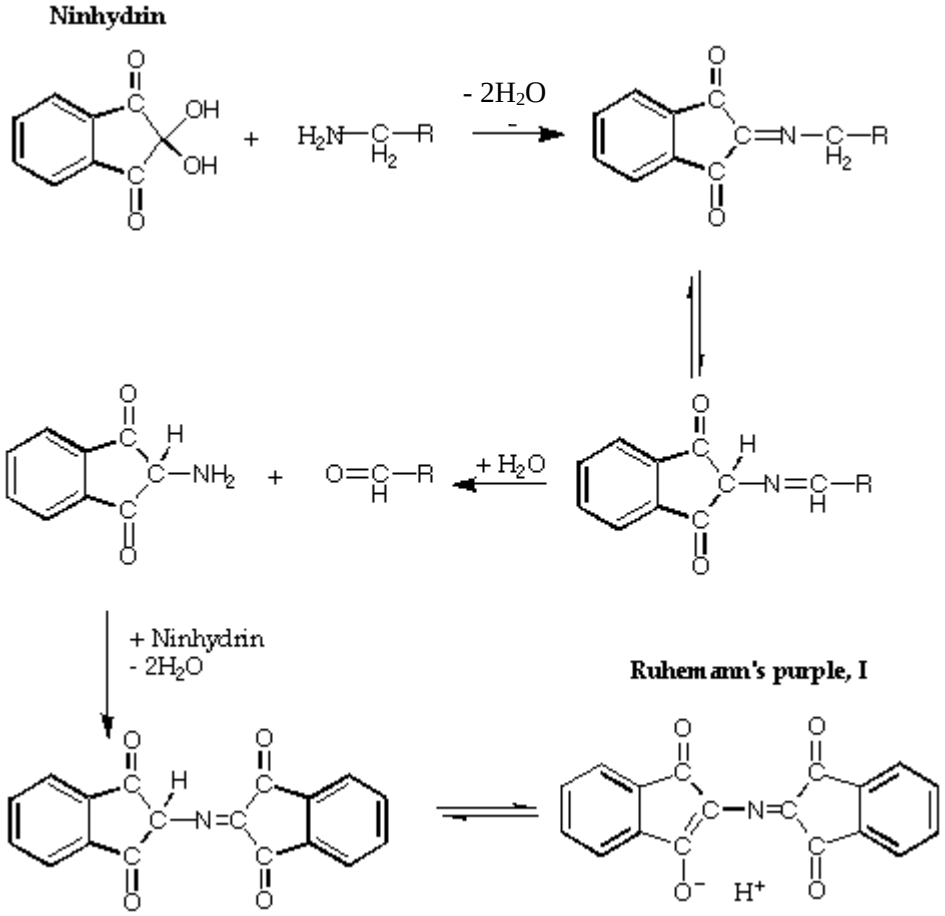

Figure 3.1. Reaction scheme for the Kaiser test.

3.2.2 Experimental

The Kaiser test is used as a standard test for amine groups in polypeptides at Risø. Two standard solutions are made for the test.

*Solution A***:**

Solution no. 1:

40 g reagent grade phenol was mixed with 10 ml. 99% ethanol (crystals and solution should be colorless). Heated until dissolved. Stirred magnetically for 45 min with 4 g of Amberlite mixed-bed resin MB-3 to remove traces of ammonia. Filtered by suction.

Solution no. 2:

33 mg of KCN was dissolved in 50 ml of distilled water. 2 ml of this solution was blended with 98 ml of pyridine (Fluka for UV spectroscopy). Stirred magnetically for 45 min with 4 g of Amberlite mixed-bed resin MB-3 . Filtered by suction.

Solution 1 and 2 was mixed (exothermic reaction!) to give Kaiser solution A. Stored dark.

Solution B:

7.5 g of Ninhydrin was dissolved in 50 ml absolute ethanol. (Solution is yellow, ninhydrin crystals are slightly yellow). Stored dark.

Procedure of testing:

2-20 mg of sample was placed in a 4 ml reagent glass. The mass was determined with 0.1 mg accuracy. From a standard Pasteur pipette 12 drops of solution A and 4 drops of solution B were added. The reagent glass was then sealed with aluminum foil and put in a 100°C heating block for 10 min. 1 ml of 60% ethanol in distilled water was added and the solution was cooled in ice water. If a visual blue color was observed the procedure was carried on. The sample solution was centrifuged at 2000 rpm for 5 min and the supernatant was transferred via a syringe through a 0.22 µm hydrophilic filter (Millipore) to a suitable graduated flask (i.e. 25 ml) and diluted with 60% ethanol/water. The size of the flask depends of the color intensity. The absorbancy should be between 0.2-0.4 for a reliable result. A reference solution was prepared using the same procedure without adding any sample. The solution was transferred to standard 1 cm cuvettes. The absorbancy difference at 570 nm between the sample and the reference solution was measured using a Carry 1E UV-Visible spectrometer.

The concentration of amino groups (C (µmol/g)) is determined by formula (3.1).

(3.1)

$$C = \frac{A(570\ \text{nm}) \cdot V_{sol}}{e_{570}' \cdot M_s},$$

where A(570 nm) is the measured UV absorbency difference at 570 nm, V_{sol} is the volume of the solution in ml, M_s is the weight of the sample in mg and e_{570} the effective extinction coefficient in l/µmol. The effective extinction coefficient is determined by performing the test using a number of aminosilane solutions with known concentrations.

The method has been used to measure the efficiency of specific surface treatment with γ-aminopropylsilane compared to commercially treated fillers. The filler $Mg(OH)_2$ platelets (H7 form Magnifin) were stirred in 1% solution of γ-aminopropyl-trimethoxysilane in 96% ethanol in water for 20 min., then filtered and dried under vacuum. ~3 mg of the filler was tested using the Kaiser test. The untreated filler was also tested for amine contamination. Magnifin H7B (amine modified $Mg(OH)_2$ platelets form Magnifin) was tested for comparison. Finally, an amino modified high surface area silica column material for liquid-chromatography (Nucleosil 5 NH_2) was tested to compare the surface coverage.

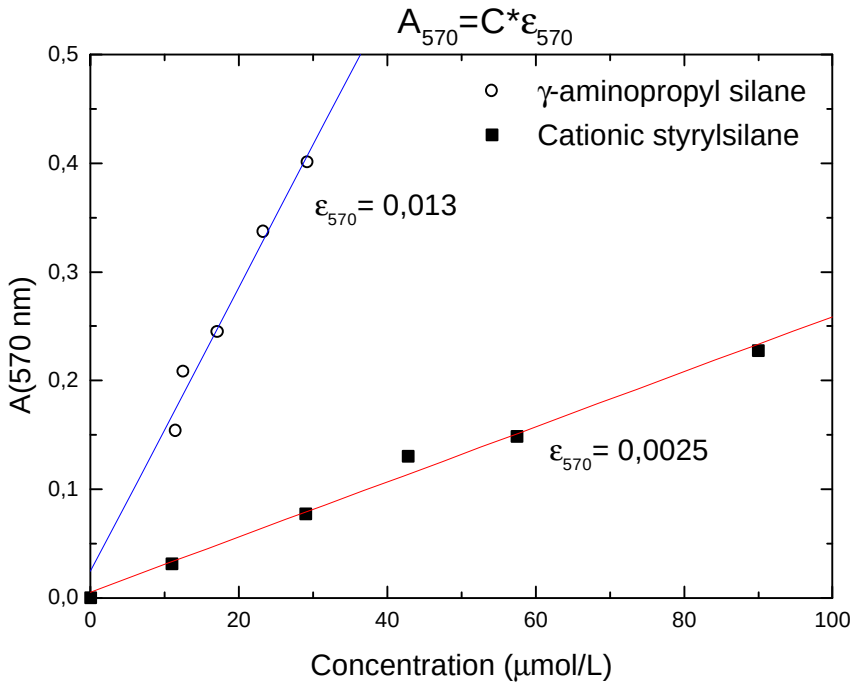

Figure 3.2. Calibration curves for the Kaiser test for γ-aminopropyltrimethoxy-silane and 3-(N-Styrylmethyl-2-aminoethylamino)-propyl-trimethoxysilane hydrochloride, known as (Cationic styrylsilane)

3.2.3 Results and discussion

The qualitative Kaiser test showed a positive reaction for glass fillers treated with γ-animopropylsilane, but also for glass fillers treated with 3-(N-Styrylmethyl-2-aminoethylamino)-propyl-trimethoxysilane hydrochloride better known as cationic styrylsilane (Table 1.1.) This was unexpected because cationic styryl-silane does not contain primary amine groups, but a protonated secondary anime. Calibration curves for determination of the effective extinction coefficient e_{570} (3.1) for γ-animopropyl-silane and 3-(N-Styrylmethyl-2-aminoethylamino)-propyl-trimethoxysilane hydrochloride are shown in Figure 3.2. The calibration curves reveals a significant difference in effective extinction coefficient for the two silanes. The effective extinction coefficient is more than 5 times smaller for cationic styrylsilane than for γ-aminopropylsilane. This is in good agreement with the chemistry of the reaction with ninhydrine. It is expected that the efficiency of the reaction of ninhydrin with protonated secondary amine is either zero or less than that of a primary amine.
The essential in this investigation is the linear relationship between the concentration and the absorption at 570 nm for both amino-silanes. This makes the Kaiser test a useful tool in investigations of surface treatments involving amino-silanes. In Tast on γ-amino-propyltrimetoxysilane treated $Mg(OH)_2$ compared with commercial NH_2-treated $Mg(OH)_2$ and high surface area silica gel.
The results show that laboratory treatment of $Mg(OH)_2$ (1% g-APS in 96% ethanol in 20 minutes) yields the same surface coverage as the surface treatment given to the filler at Magnifin. Compared to the SiO_2 gel the surface coverage is more than 2 times higher on the $Mg(OH)_2$. This difference can be due to less efficient surface treatment of the silica gel or due to the fact that the surface density of OH-groups is higher on $Mg(OH)_2$ than silica gel.

Table 3.2. Results of the Kaiser test for $Mg(OH)_2$ fillers treated with γ-aminopropyl-trimethoxysilane compared with commercial filler containing amino-silane.

Sample	Specific surface area (m^2/g)	Amine conc. μmol/g	Surface coverage number/$(nm)^2$
H7 $Mg(OH)_2$	7	0	0
H7 + 1% γ-APS	7	18,2	1,6
H7B commercial NH_2	7	18,4	1,6
Nucleosil 5 NH_2	350	407	0,7

3.3 FTIR methods

Fourier transformed infrared spectroscopy (FTIR) is a powerful analytical tool in investigation of chemical bonds. The method has been used in numerous investigations of silane coupling agents and other adhesion promoters.
There are a number of different sampling techniques using FTIR. The scope of this work is to investigate three different sampling techniques in connection with silane coupling agents. The three sampling techniques are:

- Direct transmission
- Photoacoustic spectroscopy
- Diffuse Reflectance

3.3.1 The principle of FTIR

A vibrational spectroscopic instrument consists of three principal components: the source, the monochromator and the detector. In infrared instrumentation the source must be continuous and provide radiation in the spectral area of interest, which is different from Raman spectroscopy, where the source must be monochromatic.
Until about 1976, practically all commercial infrared instruments were dispersive spectrometers, where the wavelength is gradually varied using a prism and slit set-up. The reinvention of the Michelson interferometer and the commercial development of this kind of Fourier transform infrared interferometers completely changed the world of infrared spectroscopy.

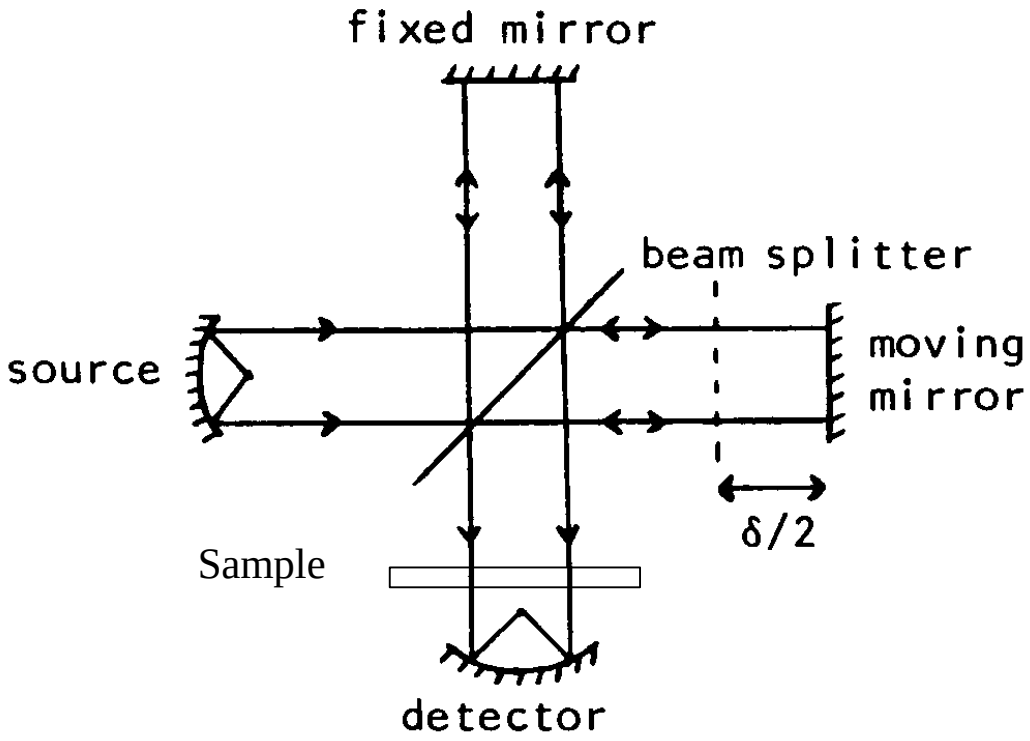

Figure 3.3 Principle of a Michelson interferometer

The principle of the Michelson interferometer (Figure 3.3) is that the radiation from the source is divided using a beam splitter in a way that half the radiation is reflected on a fixed mirror and the other half is reflected on a moving mirror. The reflected radiation from the two mirrors then interferes constructively or destructively depending on the wavelength and the position of the moving mirror. If monochromatic light is passed into the interferometer and the two mirrors are at equidistant from the beam splitter, the light beam would exit the interferometer unchanged except for a 50 % reduction in intensity from the light returned in the direction of the source. However, if the path length of the movable mirror is changed by ¼ the wavelength of the monochromatic light, then the light waves would cancel each other out by destructive interference. Scanning the movable mirror will result in alternating light and no light in a sinusoidal wave with a frequency determined by the speed of the mirror and the wavelength of the monochromatic light. For a continuos light source, this happens simultaneously resulting in a very complex signal called the interferogram. When the mirror is moved with a constant speed the frequency of the resulting sinusoidal response for each spectral element depends only on the wavelength. The spectra can then be obtained by computing the cosine Fourier transform of the interferogram.
The relation between the position of the mirror and the wavelength can be calibrated using a monochromatic source with known wavelength. This is usually done using a He-Ne laser.

Interferometers have three distinct advantages over the conventional dispersive spectrometers Durig & Sullivan (1987)

- *Fellgett's advantage* (the multiplex advantage). Simultaneous observations of all frequencies present, which offers a signal-to-noise advantage. In dispersive spectrometers each spectral wavelength is sequentially examined.
- *Jacquinot's advantage*. Greater throughput than in dispersive spectrometers because there are no slits or other obstructions in the optical pathway.
- *Connes' advantage*. Precision of wavelength measurements through laser bean calibration.

Together these advantages give the possibility to add multiple scans which gives significant improvement of the signal-to-noise ratio.
The first electronic IR detectors were thermocouples. But, thermocouples do not react fast enough for interferometers and they loose efficiency at chopping frequencies >30 Hz. The most commonly used detectors for FTIR are triglycine sulphate (TGS) or deuterated triglycine sulphate (DTGS) pyroelectric bolometers because they have good response to a wide range of infrared frequencies (5000- 33 cm^{-1}). DTGS detectors loose efficiency at chopping frequencies >1000 Hz. In the mid infrared spectral range (5000-400 cm^{-1}), a mercury-cadmium telluride (MCT) detector operated at the temperature of liquid N_2 offers faster response and increased sensitivity compared to TGS detectors. MCT detectors are commonly used in connection with FTIR microscopy where higher sensitivity is needed.

The sample is placed it the beam-way between the beam splitter and the detector. If the sample contains chemical bonds with vibrational frequencies that absorb light in the infrared region it is possible to identify these bonds by their specific vibrational frequencies. The theory of which molecular vibrations that results in infrared absorption is beyond the scope of this review. An introduction to the quantum mechanical selection rules can be found in the book by Rossiter and Hamilton (1987 pp.9-16).

3.3.2 Sampling techniques

FTIR investigations of silane coupling agents and other interface modifiers on filler materials can be difficult because of the low concentrations (usually < 1% wt.). Using the right sampling technique is crucial for the outcome of the investigation. The following is an introduction of the three different sampling techniques used in this work.

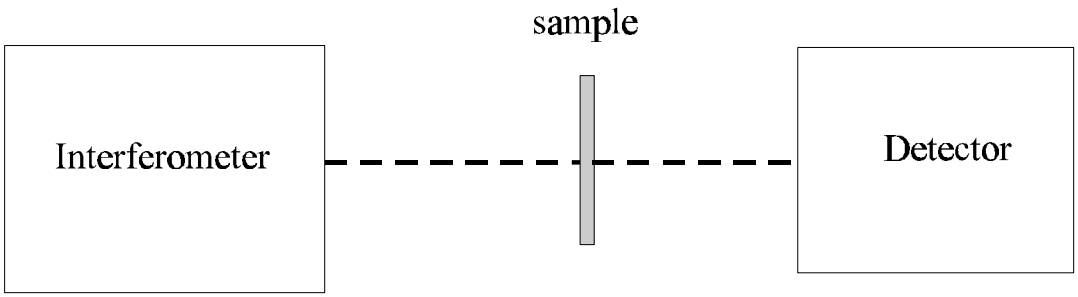

Figure 3.4. The principle of direct transmission FTIR, with the sample diluted in a KBr pellet.

Direct transmission: The principle of direct transmission is to dilute the sample in a pellet material that is transparent for infrared light in the spectral area of interest. There is a range on metal halides used as pellet materials. KBr is commonly used in the mid-infrared region because of the low cost and the extended transmission range form 4000-400 cm^{-1}. The sample material (0.5-2% wt.) is blended and grinded with dry KBr salt. The blend is pressed in to a pellet using a die connected to a vacuum pump to eliminate voids in the pellet. The blend is pressed at 300 bar for five minutes to form a solid pellet that can be mounted in the infrared beam way. In order to calculate the infrared spectrum of the sample it is necessary to subtract the background spectrum caused by other IR aborptions in the optical path way. The background spectrum for direct transmission is simply recorded with no sample in the optical path way.

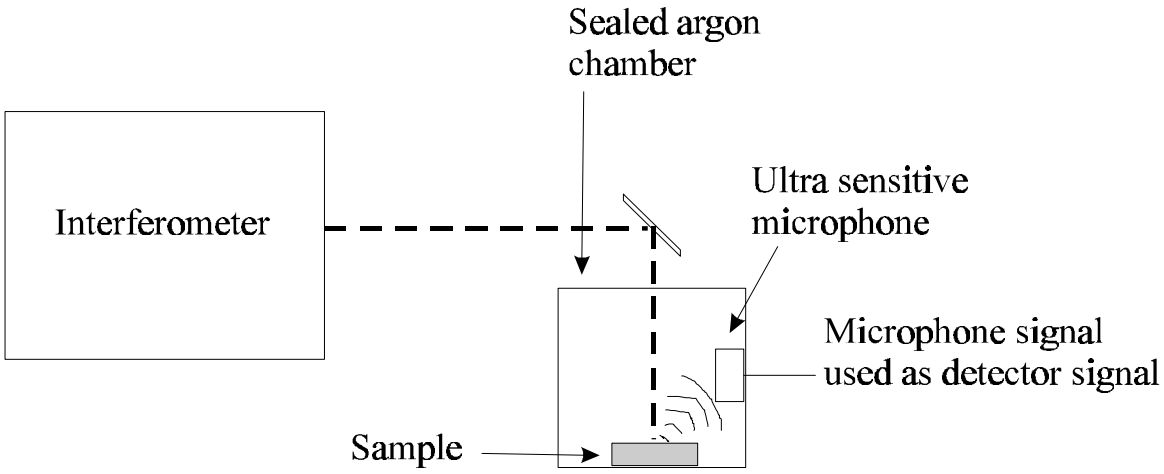

Figure 3.5. Principle of the photoacoustic sampling technique.

Photoacoustic Fourier transformed infrared spectroscopy (PAS): The photoacoustic FTIR technique is a rather unusual form of infrared sampling. The sample is placed in a small cup and inserted into a chamber with a microphone. When the infrared radiation strikes the sample, some of the energy is absorbed by the sample. The sample transfers some of this energy to the surrounding gas, which results in a pressure wave. The pressure wave is detected by an ultra sensitive microphone, amplified and fed to the detector signal of the interferometer. This method is attractive, particularly for analysis of particulate and fibrous materials, because its sample morphology presents no formidable preparation. The problem of this method is a low signal to noise ratio that sets limits to the detectable amount of a surface coating. The gas in the sealed sample chamber called the coupling gas is in this study Argon. An investigation of other noble gases as coupling gases by Koenig (1985) indicates that going from helium to xenon enhances the surface sensitivity of the PAS method.
The background spectrum for this technique is recorded using a sample of carbon black in the PAS chamber.

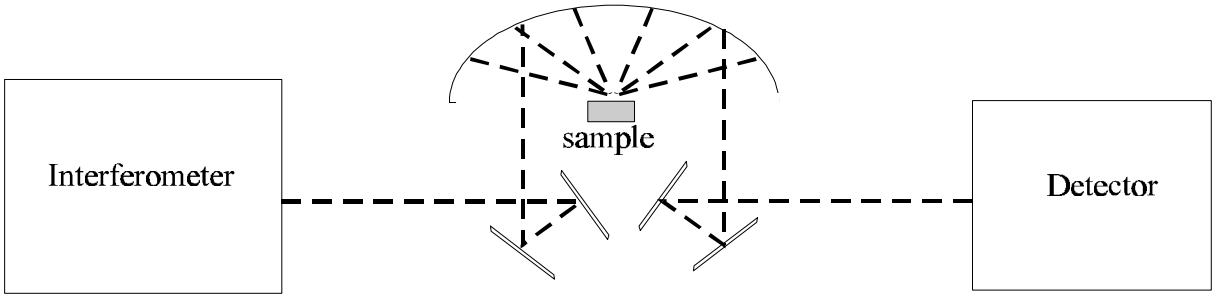

Figure 3.6. Principle of diffuse reflectance FTIR (DRIFT).

Diffuse reflectance FTIR (DRIFT): In a DRIFT experiment the sample material is placed in a small cup under a curved mirror. The infrared radiation is reflected onto the sample at multiple angles. The diffuse reflected radiation from the sample is collected by the curved mirror and guided to the detector. This technique is ideal for FTIR investigations of organic coatings on particulate or fibrous materials because of the surface enhancement originating from multiple reflections on the surface of the particles or fibers. The problem of this technique is the inversion of high absorptivity bands which is caused by the presence of specular reflections from the surface layer of the sample. The background spectra for this technique are recorded using KBr powder in the sample cup. By DRIFT, it is possible to do quantitative determination of silane coupling agents on particles or fibers using the right correction of the spectra (Porro & Pattacini 1992, Boroumand 1994).
The Kubelka-Munk correction (3.2) compensates for the ordinate reflectance non-linearity induced by the diffuse reflection process.

$$(3.2) \qquad R_{km} = \frac{(1 - R_{ob})^2}{2R_{ob}},$$

where R_{ob} is the measured uncorrected reflectance and R_{km} is the corresponding Kubelka-Munk corrected reflectance that has a linear relationship with the chromophore concentration in the sample.

3.3.3 Experimental

All FTIR experiments were conducted using a FT-IR 1760X spectrometer from Perkin Elmer with an internal TGS detector. The default settings used for most experiments were: Resolution 4 cm^{-1}, Scan speed 0,2 cm/s. and number of scans 32. Data processing were done on a computer attached to the spectrometer running the IR Data manager software from Perkin Elmer.

PAS: the photoacoustic experiments were conducted using a Model 200 PAS detector form MTEC Photo Acoustics.

DRIFT: Diffuse reflectance experiments were conducted using a the diffuse reflectance unit "Collector" form Spectra Tech inc.

KBr: Potassium bromide used for pellets for direct transmission and as background material for DRIFT was IR-spectra grade from Fluka.

To compare the different FTIR sampling techniques samples of $Mg(OH)_2$ platelets (from Martinswerk GmbH, Germany) containing an unknown surface coating were analyzed using all three sampling techniques. A number of extraction experiments in different solvents revealed that the particular coating could be removed for the $Mg(OH)_2$ platelets by boiling xylene. The xylene extract was dried under vacuum onto KBr powder, pressed into a pellet and analyzed by direct transmission FTIR for comparison.
A number of DRIFT experiments have been conducted on a particulate glass filler (Schott 8235) treated by different amounts of methacryloxy propyltrimethoxy silane (MPS) at the Danish company "Wolff og Kaaber a/s". The glass filler was treated with a ethanol/water (95/5 % wt.) containing a specific amount of MPS (0.5%,1%,2% and 4% wt.) for 20 min. The solvent and unreacted MPS were removed by evaporation. The filler were then dried at 45°C/9 mm Hg.

In order to test the ability of the block copolymer based silane coupling agents (described in Chapter 2) to covalently bond to inorganic fillers, a $Mg(OH)_2$ filler (Magnifin H5 form Martinswerk) was treated with a 1% wt. solution of the block copolymers in toluene (Romil super pure) for 1 hour. The filler was filtered and washed three times in pure toluene and three times in methanol then dried at 110°C. DRIFT spectra were recorded on the dry powder and compared with a spectrum of a powder undergone the same treatment without the block copolymers.

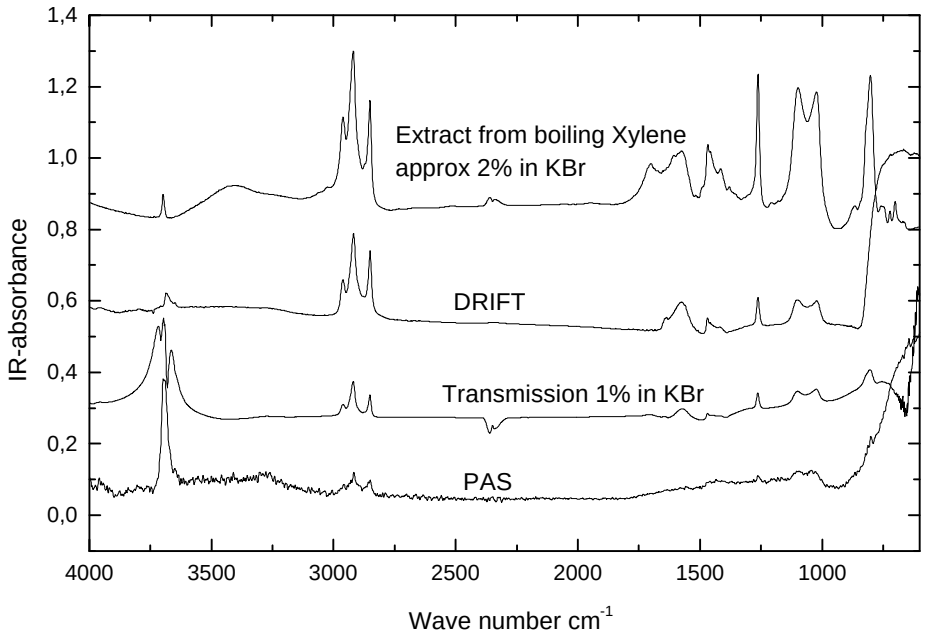

Figure 3.7. FTIR spectra of an unknown surface treatment on $Mg(OH)_2$ using different sampling technices for comparison.

3.3.4 Results and discussion

The differences between the outcome of FTIR analyses using different sampling techniques are illustrated in Figure 3.7. The figure clearly shows the low signal to noise ratio of the photoacoustic technique compared to the others. The Diffuse reflectance spectrum clearly has the largest vibrational contributions from the surface coating of the three spectra recorded on the treated filler. The problem with inversion of high absorbency bands in DRIFT caused by specular reflection can be seen in the DRIFT spectra at the band around 800 cm^{-1}. Being aware of this problem, diffuse reflection is found to be the most sensitive of the three FTIR-sampling techniques for analysis of organic surface coatings on particulate and fibrous inorganic fillers. As illustrated in Figure 3.7 the most sensitive method is to separate the coating from the filler before FTIR analysis. This is seldom possible when the surface modification is properly covalently bonded to the filler surface and, even if it is possible, it implies extensive laboratory work to find the right solvent to extract the surface coating. In conclusion, it was found that the best way to gain insight of the chemical nature of organic coatings on inorganic fillers with FTIR was to use the diffuse reflectance technique.

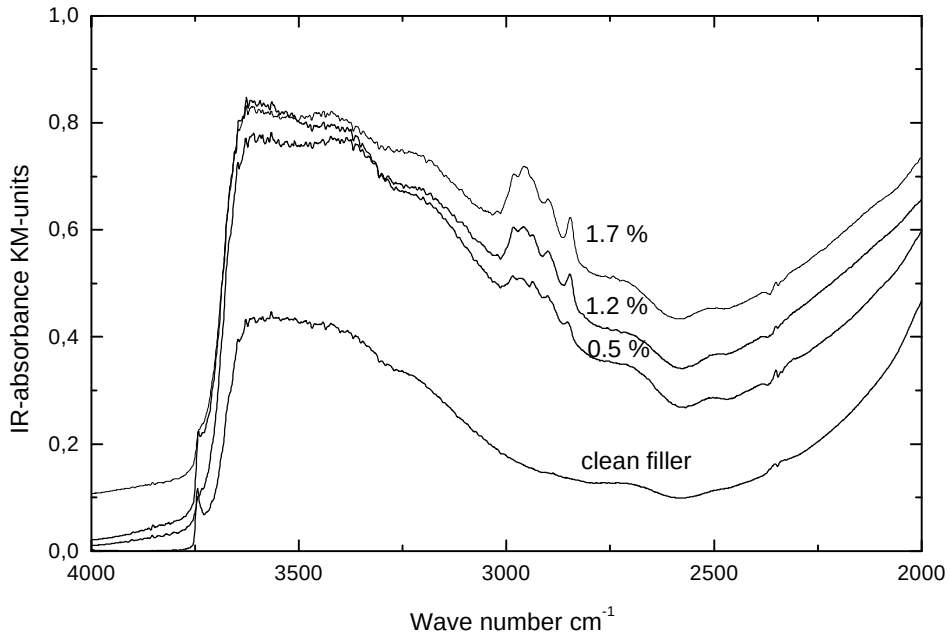

Figure 3.8. DRIFT-spectra of Schott 8335 glass filler treated with varying amount of methacryloxy-propyltrimethoxy silane (MPS). The percent values are weight % calculated on the base of carbon and hydrogen microanalysis.

In search of a simple and fast way to quantify the amount of silane coupling agent on glass fillers DRIFT experiments were conducted on particulate glass fillers treated with ethanol/water solutions containing varying amounts of methacryloxy-propyltrimethoxy silane. The resulting spectra are shown in Figure 3.8. The treated fillers were analysed for carbon and hydrogen content by microanalysis for comparison. Figure 3.8 illustrates the relationship between the absorbance intensities in the range from 2800-3000 cm^{-1} (C-H stretching) and the amount of MPS calculated on the base of microanalysis. The most distinct absorbance band in this area is the band at 2845 cm^{-1} (symmetric CH_2 stretching). Plotting the difference in absorbance at 2845 cm^{-1} between the treated and the untreated fillers ($\Delta\log(1/R_{km})$) results in a straight line as shown in Figure 3.9. The number of data points are too limited to draw conclusions of linearity, but the straight line relationship is in agreement with analogue investigations of vinylsilanes on kaolin clay and aluminum hydroxide done by Porro and Pattachini (1992).

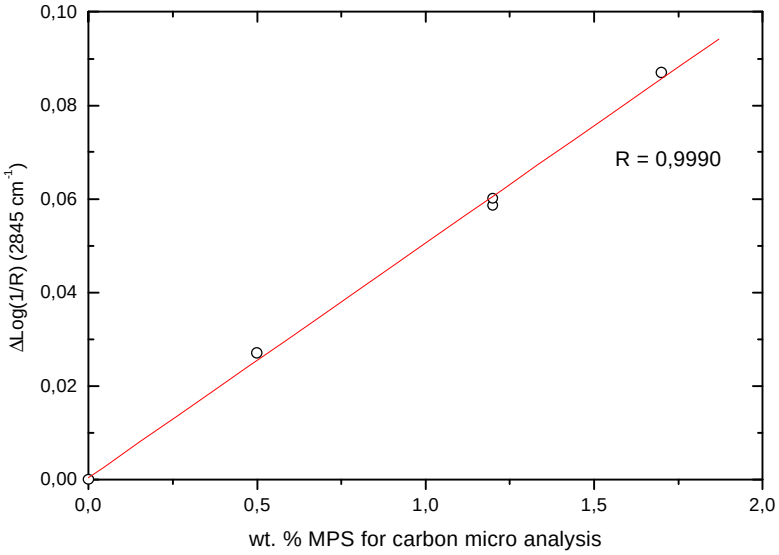

Figure 3.9. Correlation between the Kubelka-Munk corrected absorbance band at 2845 cm^{-1} (symmetric CH_2 stretching) and the wt.% MPS calculated from carbon microanalysis.

An other absorption band of interest is the band at 3747cm^{-1} corresponding to the band of unpertubated surface silanol groups. As shown in Figure 3.10 the number of free surface silanol groups decreases with increasing amount of MPS on the surface as a result of the reaction between MPS and surface silanols.

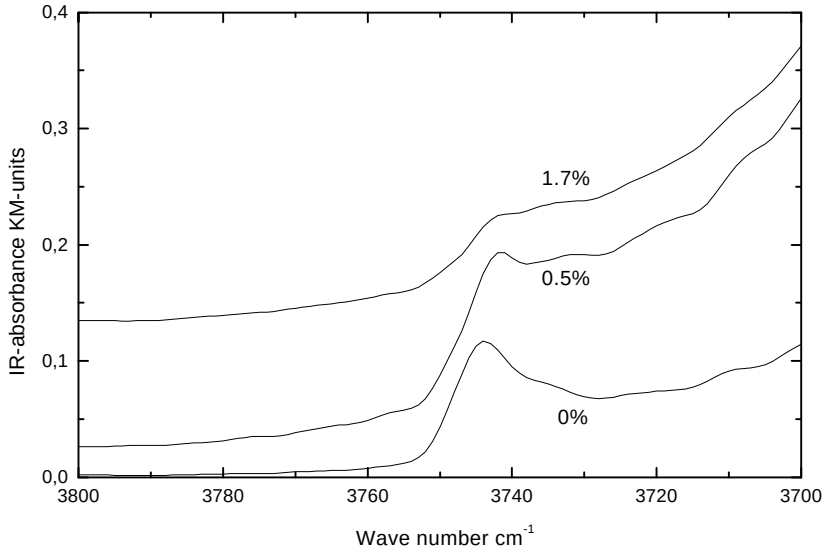

Figure 3.10. DRIFT spectra showing the absorbance band for unpertubated silanol groups on the surface of Schott glass filler treated with various amounts of MPS.

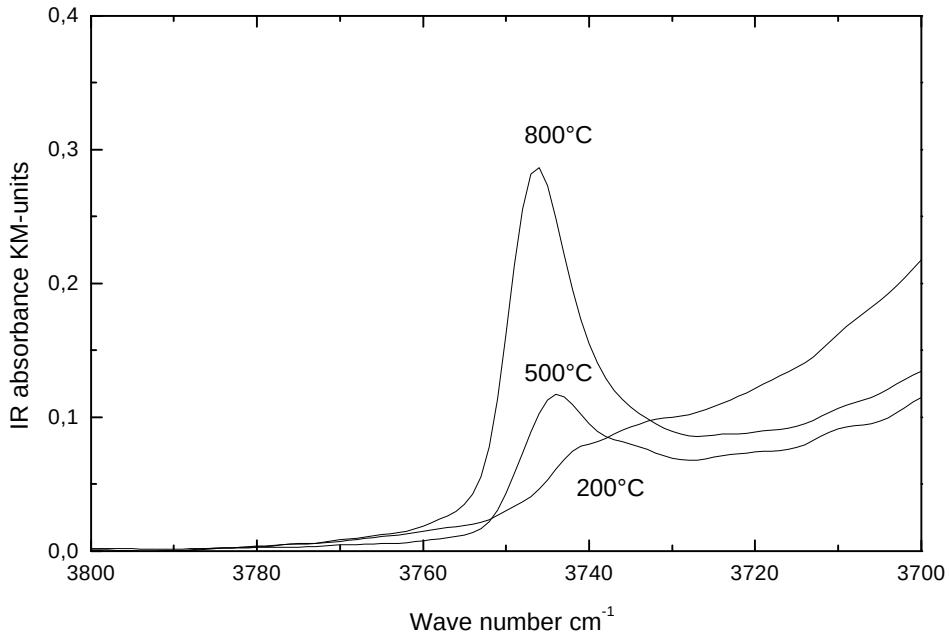

Figure 3.11. DRIFT spectra showing the IR absorbance band for unpertubated silanol groups on the surface of Schott glass fillers treated at various temperatures.

As shown in Figure 3.11 the amount of unpertubated surface silanols is highly dependent on the pre-treatment of the glass filler. The particular fillers show in Figure 3.11 were pre-treated in 1M HNO_3 in a ultrasonic bath to increase the specific surface area form ~10 to ~19 m^2/g, then washed with water and dried at various temperatures. According to Piers & Rochester (1995) and Ying et al. (1993) the increasing absorption of the band at 3747cm^{-1} by raising temperature is caused by the removal of surface water and organic contaminations capable of hydrogen bonding to the surface silanols. The band can be used as a direct indicator for reactions between silanes and surface silanols but only if the surface is dried at sufficiently high temperature to remove all surface water. Piers & Rochester (1995) have done this in a study of the reaction between trimethylmethoxysilane and silicagel preheated at 900K. The Schott glass filler in Figures 3.9 & 3.10 was dried at 500°C prior to silane treatment. This is obviously not a high enough temperature to remove all water from the surface.

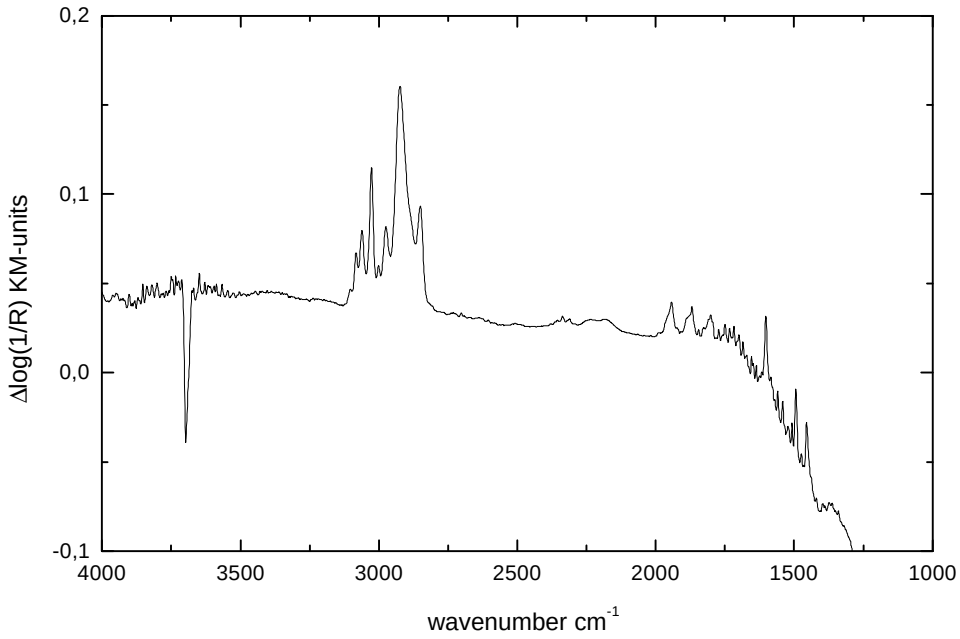

Figure 3.12. DRIFT spectrum of a block copolymer silane coupling agent (sPB-PS 30k) on $Mg(OH)_2$ filler (Magnifin H5 form Martinswerk).

A difference DRIFT spectrum of a PS-silylatede PB block copolymer on $Mg(OH)_2$ is shown in Figure 3.12. The spectrum shows a positive absorbance pattern that is equal to the absorbance pattern of atactic polystyrene which shows that the block copolymer stays on the surface of the filler during washing with toluene. Furthermore, the spectrum contains a negative absorption band around 3700 cm^{-1} corresponding to Mg-OH stretching. This negative band can be interpreted as an indication of interaction between the block copolymer and Mg-OH groups on the surface. A more simple way of testing the surface treatment is to put the treated powder in water. The untreated $Mg(OH)_2$ powder is easily dispersed in water and because of the density difference the powder will slowly sedimentate. The treated powders are completely imiscible with water and the powder forms a dry layer on top of the water indicating successful surface modification.

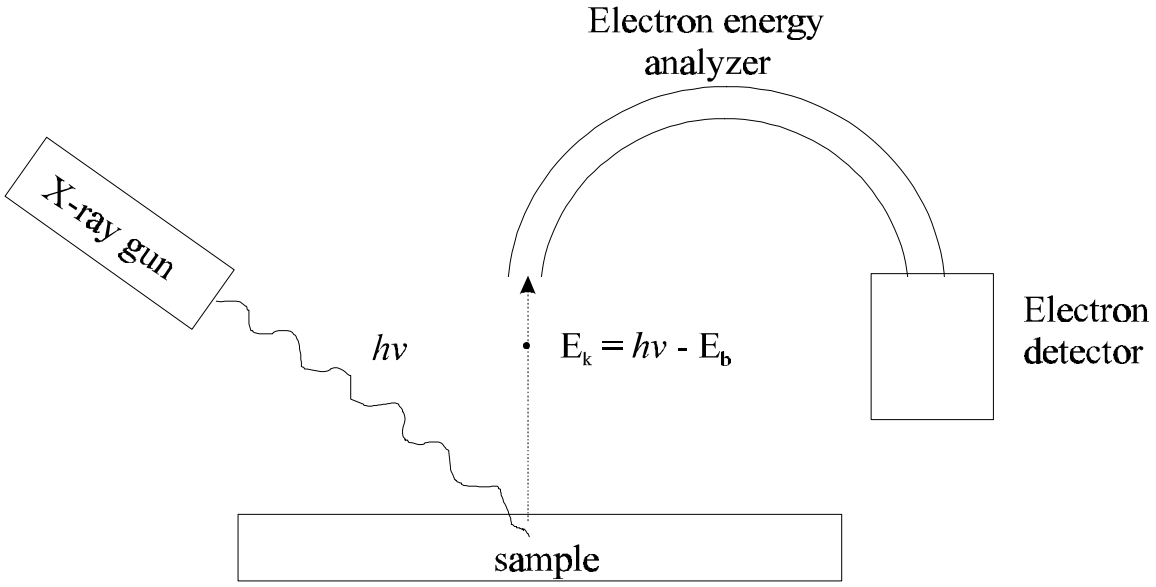

Figure 3.13. Principle of X-ray photoelectron spectroscopy (XPS)

3.4 X-ray photoelectron spectroscopy (XPS)

The principle of X-ray photoelectron spectroscopy is to radiate the sample with monochromatic X-ray radiation with known frequency (v) and hence a known photon energy (hv). The energy of the incident photon has to be sufficiently high to eject electrons from the inner cores of the atoms in the sample. The kinetic energy (E_k) of the photoelectron generated is then the difference between the photon energy and the binding energy (E_b) of the ejected electron as expressed in Figure 3.13. Each element has its own set of characteristic binding energies, which makes element identification possible based on determinations of the observed binding energies.
The XPS technique is very surface sensitive. Although photoelectrons is generated in a thick surface layer only the photoelectrons generated in the very top layers of the surface can escape to the detector. The reason is the very short inelastic mean free path (IMFP or λ) for the photoelectrons in solid matter. The IMFP is defined as the distance that an electron will travel before it suffers an inelastic collision with a nucleus in a solid. Inelastic meaning a collision that causes the electron to loose kinetic energy. Only 37 % (1/e) of the electrons ejected in the depth of 1λ will reach the surface with their characteristic kinetic energy and from a dept of 5λ only 0.7 % ($1/e^5$) of the electrons will reach the surface unchanged. The generated photoelectrons in XPS have typical kinetic energies for 50 to 2000 eV corresponding to λ values from 0.5 to 3 nm. This means that 99.3% of the information in the characteristic binding energy peeks originates from the top 25-150 Å of the sample.
Photoelectrons also experience inelastic collisions with atoms in the gas phase, therefore XPS experiments have to be conducted in ultra high vacuum.

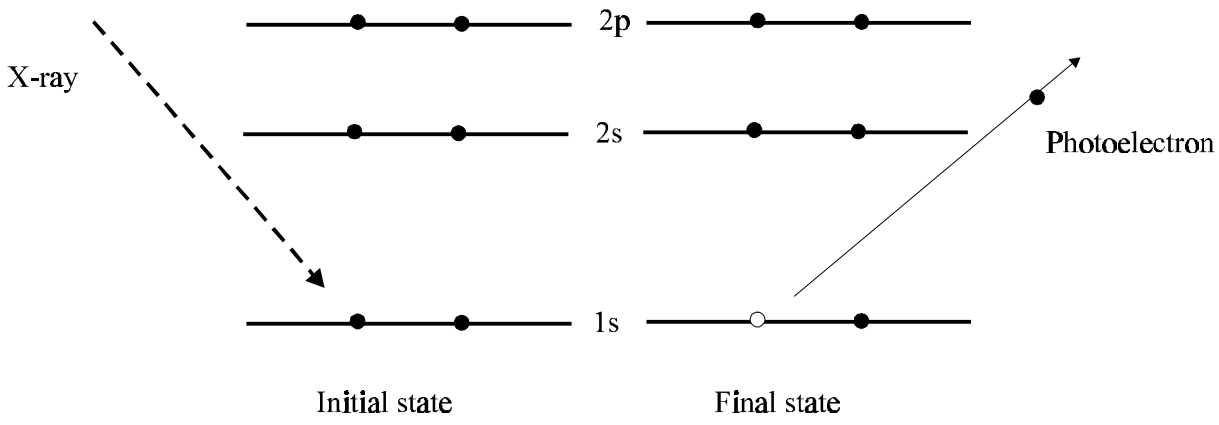

Figure 3.14. Energy level diagram for the production of a 1*s* photoemission electron from a carbon atom.

The energy conservation relationship for XPS is given by (3.3)

(3.3) $$E_i(N) + h\nu = E_f(N-1,k) + E_{KE}$$

where $E_i(N)$ is the total initial energy of the atom, $E_f(N\text{-}1,k)$ is the total final energy after an electron with a kinetic energy E_{KE} has been emitted form the *k*th level of the atom and N is the total number of electrons in the atom. The binding energy of the emitted electron from the *k*th level , $E_{BE}(k)$ is given by (3.4).

(3.4) $$E_{BE}(k) = E_f(N-1,k) - E_i(N)$$

The binding energy does not only depend on the state of the emitted electron but on the state of all electrons in the atom including bonding electrons. This means that the binding energy depend on the atomic environment of the element in question. For example, the observed binding energies for the C 1s peeks in $-(CF_2\text{-}CH_2)_n-$ [poly(vinylidene flouride)], are 292 and 286 eV for the CF_2 and CH_2 groups respectively. Moreover the CH_2 peek is shifted by about 1.5 eV higher in binding energy in comparison to the CH_2 group in $-(CH_2\text{-}CH_2)_n-$ [polyethylene] (Turner 1993).
Changes in the binding energies for different oxidation states in the same sample are illustrated in the Si 2*p* peak in chemical oxidized silicon wafer. The observed binding energies are 103.5 and 99.6 for SiO_x and Si-Si respectively. This phenomenon is often called chemical shift. XPS photoelectron binding energies for all detectable elements in a range form 1200 to 0 eV with a variety of different chemical environments are tabulated by Moulder et al. (1992).

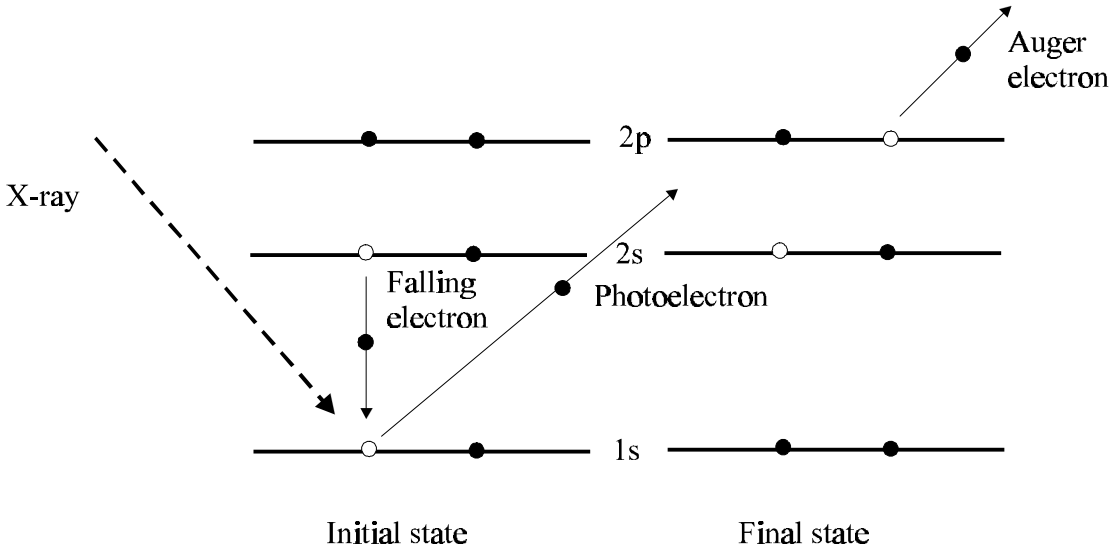

Figure 3.15. Energy level diagram for the production of a *KLL* Auger electron from a carbon atom.

When an atom has lost a core level electron one way of relaxing is that an electron from a higher energy level fall to fill the induced hole. This process induces enough energy to emit an electron for a higher energy level. This is called an Auger process and the ejected electron is called an Auger electron. As the X-ray energy in XPS always are large enough to generate core level electron hole XPS spectra often contain Auger Peaks. The kinetic energy of an Auger electron is given by (3.5).

(3.5) $$E_{KE}(jkl) = E_{BE}(j) - E_{BE}(k) - E_{BE}(l) - U$$

where $E_{BE}(j)$ is the binding energy of the photoelectron that is ejected from the initial ionization event; $E_{BE}(k)$ is the binding energy of the electron that falls into the empty hole; $E_{BE}(l)$ is the binding energy of the ejected Auger electron; and U is the hole –hole repulsion energy between the final state electron holes. (3.5) shows that the kinetic energy of the Auger electron does not depend on the X-ray energy like the kinetic energy of the photoelectrons. That means that the Auger peaks are identified by their kinetic energy and not by their binding energy. When presented as binding energy in a XPS spectra the Auger peak positions is dependent on the X-ray energy used. Auger peak positions is tabulated for the most common used X-ray sources in XPS by Moulder et al. (1992).

XPS does not only give the possibility to identify elements and give insight in their chemical environment but also give the ability to quantitatively measure the abundance of the elements. The intensity of a photoelectron peek $N(E)$ at a given kinetic energy is a function (F) of several factors as indicated in (3.6).

(3.6) $$N(E) = F(f, d, s, q, l, T, E_{KE}, D)$$

f is the X-ray flux, *d* is the number density of the element that is producing the photoelectron in the analysis volume, *s* is the photoelectron cross section (or sensitivity factor) for the particular transition being considered, *q* is the solid angle from which the energy analyzer accepts electrons, *l* is the loss function for emitted electrons, that is, electrons that are emitted in the analysis volume, but suffers some energy loss before leaving the solid, *T* is the transmission efficiency of the analyzer as a function of electron kinetics energy, and *D* is the electron detector efficiency , which may also be a function of the electron kinetic energy. It is readily apparent that the intensity of a photoelectron peak is dependent on several different and independent factors. But some of the factors and functions in (3.6) are specific for the apparatus used and even more factors are constant during a single experiment, so there are not any practical use for a full analytical description of the function in (3.6).
In practice the quantification is done by integrating a specific peak for all detectable elements in the sample correcting the areas for instrumental factors and dividing with relative photoelectron cross sections for each peak to give the relative concentrations of elements. The photoelectron cross sections for all of the peaks that can be observed by either Mg or Al anode X-ray have been computed by Scofield and referenced to the C 1s level which has an assigned value of 1.000.

3.4.1. Experimental

XPS experiments were performed with a SpecsLab Sage 100 Instrument. Spectra were acquired from a 1 × 2 mm^2 sample region illuminated by a Mg K_α X-ray source operated at 100W. The pressure in the analysis chamber was < 10^{-7} mbar during measurements. All experiments were done with 90° angle between sample and electron analyzer.
Model flat surface samples was prepared from clean Silicon [100] wafers divided in to pieces with dimension around 15 × 15 mm by making a 1-2 mm trace on the surface at the edge of the wafer with a diamond cutter. Then the wafers were broke on top of a 0.5 mm diameter metal wire. The pieces of silicon wafer were oxidized in a 10:1 by volume solution of 70% H_2SO_4 and 30% H_2O_2 at 120°C in 15 min. This treatment with a mixture of concentrated sulfuric acid and hydrogen peroxide is often referred to as *Piranha treatment* because of the strong etching and oxidizing properties. After piranha treatment the samples were washed 3 times in pure water and dried in a stream of dry nitrogen. Immediately after drying the oxidized wafers were placed in 1 wt. % solutions of silane coupling agents in toluene in closed 250 ml containers. The samples were treated with n-propyl-trimethoxysilane (98% pure P0810 form ABCR, Germany), γ-aminopropyl-trimethoxysilane (98% pure A0800 form ABCR, Germany) and the six block copolymer silanes described in chapter 2. That is triethoxysilane treated polybutadiene (sPB)-polystyrene (PS) or polydimethylsiloxane (PDMS) diblock copolymers. The molecular masses of the PS and PDMS blocks synthesized to be 10, 30 and 100 kg/mole.

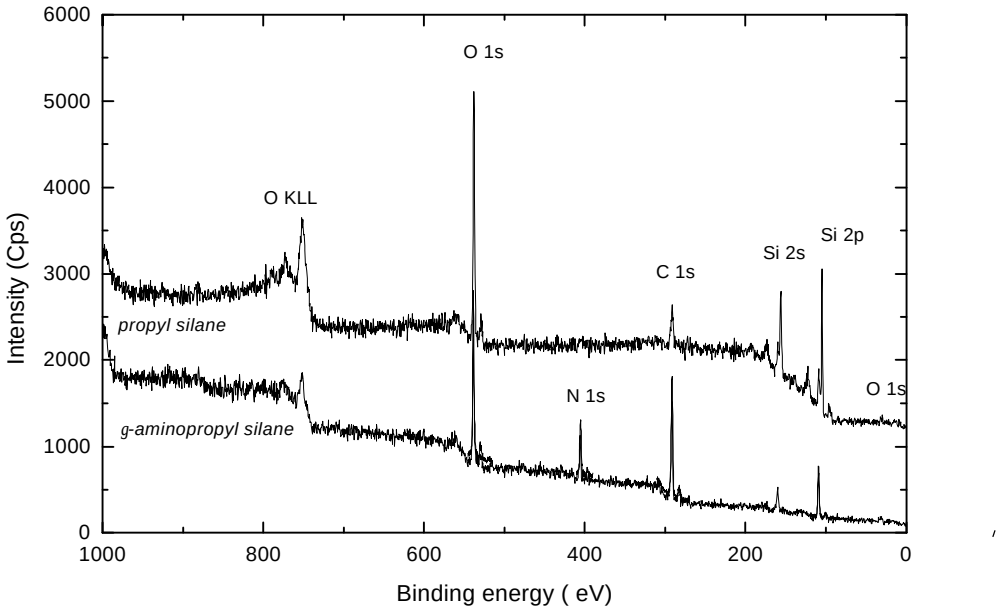

Figure 3.16. XPS wide range survey scans on piranha etched silicon wafers treated with 1 wt. % solutions of γ-aminopropyl-trimethoysilane and n-propyl-trimethoxysilane in toluene.

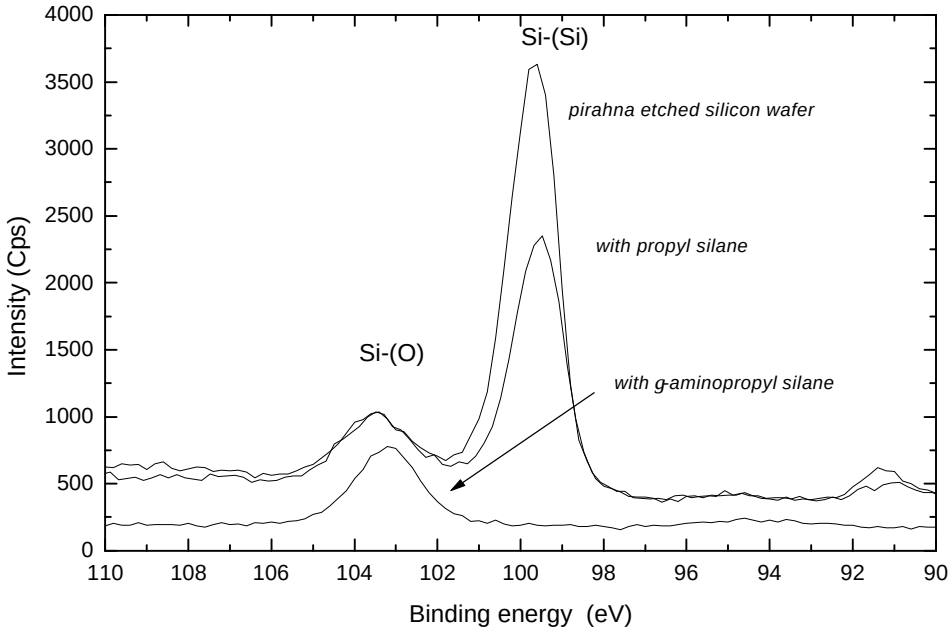

Figure 3.17. XPS detail scan of the Si 2p region of piranha etched silicon with no treatment and treated with 1% wt solutions of γ-APTMS and PTMS in toluene.

3.4.2 Results and discussion

The wide range XPS-scans of n-PTMS and γ-APTMS on piranha treated silicon wafer in Figure 3.16 shows typical examples of the kind of results obtained by XPS analysis. There are obvious differences between the spectra. Beyond the presence of the nitrogen 1s peak differences in intensities are observed for the oxygen, carbon and silicon peaks. The detailed spectra for the silicon 2p photoelectron binding energies (Figure 3.17) reveal a basic difference between n-PTMS and γ-APTMS applied from toluene. The binding energies for silicon 2p photoelectrons are as mentioned before dependent on the chemical environments of the silicon atoms. The Si 2p binding energies are 99.7 eV for Si in Silicon [100] wafers, 103.6 eV in SiO_2 and 102-103 eV for silanes and siloxanes according to Moulder et al. (1992). The Si 2p peaks from the untreated oxidized wafer shows high intensity peak at 99,7 eV originating from the silicon [100] wafer bulk phase, and a broader lower intensity peak with a maximum at 103.6 eV. originating form the oxide layer generated by piranha treatment. The oxide layer generated by piranha treatment is usually denoted as a SiO_x over-layer, because not all silicon atoms are tetra-coordinated with oxygen like in SiO_2. This give rise to broader peaks in the silicon-oxide region. The Si 2p peaks for piranha treated silicon wafer shows that the oxide layer on the surface are considerable thinner than the photon electron escape depth, which is 50-200 Å in this kinetic energy range depending on the effective absorption cross section of the surface layers. The thickness of SiO_2 layer on silicon wafers made by piranha etch measured by ellipsometry have been reported to be 10-20 Å. (Wasserman et al. 1989 & Rühe et al 1993). Applying n-PTMS from toluene results in a reduction of the intensity form the bulk Si [100] signal corresponding to a total layer thickness smaller than the photoelectron escape depth. But applying γ-APTMS from toluene completely eliminates the Si 2p signal from the bulk Si [100] and the position of the observed Si 2p correspond to the signal for silicon in silanes or siloxanes. This shows the influence on the solvent used to apply silane to a surface. The polarity of γ-APTMS is very different from that of n-PTMS and of toluene. Toluene is not a good solvent for γ-APTMS resulting in precipitation on the oxidized silicon surface, and the precipitated layer is not removed by washing in toluene. Toluene is a better solvent for n-PTMS so that only the bonded molecules are left on the surface after washing. Another very important factor is the ability of γ-APTMS to form hydrogen bonds with itself and thereby form a hydrogen bond stabilized network on the surface. The atomic distribution measured on the γ-APTMS layer in Table 3.3 corresponds to approx. C_4O_2SiN corresponding to a structure were one methoxy group is left on each silane molecule and each silane molecule has reacted with a neighboring silane molecule through a siloxane bond. More work has to be done to verify this structure but such a structure could explain the extensive layer observed here.

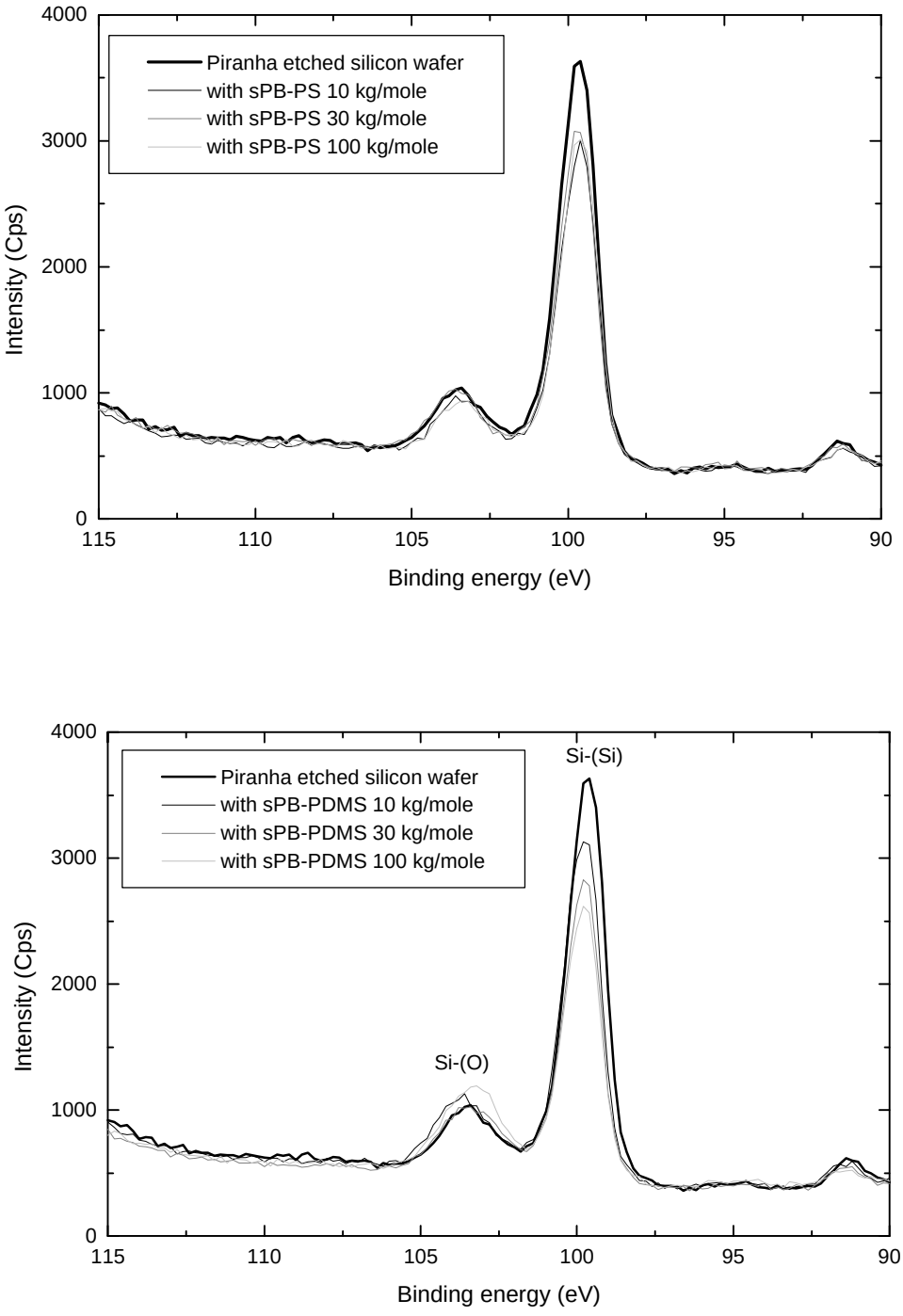

Figure 3.18 XPS detail scan of the Si 2*p* region of piranha etched silicon with no treatment and treated with 1% wt solutions of silylated polybutadiene-polystyrene block copolymers (*upper*) and silylated polybutadiene-polydimethylsiloxane block copolymers (*lower*) in toluene.

The Si 2*p* region for block copolymer silane coupling agents Figure 3.18 show the same reduction of the peak at 99.6 eV originating form bulk silicon as a result of surface covering by the block copolymers. But Figure 3.18 also reveals a difference between the two types of block copolymers. For the block copolymer containing polystyrene ends, the reduction of the bulk silicon signal is independent of the molecular mass of the polystyrene ends. This indicates that the effective thickness of the layer formed is independent of the molecular mass of the polystyrene ends. For the block copolymers containing polydimethylsiloxane ends, the reduction of the bulk silicon signal increases with increased molecular mass of the PDMS ends. This indicates that the effective thickness of the formed layers increases with increased molecular mass of the PDMS chains. This observation reveals a fundamental difference in the way the two types of block copolymers form layers on SiO_2. The quantification of elements in the surface measured by XPS shown in Table 3.3 substantiates the observations of bulk silicon reduction. For the polystyrene system the carbon concentration in the measured surface layer is independent (with in the error of the method) of the molecurlar mass, while for the PDMS system the carbon concentration increases with increased molecular mass. The results for the "clean" Si/SiO_x sample shows that the high energy surface from the piranha treatment is very easily contaminated under ambient conditions.

Table 3.3 XPS qualification of block copolymer and other silanes on oxidized silicon wafers

Sample name	C	O	Si_{total}	Si (O)	Si (Si)	N
	atom %	atom %	atom %	atom %	atom %	atom %
Si/SIO_x	6,2	32,5	61,4	9,9	51,5	
sPB-PS 10k	26,8	26,7	46,4	7,9	38,5	
sPB-PS 30k	28,0	26,2	45,8	8,6	37,2	
sPB-PS 100k	28,5	24,2	47,4	7,9	39,5	
sPB-PDMS 10k	13,6	32,6	53,8	12,2	41,6	
sPB-PDMS 30k	16,4	31,7	52,0	13,9	38,1	
sPB-PDMS 100k	27,0	28,0	45,0	14,5	30,5	
PTMS	21,2	36,9	41,9	12,0	30,0	
APS	48,4	24,5	14,9	14,9	0,0	12,2

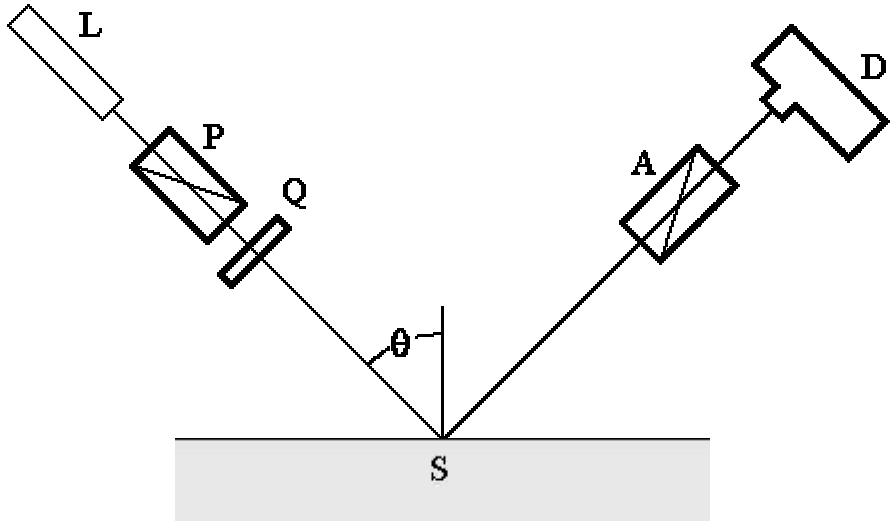

Figure 3.19. Schematic diagram of a ellipsometer. **L** is the light source; **P** is the polarizing prism; **Q** the quarter-wave plate compensator; **S** is the sample under study; **A** is the analyzer prism and **D** is the light detector, that in the actual case contains a spectrometer.

3.5 Ellipsometry

Ellipsometry is a sensitive optical technique for determining properties of surfaces and thin films. If linearly polarized light of a known orientation is reflected at oblique incidence from a surface then the reflected light is elliptically polarized. The shape and orientation of the ellipse depend on the angle of incidence, the direction of the polarization of the incident light, and the reflection properties of the surface. We can measure the polarization of the reflected light with a quarter-wave plate followed by an analyzer; the orientations of the quarter-wave plate and the analyzer are varied until no light passes though the analyzer. From these orientations and the direction of polarization of the incident light we can calculate the relative phase change $\cos(\Delta)$ and the relative amplitude change $\tan(\psi)$ introduced by reflection from the surface.
An ellipsometer measures the changes in the polarization state of light when it is reflected from a sample. If the sample undergoes a change, for example a thin film on the surface changes its thickness, then its reflection properties will also change. Measuring these changes in the reflection properties can allow us to deduce the actual change in the film's thickness.
The most important application of ellipsometry is to study thin films. In the context of ellipsometry a thin film is one that ranges from essentially zero thickness to several thousand

Angstroms, although this range can be extended in some cases. If a film is thin enough that it shows an interference color then it will probably be a good ellipsometric sample. The sensitivity of an ellipsometer is such that a change in film thickness of a few Angstroms is usually easy to detect.

The complex description of the difference between the incoming and the reflected polarized light (r) is given in (3.7)

(3.7) $$r = \tan(y)e^{i\Delta},$$

where $\tan(y)$ is the chance in amplitude and *D* is the chance in phase. These two parameters are the output of an ellipsometry measurement and can be interpreted into layer thickness provided the right model for the surface. In order to interpret the ellipsometry data into layer thickness it is necessary to know or assume values for the refractive index (n) for each separate layer on the surface.

3.5.1 Experimental

All ellipsometry measurements were carried out using a Sobra^{TM} spectroscopic ellipsometer ES4G at Center for Interfacial Engineering (CIE), University of Minnesota (UM), Minneapolis. The instrument is capable of making ellipsometry measurement at various wavelengths. All measurements were carried out using an angle of incidence of 75°.
The samples for ellipsometry are the same as for XPS-analysis: Silicon [100] wafers Piranha treated at 120°C for 15 min washed and dried, then emerged in 1% solutions of block copolymers silanes in toluene for 1 hour at r.t., then washed three times in toluene and three times in methanol. All sample preparation were carried out in dust free environments in clean room facility at the micro electronics center, UM.

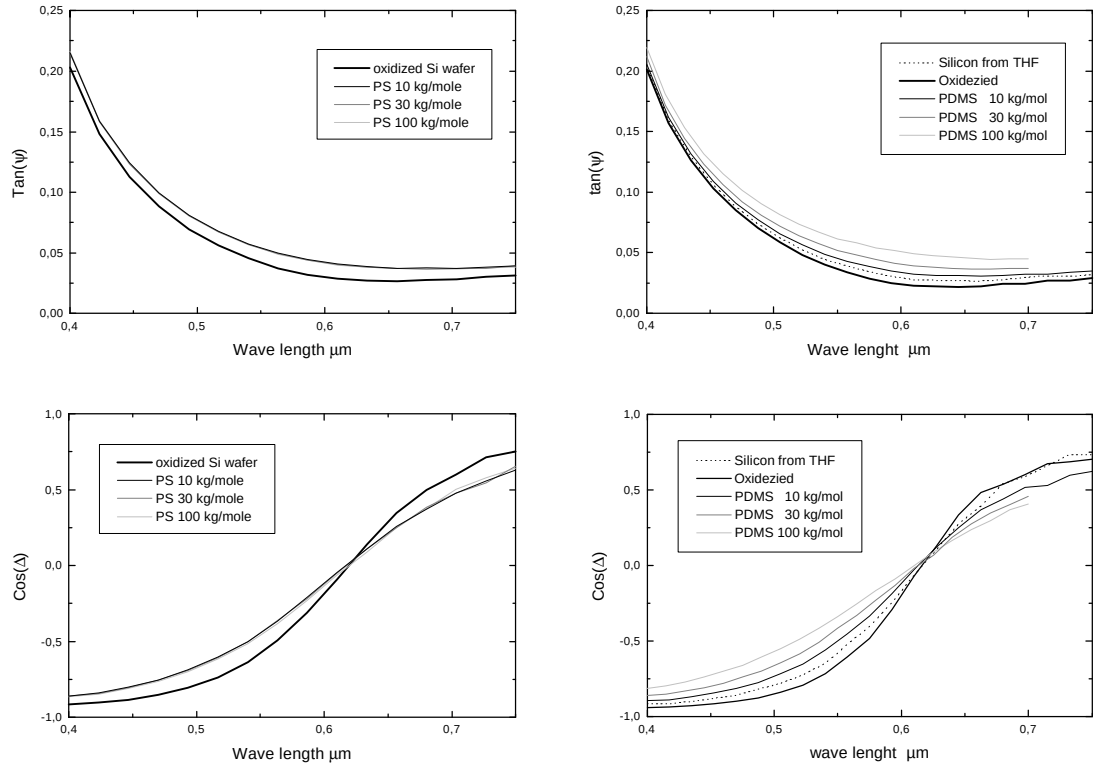

Figure 3.20 Amplitude change tan(ψ) and phase change cos(Δ) as functions of wave length for Si/SiO_2 treated with block copolymer silanes. Measured by ellipsometry

3.5.2 Results and discussion

The measured values for amplitude and phase change as a function of wavelength is shown in Figure 3.20. It is obvious that the optical properties of the surface change when the surface is treated with silylated block copolymers. For the polystyrene system the change in optical properties appear to be independent of the molecular mass of the polystyrene chains. For the polydimethylsiloxsane system the change in optical properties appear to increase with growing molecular mass of the PDMS chains. This observation is in full agreement with the XPS analysis of the same samples. Calculations of layer thickness from the ellipsometry data gave very consistent values of 17±1 Å for the SiO_2 layer on Si using a one over-layer model and standard values for the reflective indexes. But the computer program used could not calculate the layer thickness of the organic layer on top of the SiO_2 by using a two over-layer model. The program could not fit the data to a two over layer model with fixed refractive indexes. This could be because the refractive index of the polymer over-layer varies with distance from the surface as should be expected for a surface selective block copolymer. The program used could not calculate multilayer models. Instead the layer thickness was calculated by a one over-layer model not distinguishing between the SiO_2 and block copolymer layers. The thickness of the polymer layer is then calculated by subtracting the thickness of the SiO_2 layer. The results are listed in Table 3.4.

Table 3.4. Layer thickness measurements by ellipsometry using a one over-layer model not discriminating SiO_2 and block copolymer over-layers.

Sample	Layer thickness (Å)	Polymer layer (Å)
Clean Si/SiO_2	17	-
sPB-PS 10k	35	18
sPB-PS 30k	35	18
sPB-PS 100k	40	23
sPB-PDMS 10k	24	7
sPB-PDMS 30k	34	17
sPB-PDMS 100k	45	28

The values calculated by using the one over-layer model show the same trend as the raw ellipsometry data. The values are not exact due to the calculation method but the order of magnitude is in agreement with the XPS results. A plot of the calculated layer thickness as a function of $M^{1/2}$, where M is the dimensionless molar mass of the end chains with respect to the molar mass of hydrogen is shown in Figure 3.21. The layer thickness of the PDMS system is dependant on the molar mass of the end block while this is not the case for the PS-system. The reason for plotting the layer thickness as function of $M^{1/2}$ and not M is that the radius of gyration (R_g) for a polymer chain in (near) theta solvent can be expressed as in (3.8)

(3.8) $$R_g = aM^{1/2},$$

where *a* is constant specific for each polymer system. Values for a number of common polymer solvent systems are listed by Fleer et al. (1993) p.463.
The ellipsometry and XPS data indicates that the thickness of the collapsed layer is dependant on the radius of gyration of the polymer chain in the solvent for the PDMS system while this does not appear to be the case for the PS system.

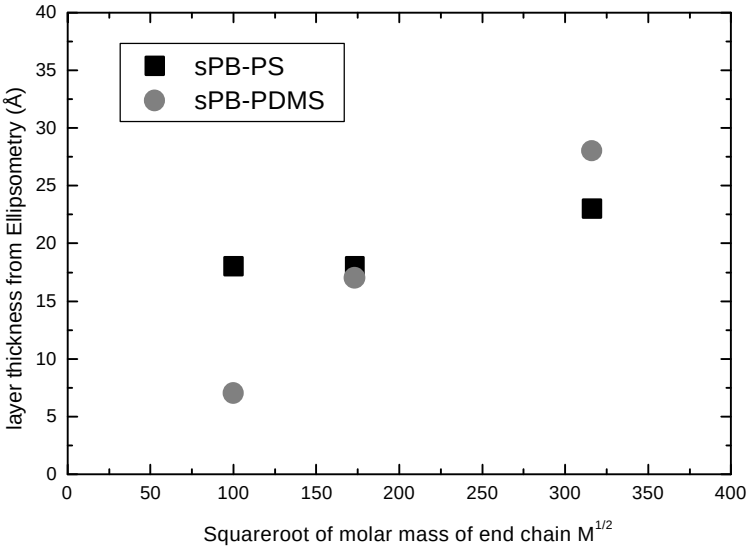

Figure 3.21 Layer thickness calculated for ellipsometry data by a one over-layer model as a function of the square-root molar mass of the end chain.

The thickness of the collapsed layer is determined by the block copolymer structure in the solvent at the end of the surface treatment. The polymer-solvent interaction parameter (χ) for the homopolymers and toluene at 20°C are 0.40 and 0.50 for PS and PDMS respectively (Fleer et al. 1993). Toluene being a θ-solvent for PDMS and better than θ-solvent for PS at room temperature. This difference in solvency is not sufficient to explain the difference in absorption behavior. The surface tensions of the homo-polymers, the solvent and the surface are listed in Table 3.5. with decreasing surface tensions. The surface tension of toluene has a value between those of PS and PDMS.

Table 3.5 Surface tensions at 25°C *from* Wu (1982)

Material	Surface tension (mJ/m^2)
SiO_2	~ 400
PS	40.5
Toluene	28.5
PDMS	19.5

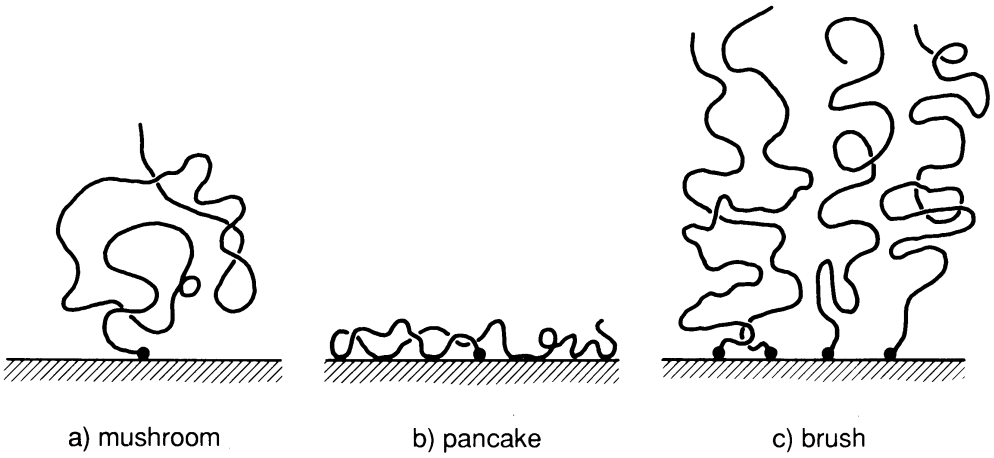

Figure 3.22. Schematic representation of the possible structures of terminally attached polymer chains from (Fleer *et al.* 1993)

For homopolymers in toluene solution on SiO_2 polystyrene will have a strong affinity to absorb on the interface between SiO_2 and toluene while PDMS rather will absorb at the toluene/air interface. This difference, that PS/toluene/SiO_2 is an absorbing system while PDMS/toluene/SiO_2 is not, can account for the major difference in absorption behavior for the two systems. The possible structures of terminally attached polymer chains are schematically drawn in Figure 3.22. Generally speaking the mushroom structure is characteristic for non-absorbing systems, while the pancake structure is characteristic for absorbing systems. The brush structure becomes relevant when the grafting density on the surface becomes so high that the chains overlap causing a stretch of the polymer chains. The brush case is not relevant in this specific case considering the size of the anchoring block.

Considering that the PS/toluene/SiO_2 is an absorbing system forming a pancake like structure on the surface, increasing the molecular mass of the PS chain, will decrease the grafting density on the surface and not effect the layer thickness of the collapsed layer very mush. For the PDMS/toluene/SiO_2 system being non-absorbing forming a mushroom like structure increase of the molecular mass of the PDMS will result in increase in the layer thickness of the collapsed layer. Small angle neutron scattering data of silane terminated deuterated polystyrene grafted onto silica from toluene were fitted by various pre-assumed profiles by Cosgrove et al. (1994). The result of this investigation was that the best fit to the data was an exponential profile corresponding to a pancake like structure. Exchanging toluene with dimethyl formamide (DMF), which have a surface tension at 25° around 58 mJ/m^2 changes the system to nonabsorbing. The surface profile PS grafted from DMF is best fitted with Gaussian profile indicating a mushroom like structure.

The choice of solvent in connection with surface grafting of polymer is essential for the grafting density and the thickness of the resulting layer. Toluene is not the best choice for grafting PS chains onto SiO_2 and it should be considered to exchange the solvent for further experiments with PS containing silane coupling agents.

3.6 Atomic force microscopy (AFM)

Both XPS and ellipsometry suffers from the same lack of lateral surface resolution. In these methods the information is averaged over an area that is much larger than the lateral extension of a single block copolymer molecule. The new improved methods in atomic force microscopy seam promising in order to resolve the lateral distribution of polymer chains on a flat model surface.

The principle of atomic force microscopy is illustrated in Figure 3.23. The tip is brought very close to the surface until a preset deflection of the tip is reached. The deflection of the tip is measured by a laser beam reflected on the cantilever just above the tip. A circular laser detector divided into four quadrant sections, detects the reflected laser beam. The deflection of the tip is measured by the difference in intensity between upper two and the lower two quadrants of the laser detector. While scanning in the X and Y directions a feedback system from the laser detector to the Z-direction piezo-transducer keeps the deflection of the tip on the preset value. The X,Y and Z positions of the piezo-transducer is recorded to form a topographic picture of the surface of the sample.

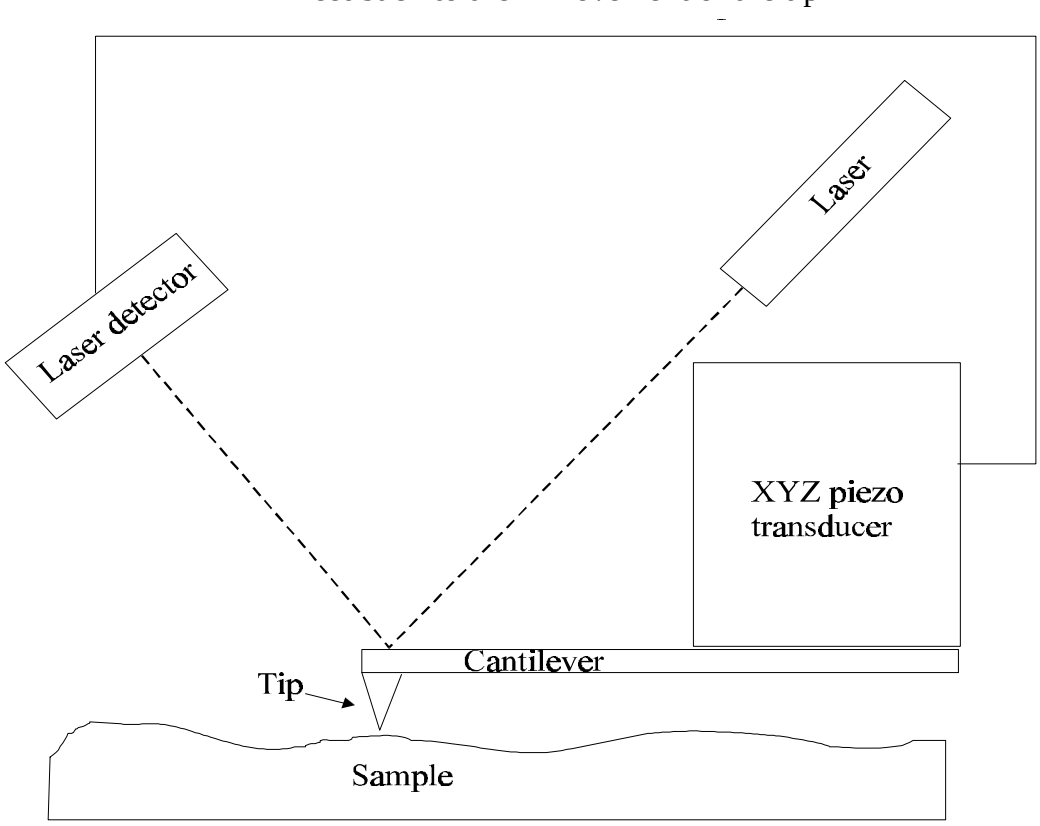

Figure 3.23 Principle of atomic force microscopy (AFM)

The AFM used here has two basic modes of operation: Contact mode and tapping mode. Contact mode is the original way the first atomic force microscopes were operated. The tip is brought so close to the surface that a preset value of deflection is reached.
The deflection of the cantilever depends on the force between the tip and the sample surface on the spring constant of the cantilever. The deflection of the cantilever can be adjusted during scanning adjusting the operational force between the tip and the surface. The operational force in contact mode AFM varies from one to several hundred nanonewtons.
The image formations can be done in two different ways in contact mode AFM. By recording the z-position at constant deflection (force) resulting in a topographic picture of the surface. As mentioned before the photo detector is divided into four quadrants making it possible to detect the lateral deflection of the cantilever as it scans the surface. This can be utilized in analysis of apparently flat samples containing domains with different friction to the tip. This technique is referred to as friction mode or lateral force microscopy. Contact mode is excellent for investigations of hard solid surfaces but the force between the tip and surface is often sufficiently high to disorder soft material on the surface during scanning by inelastic deformation.

To overcome the limitations of the contact mode in studying soft materials, modulation techniques have been developed. In these methods either the cantilever is vibrated at its resonance or the vertical sample position is modulated. The tip-sample force interaction causes a change in the amplitude, the phase and the resonance frequency of the vibrating cantilever. Tapping mode is a modulation mode where the tip is vertically oscillated at its resonance frequency. When the sample approaches the vibrating tip, they come into intermittent contact, thereby lowering the vibrational frequency as detected by the reflected laser beam at the photo detector. The amplitude drop is used as feed back to the z-direction. By tapping instead of constant contact, the tip sample lateral force is greatly reduced and the short tip-sample contact time prevents inelastic surface modification. Topographic images of the surface are recorded at a preset amplitude drops value. Tapping mode also gives the possibility to image the phase shift between the driven and the actual oscillations of the cantilever as a function of the x,y coordinates analogue to the topographic image. The phase shift is connected to the dissipation of energy through inelastic processes. The phase image can reveal differences in viscoelasticity, friction and adhesion between domains on the surface.

3.6.1 Experimental

AFM tapping mode images were recorded using a Dimension^{TM} 3000 Scanning Probe Microscope from Digital Instruments. The samples were the same as for XPS and ellipsometry analysis. AFM images of these samples prepared in Minnesota were recorded about 6 months after preparation stored at ambient conditions. New samples were prepared at Risø for the sPB-PS system. AFM images were recorded immediately after preparation and drying and after annealing at 100°C for 12 hours.

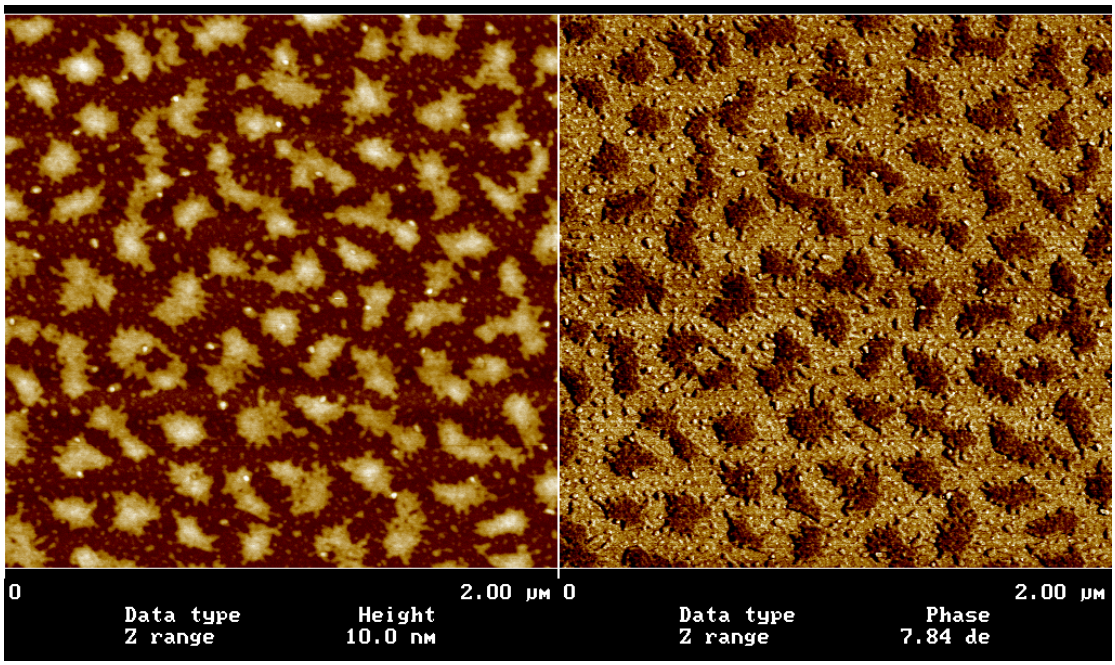

Figure 3.24. Tapping mode AFM image of piranha treated silicon wafer treated with 1% solution of sPB-PS 100k in toluene. Stored 6 months at ambient conditions. Topographic image (left); Phase image (right).

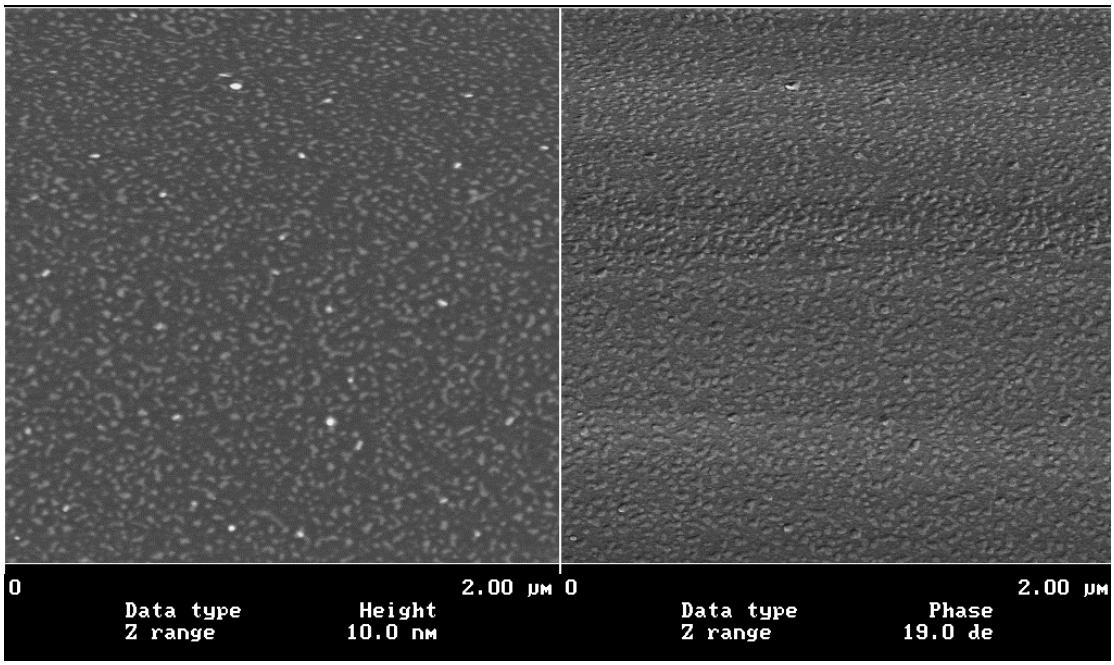

Figure 3.25. Tapping mode AFM image of piranha treated silicon wafer treated with 1% solution of sPB-PS 30k in toluene. Stored 6 months at ambient conditions. Topographic image (left); Phase image (rigth).

3.6.2 Results and discussion

The tapping mode AFM images Figure 3.24 & 25 show that the sPB-PS block copolymers form a domain structure on the surface of oxidized silicon with lateral extensions much larger than the size of single chains. This segregation appears to be very dependent on the molecular weight of the polystyrene chain ends. The AFM image of sPB-PS 10k is not included because it shows no features on this length scale.
Similar surface patterns have been reported independently by Zhao et al. (1994), Karim et al. (1995) for silane end-functionalized polystyrene on silicon. Karim et al (1995) and Tsukruk and Reneker (1995) observe an island like structure at low surface coverage evolving to a spinodal-like patterns at higher surface coverage. The island structure was also observed by Stamouli et al (1996) for poly(2-vinylpyridine)/polystyrene diblock copolymers adsorbed from toluene on mica. They explain the island structure with formation of “octopus-like” surface micelles, where the polystyrene blocks segregate in to larger domains with the poly(2-vinylpyridine) blocks attached to the mica surface. This kind of domains on the surface is not observed in the PDMS system at any molecular mass of the PDMS chains. The observed island formation can be a result of too low concentration or too short reaction time to cover the entire surface of the wafer or a result of surface segregation subsequent to the surface treatment. To investigate these, new samples were prepared using the same concentration on reaction time. The freshly prepared samples showed no island structures on the surface Figure 3.26. This indicates that the surface segregation happens subsequent to the surface treatment. To test this hypothesis, the freshly prepared samples were heated 12 hours at 100°C.

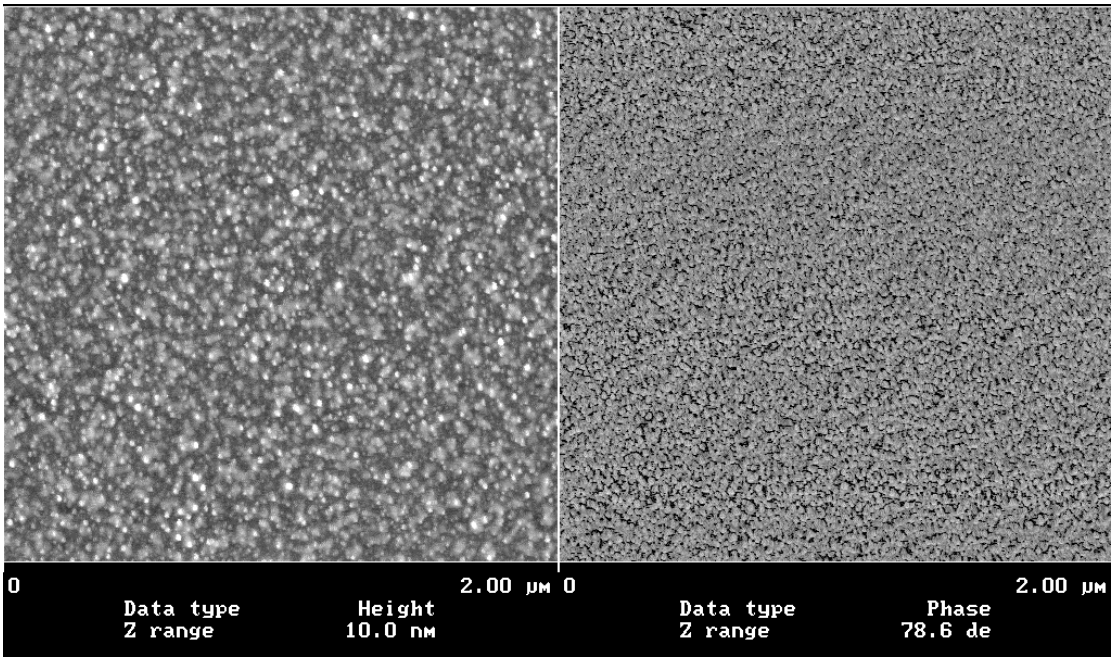

Figure 3.26. Tapping mode AFM image of piranha treated silicon wafer treated with 1% solution of sPB-PS 100k in toluene. Image recorded immediately after preparation. Topographic image (left): Phase image (right).

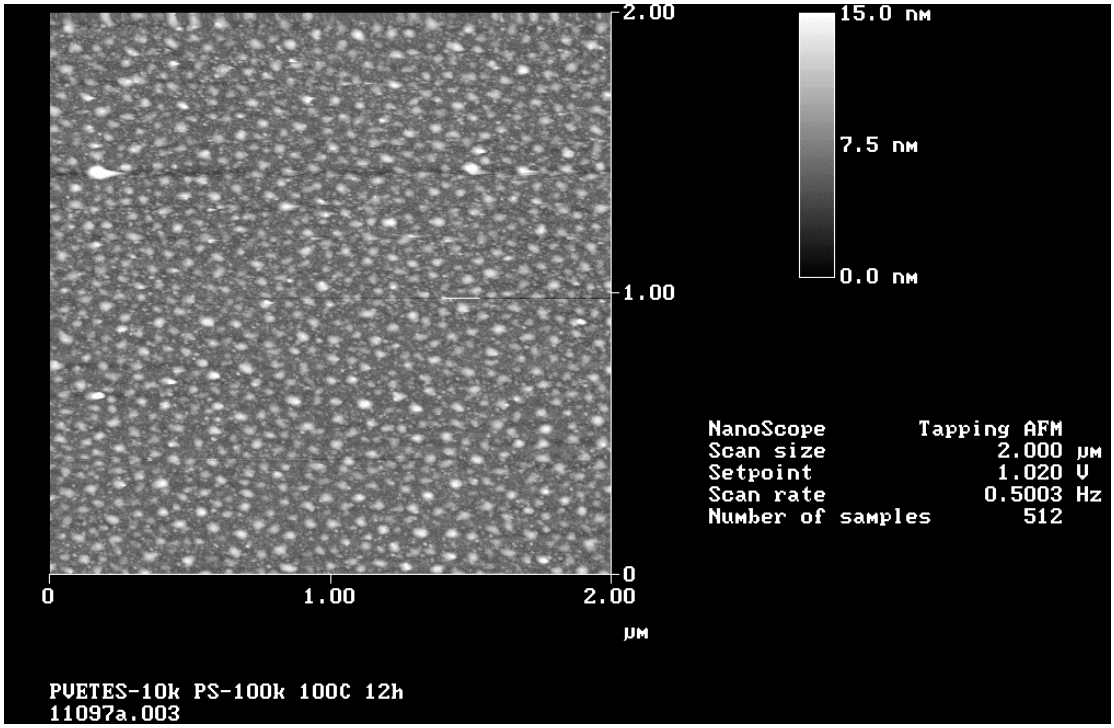

Figure 3.27 Tapping mode AFM image of piranha treated silicon wafer treated with 1% solution of sPB-PS 100k in toluene. Annealed at 100°C for 12 hours.

Figure 3.27 show that heat treatment does change the lateral structure of the surface but not at all to the extent of the samples stored at ambient conditions for 6 month (Figure 3.22). Segregation at room temperature could be questioned considering that the mobility of polystyrene on the surface will be very low at room temperature, because the glass transition temperature for pure polystyrene is above 100°C.

These AFM analysis show that sPB-PS 100k segregate into larger surface features when heated to 100°C for 12h but it is inconclusive weather the very large features observed after long time at room temperature, are caused by segregation at room temperature or insufficient surface coverage.

a) Freshly prepared

No characteristic length scale

b) Annealed at 100°C for 12 hours

Characteristic length scale
Around 80 nm

c) Stored at ambient conditions for six month.

Characteristic length scale
Around 200 nm

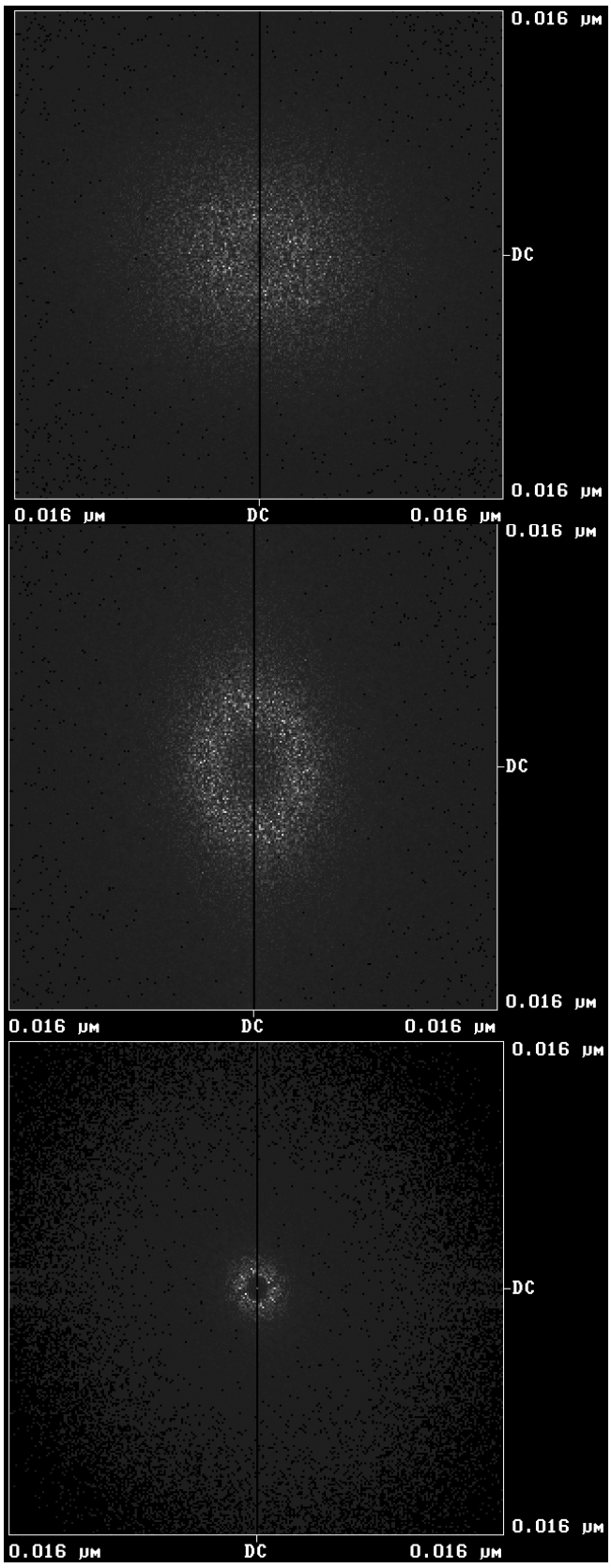

Figure 3.28. 2D Fourier transformation of AFM topography images sPB-PS 100k on piranha treated silicon wafer with different subsequent treatments.

Fourier transformation of AFM images can be used to analyse the images for repeating structures and can also be used to determine characteristic lateral length scales in the images. The 2D Fourier transforms of the AFM images (Figure 3.24,26&27) of sPb-PS 100k are show in Figure 3.28. The freshly prepared sample show no structure while the annealed and the stored sample both show halo patterns in the 2D Fourier images. A halo pattern in the 2D Fourier image means that a structure in the real image is repeated at a characteristic length scale with no preferred direction. The same halo patterns was observed by Karim et al.(1993) and was interpreted as a spinodal like phase separation on the surface. The 2D Fourier analysis indicates that the thermal phase separation is related to the phase separation observed on the stored samples. But it is inconclusive whether the phase separation observed in the stored samples originated from the treatment or the storage time. The important issue is that phase separation is observed in the PS system and not in the PDMS system. That the block copolymers phase separates on the surface have effects on the wetting properties of the surface and can effect the properties of the interface in a polymer composite.

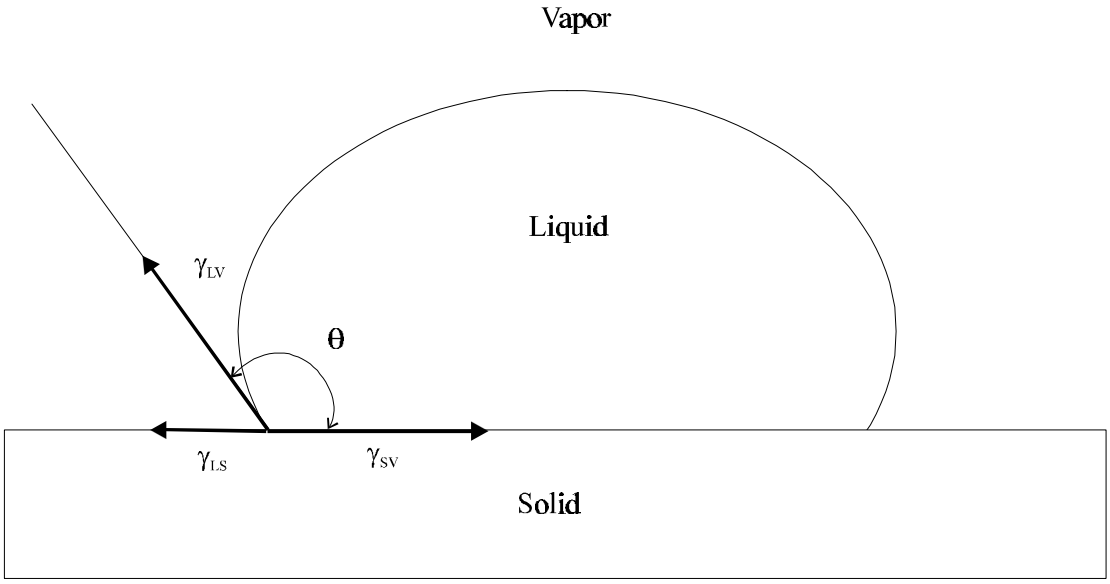

Figure 3.29. Contact angle equilibrium on a smooth, homogeneous, planar and rigid surface.

3.7 Contact angle measurements

Measurement of contact angles can give insight in the physical state of a surface and can in collaboration with other surface analytical techniques reveal the chemical and structural influence on the surface energetics. The contact angle equilibrium (sketched in Figure 3.29) gives the Young equation (3.9) correlating the equilibrium contact angle to the surface and interfacial tensions of the system.

(3.9) $g_{LV}\cos(q) = g_{SV} - g_{SL}$,

where γ_{LV} is the surface tension of the liquid in equilibrium with its saturated vapor, γ_{SV} is the surface tension of the of the solid in equilibrium with the saturated vapor of the liquid, and γ_{SL} is the interfacial tension between the solid and the liquid. The Young equation expresses that the contact angle of a liquid with known surface tension on a sample with an unknown surface tension does not only depend on the surface tension of the sample but also on the interfacial tension. In practice this means that the surface tension of the sample can not be determined by contact angle measurements with a single liquid. In many cases, particular for nonpolar solids, their wetting by members of homologue series of liquids such as alkanes or alkyl halides, is described by an empirical equation (3.10).

(3.10) $\cos(q) = 1 - b(g - g_c)$,

Where γ_c is the critical wetting tension of the solid and b is a constant whose value is usually in the range 0.03 to 0.04. The contact angle falls to zero as the surface tension of the liquid γ approaches γ_c. The problem with this technique is that γ_c to some extent depends on the choice of homologue series.

Exact surface tension determination by contact angle measurement is difficult, but contact angle measurement, by a single liquid can by used qualitatively in examination of surfaces given different surface treatments.

Contact angle hysteresis

Many real surfaces are rough or heterogeneous. A liquid drop resting on such a surface may reside in the stable equilibrium (the lowest energy state), or in a metastable equilibrium (energy state separated form neighboring by energy barriers).
Consider a liquid drop having a steady contact angle on a planar surface. If the surface is ideally smooth and homogenous, addition of a small volume of liquid to to drop will cause the front to advance, and the same contact angle will reestablish. Subtraction of a small volume of the liquid from the drop will cause the drop front to recede, but the same contact angle will again reestablish. On the other hand, if the surface is rough or heterogeneous, addition of the liquid will make the drop grow taller without moving its periphery, and the contact angle becomes larger. When enough liquid is added the drop will suddenly advance with a jerk. The angle at the onset of this sudden advance is the maximum advancing contact angle (θ_a). Removal of the liquid will make the drop become flatter without moving its periphery, and the contact angle will become smaller. When enough liquid is removed, the drop front will suddenly retract. The angle at the onset of this sudden retraction is the minimum receding angle (θ_r). This is known as contact angle hysteresis. The difference θ_a-θ_r is the extent of hysteresis.
In the case of roughness the hysteresis is determined by the actual local contact angle to the surface at the drop front. The contact angle depends on if the drop front is on the top of a surface feature or on the slopes of a feature.
In the case of compositional heterogeneity energy barriers exist at the boundaries between region of different intrinsic contact angles. The liquid front tends to stop at the phase boundaries. Advancing angles tend to reflect the higher intrinsic angle regions (or lower surface energy region). Receding angles tend to reflect the lower intrinsic angle regions (or higher surface energy regions) of a heterogeneous surface.
Contact angle hysteresis measurements give the possibility to detect surface heterogeneity.

3.7.1 Experimental

In order to measure contact angles an experimental setup were build at Risø. A sketch of the principle and a picture of some of the setup are shown in Figure 3.30. The central components are: A 250 µl Hamilton syringe applying liquid drops the sample surface by a standard HPLC needle. The piston is moved by a micrometer to obtain good control in applying and removing liquid from the surface. The sample is placed on a X,Y,Z-translation stage to control placement of the liquid drops. The liquid drop is illuminated by a diffuse cold light source. The outline of the liquid drop on the surface is recorded using a CCD camera connected to a monitor and a frame-gabber card in a PC. The image is analyzed using the "VCA-2500 Dynamic/Windows Software" form AST products. The contact angles are determined by fitting a curve to the outline of the drop on the surface. this is done by placing 5 points on the outline of the drop as shown in Figure 3.31. The samples are the same as analyzed by XPS, ellipsometry and AFM. Advancing and receding contact angles are measured using double distilled water (Water for injections, NPBI). The advancing and receding contact angles are calculated as the mean value of 6 separate measurements. The standard deviations on the measurements were all < 2°.

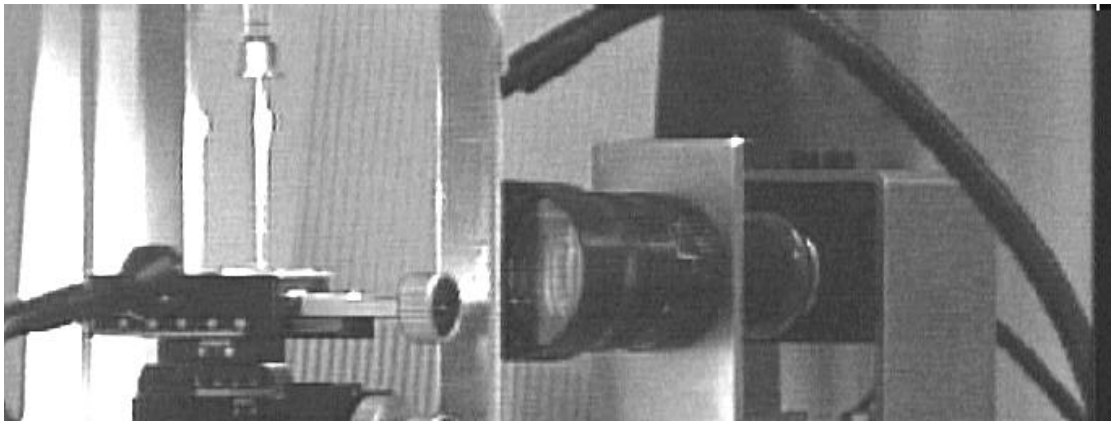

a)

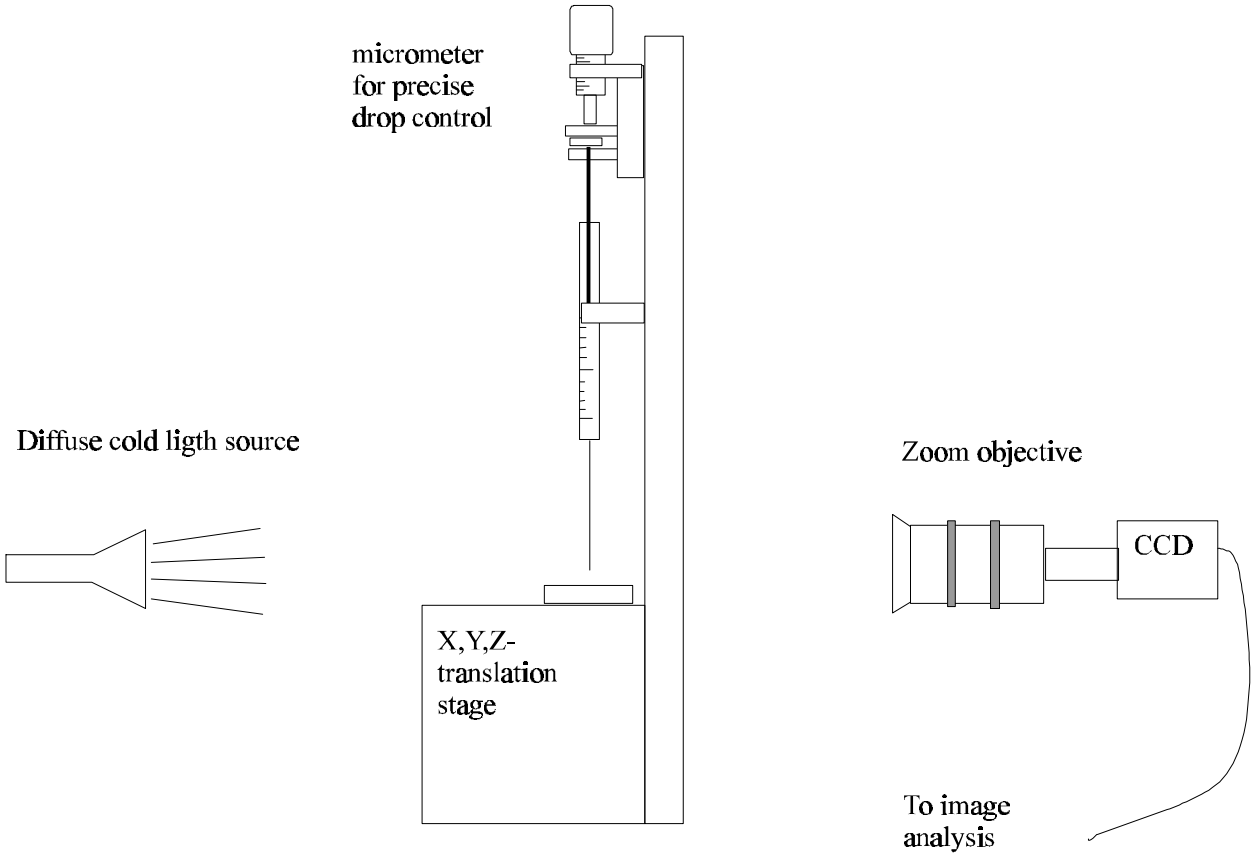

b)

Figure 3.30. Contact angle measurement using the sessile drop method. a) picture of the actual setup. b) principle sketch.

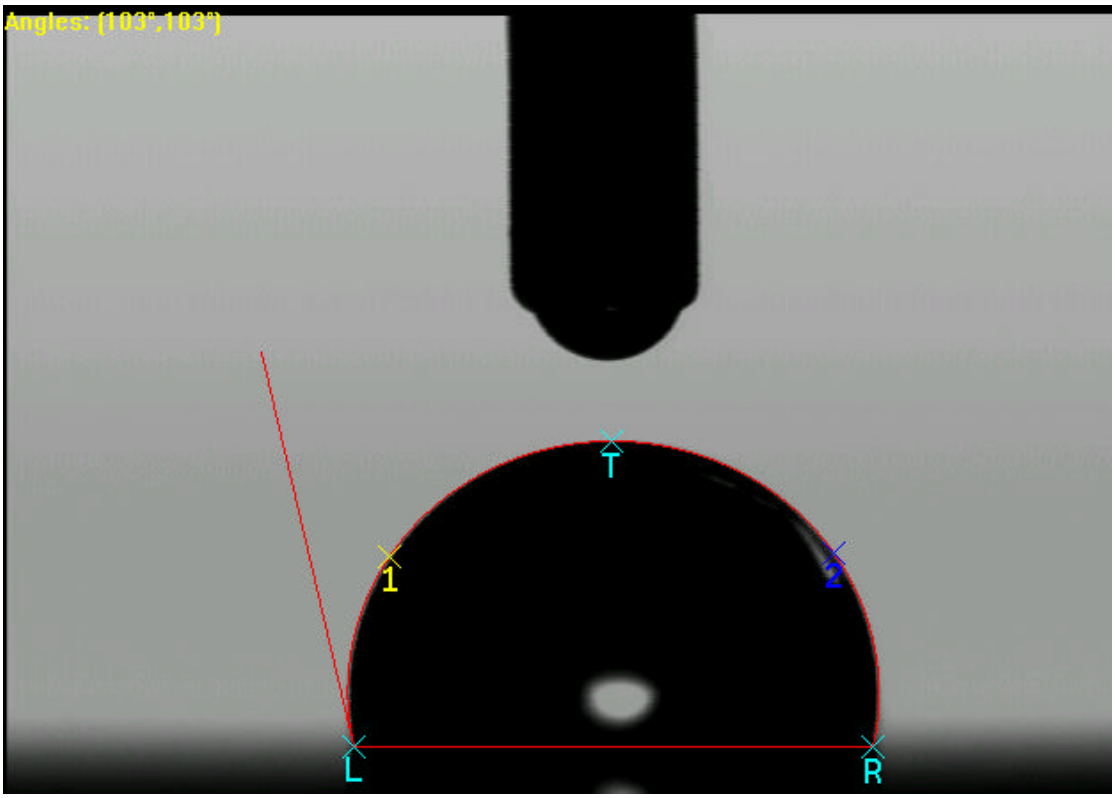

Figure 3.31. Example of a contact angle measurement. Water on piranha treated silicon wafer treated with sPB-PDMS 100k.

Table 3.6 Contact angle measurement on piranha treated silicon wafers treated with various block copolymer silane coupling agents. Advancing (θ_a) and receding (θ_r) contact angles measured in °.

Sample	θ_a	θ_r	$\Delta\theta$
sPB-PS10	69	48	21
sPB-PS30	69	47	22
sPB-PS100	73	50	23
sPB-PDMS10	77	74	3
sPB-PDMS30	94	90	4
sPB-PDMS100	102	100	3

3.7.2 Results and discussion

Comparing the measured contact angles in Table 3.6 with the equilibrium contact angles for bulk PS (θ_{ps} = 91°) and PDMS (θ_{pdms} =110°) reveals that none of the surfaces exhibits the bulk properties of the tail polymers. This shows that none of the surfaces is covered in a way that only the tail polymers are exposed. For the PS system there are little to no difference in advancing contact angles and receding angles in respect to the molecular mass of the PS tail and the system shows significant contact angle hysteresis. The PDMS system on the other hand does show higher contact angles with higher molecular mass of the PDMS tail and the system shows little or none contact angle hysteresis. These observations are in full agreement with the XPS, ellipsometry and AFM analysis on the same samples.
The contact angle hysteresis observed in the polystyrene system is interpreted as heterogeneous surface composition as observed by AFM. The contact angle hysteresis show that the island structure consists of higher and lower surface tension areas. This is consistent with the assumption that polystyrene segregate into domains. The contact angle independence of the molecular mass can be explained by constant average surface coverage independent of the molecular mass. This would be the result of the pancake like structure on the surface during treatment in toluene caused by the absorption of polystyrene on the surface.
For the PDMS system the contact angle dependence on the molecular mass of the PDMS is interpreted as a lack of screening by the PDMS chains of the underlying hydrosilylated polybutadiene and the strongly hydrophilic surface. As the molecular mass of PDMS grows the PDMS chains can cover the surface completely. The low values of contact angle hysteresis ($\Delta\theta$) indicates that the surface is homogenous in composition.

3.8 Summary of surface characterization

This chapter describes a number of different analytical methods suitable for investigations of silane coupling agents on filler surfaces.
The wet chemical methods were found useful in qualitative analyses of unknown surface treatments. A new method was introduced for quantitative determination of aminosilanes on filler surfaces based on the Kaiser test.
An investigation of different FTIR methods (Direct transmission, photo acoustic and diffuse reflectance) showed that diffuse reflectance (DRIFT) is the most efficient method in analysis of silane coupling agents of fibrous or particulate fillers. DRIFT analysis of γ-methacryloxy propyltrimethoxysilane on particulate glass fillers showed that this simple method can be used for quantitative analysis of silane coupling agents on filler surfaces.
X-ray photoelectron spectroscopy (XPS) is found to be a powerful tool in chemical investigations of silane coupling agents on inorganic surfaces. XPS analysis of various silane coupling agents on chemically oxidized silicon showed that XPS analysis also can be used in qualitative determination of average surface thickness for silane coupling agents on silicon.
The quantitative differences in average layer thickness were confirmed by ellipsometry measurements. Average layer thickness determinations revealed a fundamental difference in the way polystyrene (PS) and polydimethylsiloxane (PDMS) based block copolymer silanes absorbs on the surface of oxidized silicon form a toluene solution.
The average layer thickness for PDMS based silanes increases with increased molecular mass of the PDMS tail end. For PS based silanes the average layer thickness is independent of the molecular mass of the PS tail ends. This is interpreted as a result of the affinity for PS to adsorb on the surface from toluene forming a pancake like structure. PDMS on the other hand does not have affinity to adsorb on the surface from a toluene solution resulting in a musroom like structure on the surface where the extent of the layer is dependant on the molecular mass of the tail end.
Atomic force microscopy (AFM) gave valuable information concerning the lateral structure of block copolymer based silane coupling agents on oxidized silicon. AFM revealed that block copolymer silane coupling agents with polystyrene tail end from island structures on the surface. The lateral structure of the block copolymer silanes have effect on the wetting properties of the surface. Contact angle measurements with water on oxidized silicon treated with PS based silanes reveals a difference in the advancing and receding contact angles. This contact angle hysteresis show that the island structure observed by AFM consists of higher and lower surface tension areas. PDMS based silanes show little or no contact angle hysteresis but does in contrast to the PS system show contact angle dependence on the molecular mass of the PDMS tails. This shows that at the surface density given by the hydrosilylated polybutadiene chains, the low molecular mass PDMS chains do not have the physical size to cover the surface. Increasing the molecular mass of the PDMS chain increases the part of the surface covered by PDMS.

4 Characterization of the interface

4.1 Introduction

The reason for synthesizing new block copolymer based silane coupling agents was to achieve better adhesion between inorganic fillers and a polymer equal to the tail end of the block copolymer silane coupling agent. The task is then to find methods suitable for investigation of adhesion between inorganic fillers and polymers. A goal of these investigations is also to determine the influence of the molecular mass of the tail ends on the adhesion properties. There have been reported a number of ways to evaluate the influence of silane coupling agents on the adhesion to polymer materials. Plueddemann introduced the simplest method as the “microscope slide test”. A microscope slide is treated with the possible coupling agent from solution and a polymer layer is placed on the slide by melting, for thermoplastics, or by casting and curing, for thermosetting materials. The adhesion is then measured directly as peel strength. This method can only be used for elastic polymers because rigid glassy polymers cannot be peeled. Examples of evaluation of coupling agents using peel tests are given by Plueddemann (1982), Buchwalter et al. (1992 a&b) and Lund et al. (1992).
Other methods for determination of adhesion are the single fiber methods, where a single fiber treated with silane is embedded in polymer matrix. The adhesion is measured as interfacial shear strength by applying stress to the fiber or matrix until the fiber debonds. There are a number of different types of single fiber methods like microdebond, single-fiber fragmentation and micro-indentation. Herrera-Franco and Drzal (1992) give a good review of these methods. The single fiber methods will be described in more detail later.
A third type of method to compare the influence on coupling agents on the interface adhesion is to perform various mechanical tests on composite samples where the filler is pre-treated in different ways. Tensile, flexural and notched impact strengths have been used to investigate the influence of coupling agents for various polymer filler systems. Examples are given by Plueddemann (1982 p 141-207). The advantage and drawback for these methods are that they give the overall properties of the composite. These methods do not give an exact measure of the interface adhesion but a measure for the influence of the interface adhesion on the mechanical properties which is very useful from a design point of view. Composite laminate tests like $(\pm 45°)_s$-tensile test (Petit 1969 and Rosen 1972), Iosipescu shear test (Waltrart and Adams 1983) and Short beam shear test (Whitney at al 1982) are composite test methods yielding a value for the interfacial shear strength. Interfacial shear stress in used as a measure for interfacial adhesion in composite materials.

A more direct method for measuring the interfacial adhesion was developed by Johnson, Kendall and Roberts in the late sixties (Johnson et al 1971). This method, called the JKR-method, gives a measure of the work of adhesion between materials, and has been used for model studies of adhesion between polymers.

In order to investigate the influence of polymer based silanes at the interface between inorganic filler and a polymer matrix, two different methods have been employed.

- The JKR method for measuring the adhesion between model flat surfaces treated with block copolymer silanes and cross-linked PDMS.
- A microdebond method to measure the interfacial shear strength between single glass fibers treated with silane coupling agent and micro drop of polymer.

The JKR method was selected for the ability to measure the thermodynamical work of adhesion (W_a) and the ability to measure interfacial rearrangement at the interface between a PDMS elastomer and the block copolymer silane coupling agent. The samples for the JKR method are also the same as for most of the surface analytical techniques (treated oxidized silicon wafers), which make comparison of the results from the different techniques more simple.
The microdebond method is a single fiber method, which makes the results more applicable to real composites. This method was chosen because of the flexibility to measure interfacial shear strength between glass fibers and both thermosetting and thermoplastic matrixes. The small volume of the polymer drop on the fiber (embedded length 100-800 µm) make this method ideal to study the effect of the environment on the interfacial adhesion.

A third method was investigated to determine the influence of block copolymer silane coupling agents from tensile measurements on polystyrene glassfiber laminates. The laminates were to be made from glassfiber rowing and polystyrene film or plate materials. The process involves melting the polymer under applied pressure in a special designed oven at department of Materials Science, Risø National Laboratory. This work was terminated because it was impossible to obtain polystyrene film materials with sufficiently low melt viscosity to make laminates using this method.

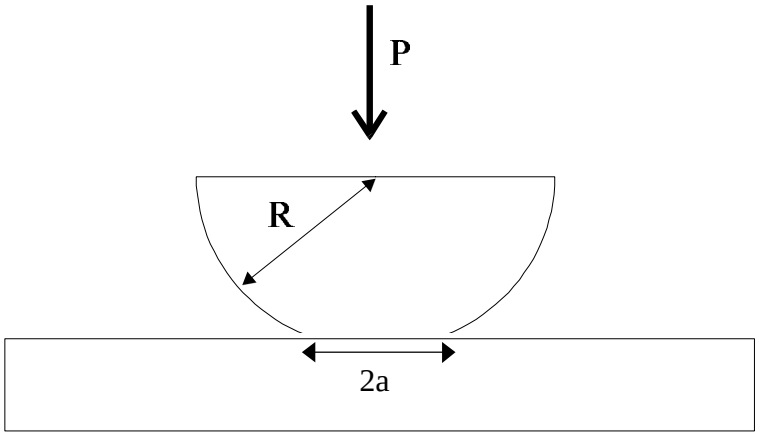

Figure 4.1. Principle of the JKR-method. A spherical elastomer lens with the radius (R) is brought in contact with a flat sample under the load (P) forming a contact with radius (a).

4.2 The JKR-method

The force/contact radius relationship for glass spheres was first described by Hertz in 1898, who found that load (P) was proportional to the cube of the contact radius (a^3).
Hertz proposed the law $a^3 = RP/K$, where K is the compression modulus and R the radius of the two spheres.
In the late 1960´s a group at Cambridge University found deviations from the Hertz description at small loads, caused by adhesion. After careful theoretical and experimental analysis Johnson, Kendall and Roberts proposed a more precise description of the deformation of spherical bodies known as the JKR-formula (4.1)

$$(4.1) \quad a^3 = \frac{R}{K}\left(P + 3pW_a R + \sqrt{\left(6pW_a RP + \left(3pW_a R\right)^2\right)}\right),$$

where a is the radius of the contact area R is the radius of curvature of the sphere, K is the compression modulus of the sphere (4.2), P is the applied load and W_a is the work of adhesion for the two bodies in contact. The compression modulus can be expressed in terms the Young modulus (E) and the Poisson's ratio (ν) for the elastomer (4.2)

$$(4.2) \quad K = \frac{2E}{3(1-n^2)}$$

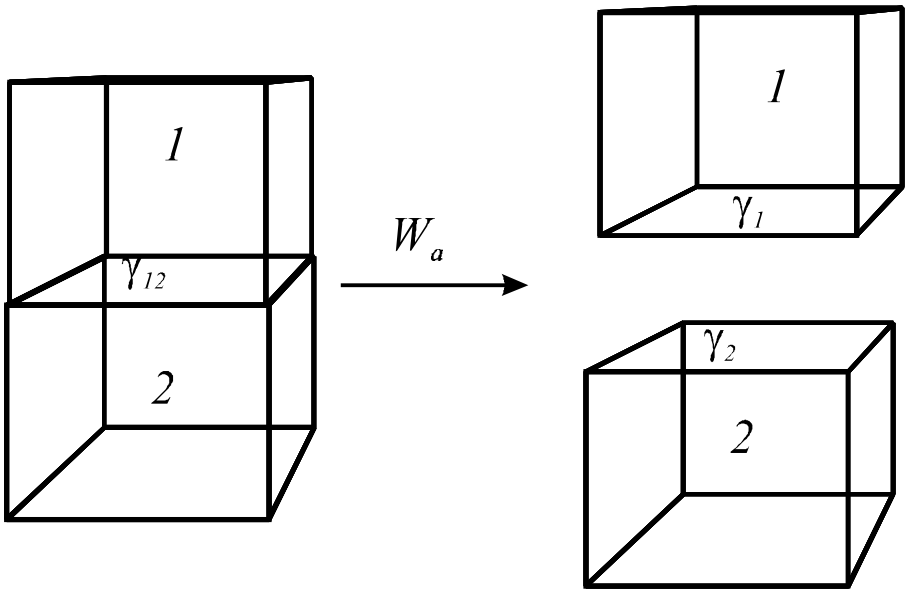

Figure 4.2. Work of adhesion

The work of adhesion (W_a) is defined by the Dupré equation (4.3) which describe the work required to separate reversible the interface between two bulk faces *1* and *2* from their equilibrium separation to infinity:

(4.3) $W_a = g_1 + g_2 - g_{12}$,

where γ_1 and γ_2 is the surface tensions of the materials and γ_{12} is the interfacial tension between the two in contact. If the two materials are identical, the reversible work is the work of cohesion,

(4.4) $W_c = 2g$,

where W_c is the work of cohesion for a material with the surface tension γ. This gives raise to the description that the interface tension is the energy per area needed for combining two different materials. This is a very simplified picture, but it gives a conceptual understanding of why interfacial tension is an important parameter in polymer blends and composites.

The principle of a JKR measurement used in this study is to move a PDMS hemisphere into contact with a flat sample mounted on a balance. Moving the hemisphere in steps closer to the sample applying more and more load. Measuring coherent equilibrium values of load (P) and contact radius (a). By fitting these load-data to the JKR theory (4.1) both the compression modulus (K) and the work of adhesion (W_a) can be determined.

When the load has reached a pre-determined maximum value the hemisphere is removed in steps from the sample. While unloading the system is no longer in equilibrium. A driving force larger than the thermodynamic work of adhesion (W_a) is needed for the contact area to move in to equilibrium or in other words for the crack at the periphery to propagate. For unloading data the thermodynamic work of adhesion (W_a) in (4.1) is exchanged with the strain energy release rate (G) for the non-equilibrium situation.
The strain energy release rate can be expressed by rearranging (4.1) and is given in (4.5)

$$G = \frac{(P - P_h)^2}{6pKa^3}, \quad (4.5)$$

where $P_h = a^3K/R$ is the so called Hertzian load, that is, the load that would have been necessary to produce the observed contact radius in a purely Hertzian situation, with no adhesion between the surfaces. The strain energy release rate is dependent on the rate the contact area moves. Because of this, the unloading is done by moving the hemisphere away from the sample and measuring coherent values of a end P while the system relaxes. Some systems relax back to thermodynamically equilibrium so that $G_0 = W_a$, while other systems end up in a situation where $G_0 >> W_a$. This load/unload hysteresis is the subject of some discussions in recent literature (Brown 1993, Silberzan et al 1994, Deruelle et al 1995, Tirrell 1996). The basic conception is that hysteresis means that some transformation has taken place during contact like inter-penetration between layers of tethered polymer chains or hydrogen bonding.
The ability of the JKR method to measure both the thermodynamical and the non-thermodynamical adhesion has caused a growth in interest for the JKR-method in the recent years. Pioneering work by Chaudhury (1991,92,93) using the JKR method to measure adhesion between PDMS clean and modified by various alkyl- and fluoro-silane caused a reinvention of the JKR method. Adhesion measurements between a number of different polymer systems have been reported by Mangipundi et al. (1994&96), Ahn & Shull (1996), Choi et al. (1997) and Perutz et al. (1997). Recent theoretical considerations for the phenomenas observed in JKR experiments have been published by Ligoure (1996) and Shull et al. (1996).
The outline of the present work is to determine the thermodynamic work of adhesion and explore the possibility of interpenetration in the s-PB-PDMS/PDMS system.

4.2.1 Experimental

The JKR- measurements were carried out on an experimental setup (Deruelle et al. 1995) at department of Chemical Engineering and Materials Science (CEMS), University of Minnesota, Minneapolis. A similar experimental setup with small modifications was built at Risø and further clarifying experiments were carried out using this setup.
Sample preparation: The samples measured were the same as those for ellipsometry: Polished [100] silicon wafers were oxidized in a 10:1 by volume solution of 70% H_2SO_4 and 30% H_2O_2 at 120°C for 15 min then washed three times in pure water and dried under dry nitrogen. The oxidized wafers were immediately treated with 1 % wt. solutions of block copolymer silanes in toluene for 1 hour. Washed three times in toluene then three times in methanol then dried under a stream of dry nitrogen.
Preparation of PDMS-hemispheres: hemispherical PDMS caps were made from a mixture of 100 parts α, ω-vinyl PDMS (~10 kg/mole) 1.9 part oligomeric hydrosilane crosslinker (degree of polymerization ~50), 0.1 parts Pt-based catalyst and 0.5 part 2-ethyl-hexyl-hydrogen-maleate inhibitor. Small volumes were placed with a syringe on glass slides pretreated with 1H,1H,2H,2H-perflourodecyl-trichlorosilane from vapor phase. Crosslinking was done at 70°C in 2 hours. After cooling the caps were removed form the glass slide and extracted in n-heptane for 48 hours in a soxlet column to remove unreacted PDMS chains. The caps were then placed on a clean glass slide and dried at 50°C under vacuum. The hemispheres prepared this way have radii of curvature between 0.5 and 2 mm.

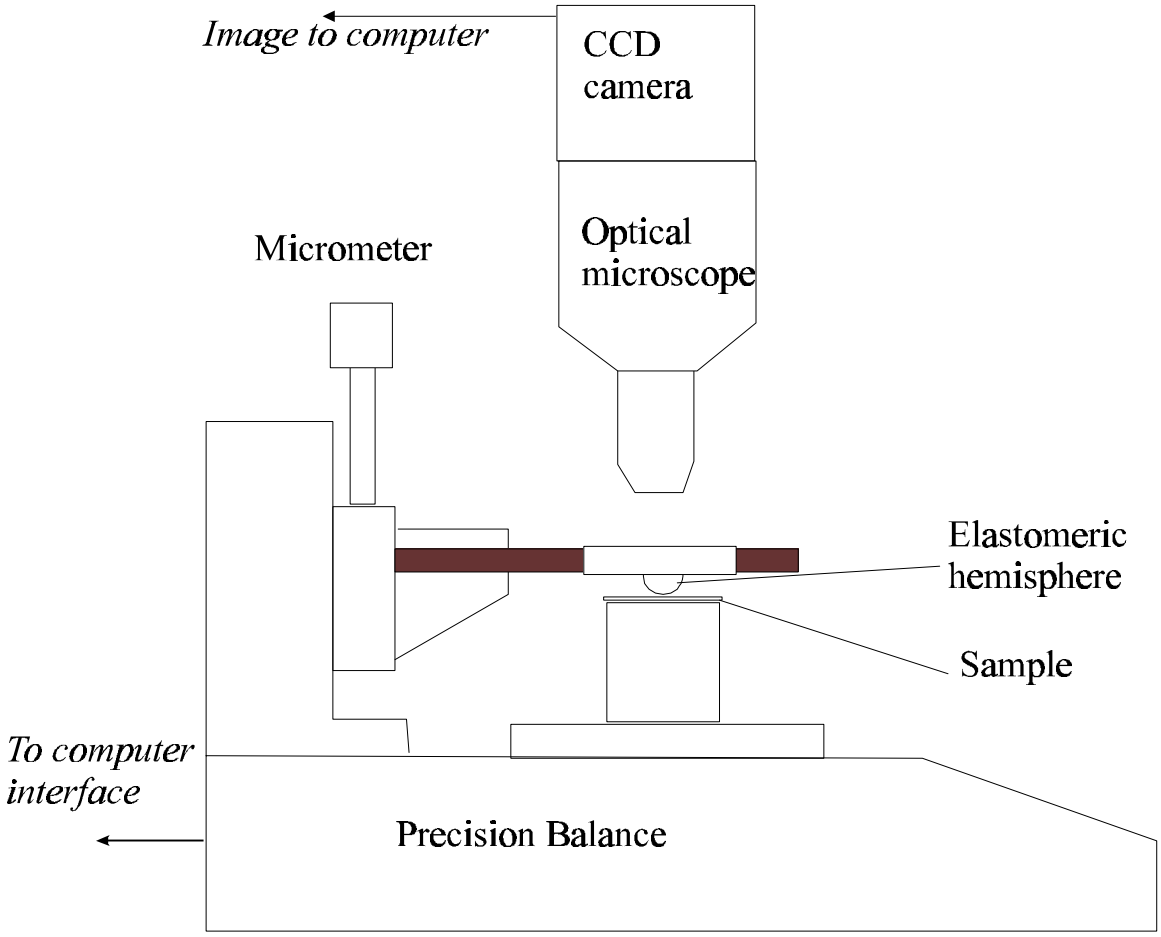

Figure 4.3. Sketch of the JKR-apparatus built at Risø

JKR-apparatus: A sketch of the JKR apparatus built at Risø is shown in Figure 4.3.
The elastomer hemisphere is placed on a glass slide mounted on a translation stage (Newport M-462) which can be moved in the z-direction using a micrometer with a precession of 0,1 µm. The load is measured on a balance with a precision of 0,1 mg (WA 210, Adams Equipment) connected to a computer. The contact radius is measured using an optical zoom microscope (Meiji Techno Co LTD) connected to a CCD camera. The image of the contact area is analyzed on the computer.
Method of testing: An extracted PDMS hemisphere was placed on a clean glass slide. The radius was measured by taking an image from the side of the hemisphere on a calibrated optical microscope. The glass slide was placed in the JKR apparatus and brought very close to the surface of the sample (observed by a Newtonian interference pattern). The hemisphere was moved in 1 µm steps down on the sample and coherent values of load and contact radius was measured after 5 minutes. This was continued until a maximum load of ~300 mg was reached where the contact was obtained for 1 hour. Unloading was done by removing the hemisphere in 3 µm steps, where the system was allowed to relax for 1 hour. Coherent values of load and contact

radius were measured while the system relaxes. This procedure was repeated until the hemisphere was completely detached from the sample.

4.2.2 Results and discussion

Typical JKR- results for a crosslinked PDMS hemisphere compressed against oxidized silicon wafers treated with block copolymer silane coupling agents are shown in Figure 4.4. All loading measurements were in perfect agreement with the JKR theory. The loading data were fitted to (4.1) using the measured radius (R) of the PDMS hemisphere. The compression modulus (K) and the work of adhesion were determined as independent parameters. The compression modulus K was found to be 3.0 ± 0.07 MPa as the mean value for all experiments. The thermodynamical works of adhesion (W_a) are shown in Table 4.1. The values for the PDMS/sPB-PDMS system are close to values measured for PDMS against PDMS (42.5 ± 0,5 mJ/m^2 Deruelle et al 1995). The measured values are almost identical to the work of cohesion $W_c = 2\gamma$ for PDMS. It is important to state, that this do not necessary mean that the surface of the wafer are completely covered by PDMS, because the same value for the work of adhesion can originate form a surface with higher surface tension and higher interfacial tension. The measured values for the PDMS/s-PB-PS system are in agreement with values measured for PDMS against PS (49 ± 2 mJ/m^2 Mangipudi et al 1996) except for the highest molecular mass (sPB-PS 100k) which can be connected to the surface segregation observed by AFM.
The JKR method show a significant difference in hysteresis between the PDMS/s-PB-PDMS and the PDMS/sPB-PS systems as observed by others for extracted PDMS/PDMS and extracted PDMS/PS systems (Silberzan 1994, Choi 1997 and Mangipudi 1996).

Table 4.1 Work of adhesion determined by the JKR method between an extracted PDMS hemisphere and oxidized silicon treated with various block copolymer silane coupling agents.

Block copolymer silane	Work of adhesion (mJ/m^2)
sPB-PDMS 10k	42,0
sPB-PDMS 30k	42,8
sPB-PDMS 100k	41,0
sPB-PS 10k	49,6
sPB-PS 30k	49,6
sPB-PS 100k	43,7

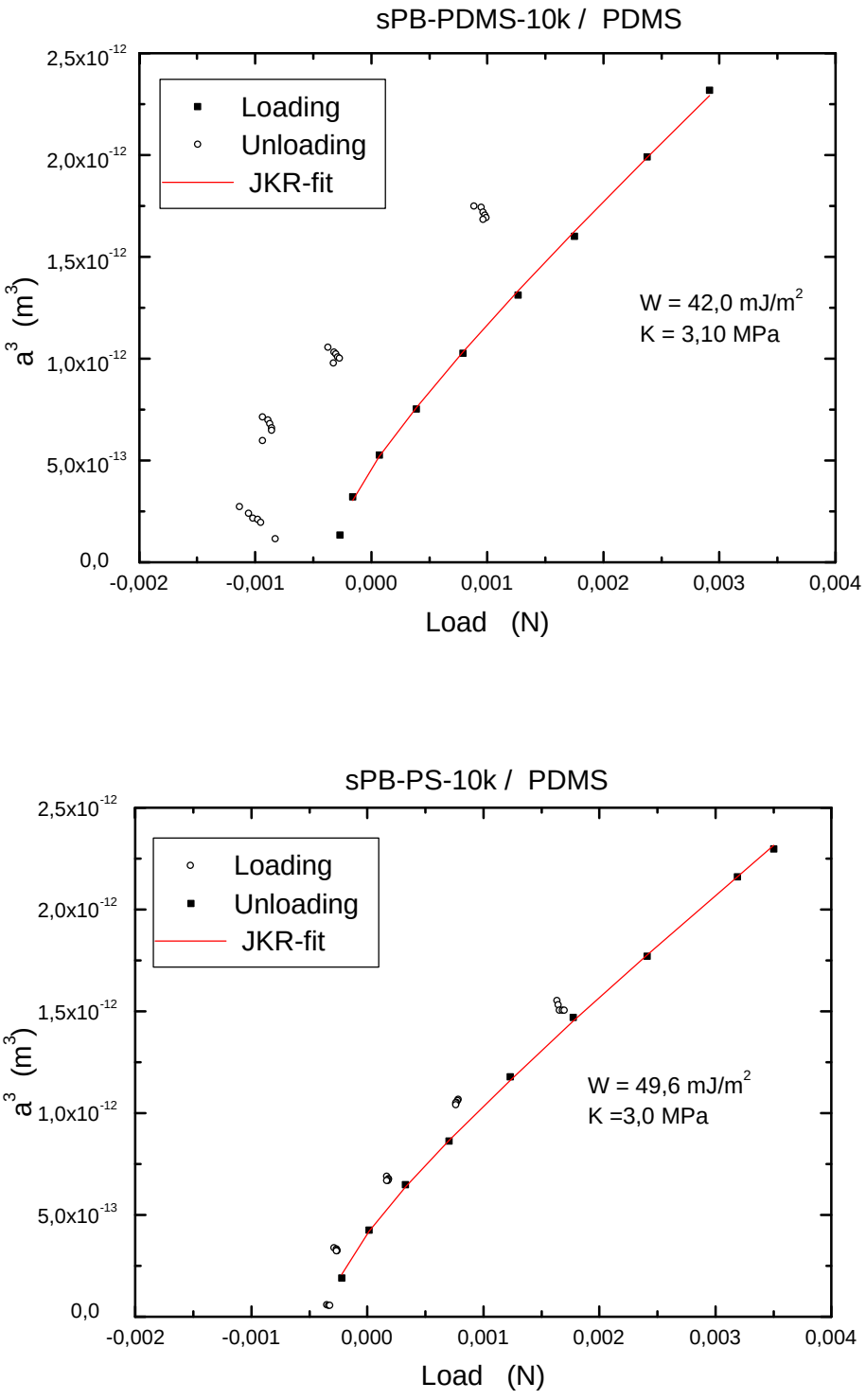

Figure 4.4. JKR-measurements of cross-linked PDMS elastomer hemisphere compressed against oxidized silicon wafer treated with block copolymer silane coupling agents.

There are two different theories for the origin of this hysteresis in the PDMS/PDMS system. One theory is that the unreacted hydrosilane groups in the cross-linking agent (Si-H) are hydrolyzed by water during handling, resulting in Si-OH groups at the surface capable of forming hydrogen bonds to PDMS in contact with the network. This theory is supported by the work of Perutz et al (1997) where the PDMS is deliberately hydrolyzed in 0.01 M HCl solutions for various time prior to JKR experiments. The JKR experiments showed significant increase in the hysteresis with increasing hydrolysis time. But this theory most be considered speculative because no direct evidence have been given for the existence of silanol groups or hydrogen bonds. A Simple attenuated total reflection (ATR) FTIR experiment on flat sheets of crosslinked PDMS before and after extraction 48 hours in hexane showed no difference in the spectra before and after extraction. The spectra showed no absorbance peeks that could be related to silanol groups.

Another theory is that the hysteresis is caused by interpenetration by layers of tethered polymer chains at the interface. This theory is supported by the work of Choi et al. (1997) that showed a significant decrease in the hysteresis with increasing crosslinker to polymer ratio. This theory is also supported by the observation of hysteresis in polymer systems where no hydrogen bonding can occur, not even hypothetical. (Brown 1993, Creton et al. 1994).

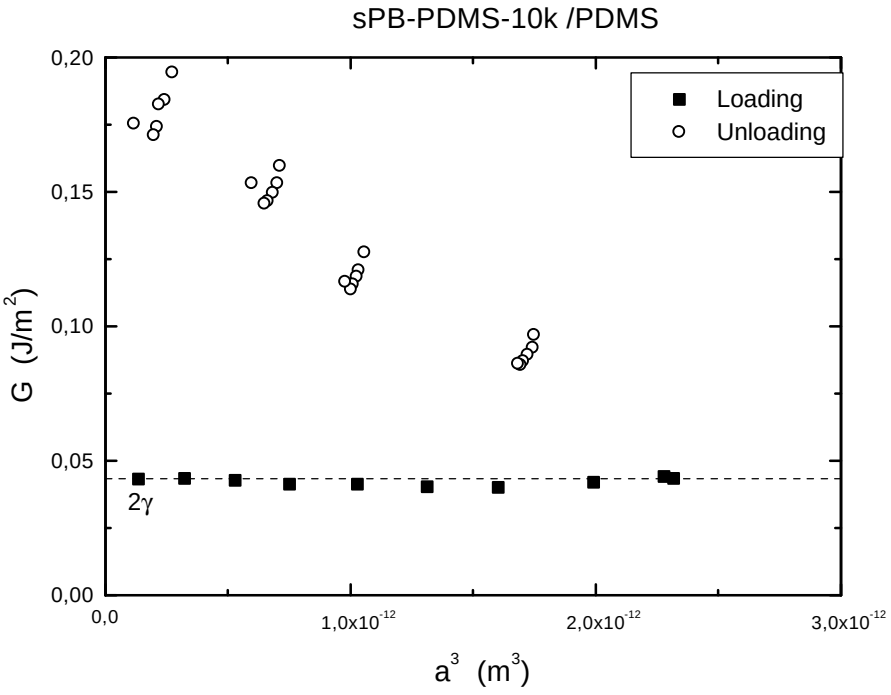

Figure 4.5. Strain energy release rate (*G*) as a function of contact radius (*a*) for extracted PDMS compressed against oxidized silicon treated with PDMS copolymer coupling agents.

Plotting the strain energy release rate (G) in (4.5) as a function of the cube of the contact radius (a^3) Figure 4.5 shows that the hysteresis increases significantly the closer the contact area comes to the center of the PDMS hemisphere. Silberzan et al (1994) gives an expression for the stress profile σ(r) at maximum load or contact radius (a_m) for an elastomer hemisphere compressed against a flat surface (4.6)

$$(4.6) \qquad s(r) = \left(\frac{3KW}{2pa_m}\right)^{1/2} \frac{1}{\left(1-\frac{r^2}{a_m^{\,2}}\right)} - \frac{3Ka_m}{2pR}\left(1-\frac{r^2}{a_m^{\,2}}\right)^{1/2},$$

This expression shows both a tensile (positive) and a compressive (negative) contribution to the stress profile. A calculated stress profile at the maximum load /maximum contact radius for PDMS compressed against sPB-PDMS on silicon is shown in Figure 4.6. The graph shows only the compression stresses, but actually the stress is tensile very close to the periphery where $r = a_m$. As it can be seen in (4.6) the stress approaches infinity for r approaching a_m. so it should be stated that (4.6) is only valid for $r > a_m$. Turning to the compressive part of the stress profile there appears to be a relation between the stress profile and the measured strain energy release rates Figure 4.5. This increasing strain energy release rate with increasing contact pressure indicates that the observed hysteresis originates from a pressure sensitive interaction at the interface.

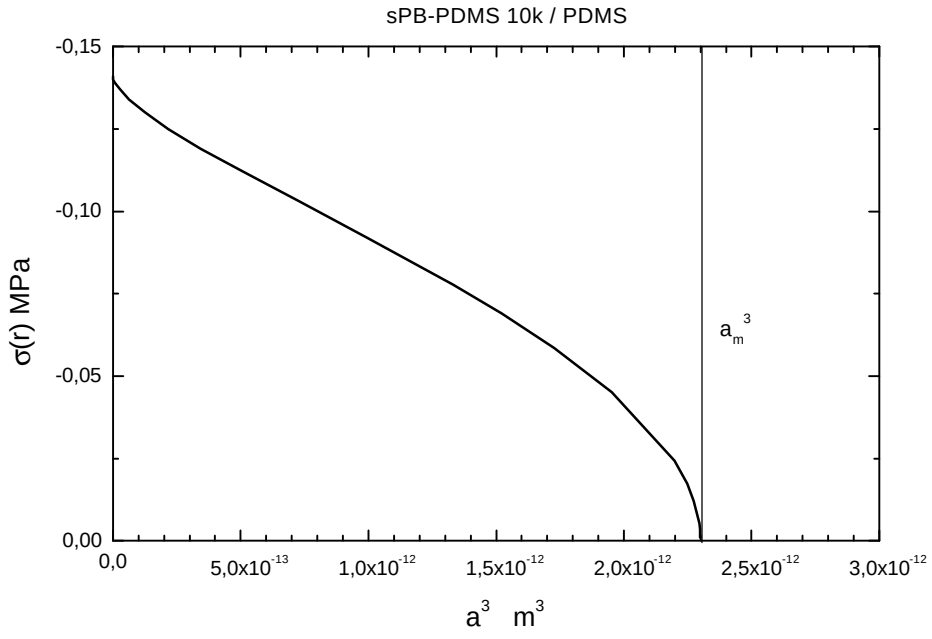

Figure 4.6. Calculated stress profile at maximum load calculated from (4.6) using the actual parameters for the JKR measurement of sPB-PDMS 10k., The negative values means compressive stress.

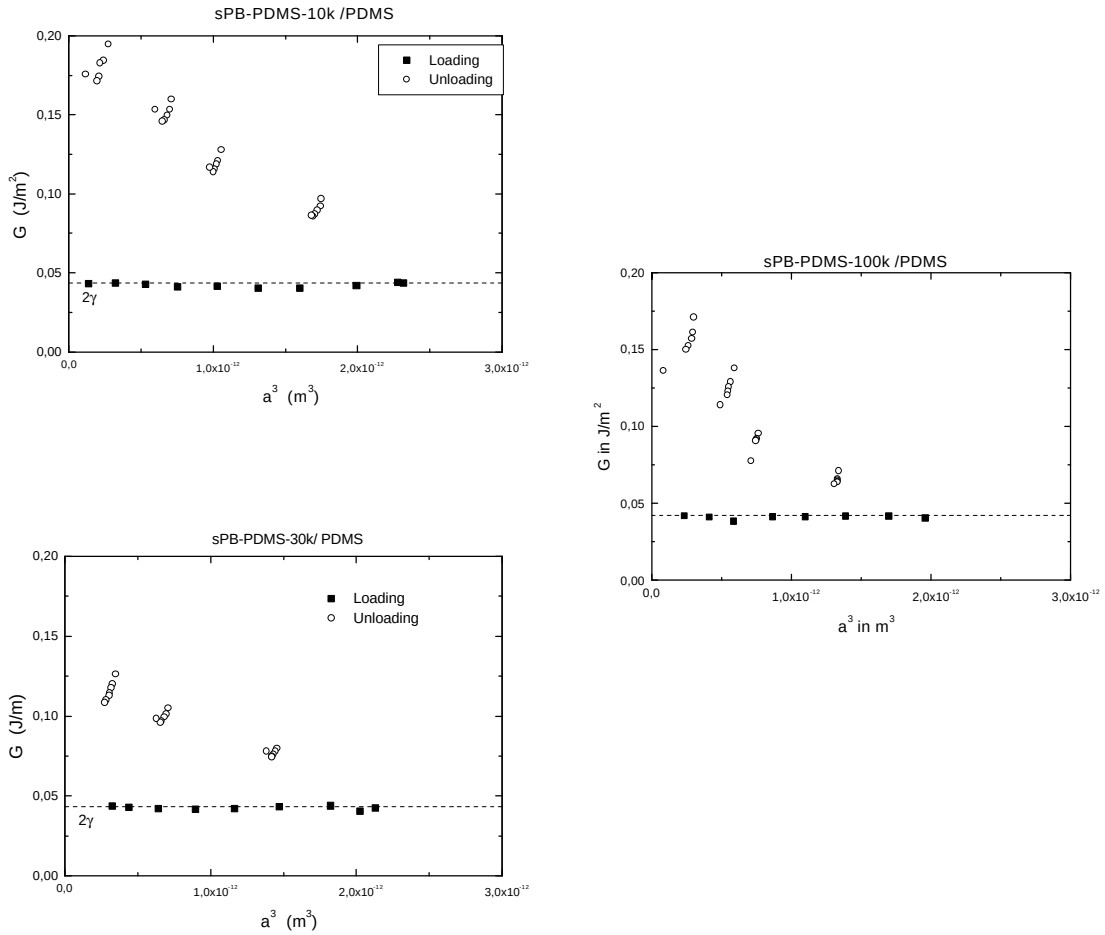

Figure 4.7. Strain energy release rates measured by the JKR method for varying molecular mass of the PDMS end block.

Whatever mechanisms are causing hysteresis, the measurements show that block copolymer silanes containing PDMS end blocks show enhanced adhesion to crosslinked PDMS.
Figure 4.7 shows that there are no apparent correlation between the molecular mass of the PDMS tail end and the extent of the hysteresis. This could be because the contact time of 1 hour is not sufficient for the high molecular mass to form optimum adhesion due to the lower mobility. But systematic variations of the contact time for an unattached PDMS with an average molecular mass of 412 Kg/mole done by Deruelle et al (1995) showed no variation in hysteresis between 30 min and 1 hours contact time.
Apparently the extent of hysteresis is largest for PDMS 10k and smallest for PDMS 30k with PDMS 100k as an intermediate. There is no apparent explanation for this behavior and further experiments are needed to understand the mechanism of adhesion hysteresis in PDMS/PDMS systems. The main conclusion is that these JKR-experiments do not show any effect on adhesion by increasing the molecular mass above the molecular mass of entanglement for PDMS.
Unpublished results for JKR experiments on various elastomer/block copolymer systems done by Falasfi (1998) show that the molecular mass of the block copolymer tail end need to be 6-10

times the molecular mass of entanglement to significantly enhance adhesion. This is also consistent with JKR experiments by Brown (1993) and Creton et al (1994). The system studied in these publications is polystyrene (PS) against a polyisoprene (PI) elastomer hemisphere and the effect on the interfacial adhesion of PS-PI block copolymers at the interface. Variation of the molecular mass over a certain critical molecular mass of the block copolymers showed significant influence on the measured strain energy release rates (G). Going from a molecular mass of 40 kg/mol to 66 kg/mol of the PI block resulted in significant increase in the interfacial adhesion while going form 66 kg/mol to 150 kg/mol showed a small increase in the interfacial adhesion. Comparing these results with the molecular mass between entanglements for PI at 25°C of 5100 kg/mol (Mark 1996) shows that the critical molecular mass is around 10 times higher than M_e.

Viewing the results in light of these studies, it is possible that the molecular mass of the tail ends used in the present work are too small to establish true entanglements between the PDMS blocks on the surface and the PDMS network in the hemisphere. Comparing the maximum molecular mass of around 100 kg/mol. with M_e for PDMS of around 12 kg/mol shows that the maximum molecular mass of the tail end is around 8 time greater than M_e. It is possible that this is insufficient to achieve real entanglements. To test this it is necessary to compare the results with results using higher molecular masses of the PDMS tail ends.

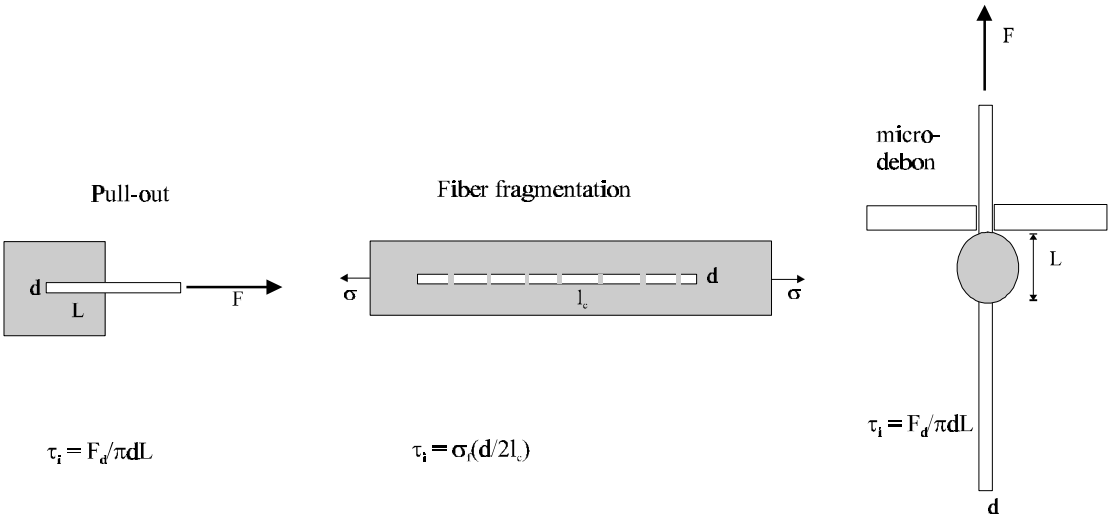

Figure 4.8. Principle of single fiber methods for determination of interfacial shear strength (τ_i), for a fiber with the diameter (d) embedded in a polymer matrix with the length (L). F_d is the debonding force, l_c is the critical fragment length and σ_f is the fiber strength.

4.3 Single fiber microdebond method

There are three single fiber methods for determination of interfacial shear strength: Pullout, fiber fragmentation and microdebond. The principles of the three methods are shown in Figure 4.8. The pullout and microdebond techniques are similar except for the sample preparation. The principle in both methods is to measure the maximum force where the fiber debonds from the matrix. The apparent interfacial shear strength (τ_i) can then be determined by dividing the debonding force (F_d) with the embedded area. These two methods also give the possibility to measure the friction between the fiber and matrix after debonding.
The principle in the fragmentation method is different in the sense that the fiber is completely embedded in a matrix with a strain to failure at least three times that of the fiber. As the applied strain increases, the embedded fiber breaks repeatedly at points where the fiber strength has been reached. Continued application of strain to the sample results in repetition of this fragmentation process until all remaining fiber lengths become so short that the shear stress transfer along their length can no longer build up enough tensile stresses to cause further failures. The maximum final fragmentation length of the fiber is referred to as the critical length (l_c). Assuming constant shear stress along the fiber and constant fiber diameter the interfacial shear strength (τ_i) can be related to the fiber strength (σ_f) by a simple force balance.

All three single fiber methods have been used to evaluate interface modifications of glass fibers in polymer matrices. Chua et al. (1992) have used the pullout method to investigate different pretreatment of glass fibers in polyester resin. Yue and Quek (1994) have used the pullout method to investigate the influence of different concentrations of cationic styrylsilane on the adhesion between glass fibers and polypropylene. Li (1995) have used the pullout method to determine interfacial shear strength between glass fibers and various types of polyethylene and Nylon 12.

Tripathi and Jones (1998) have recently reviewed the fragmentation method for various fiber matrix combinations. Salehi-Mobarakeh et al. (1997) have used the fiber fragmentation method to show improved interfacial shear strength of Nylon 6,6 condensation grafted onto glass fibers in a Nylon 6,6 matrix.

Mcalea & Gregory (1988) have used the microdebond method to determine the interfacial shear strength of Polybutylene terephthalate (PBT) in contact with silane treated glass fibers. Gaur & Miller (1989) used the microdebond method for various fiber types (aramid, carbon and glass) in epoxy. Qian et al. studied the influence of γ-APS treatment of glass fibers in epoxy resin. Herrera-Franco & Drzal (1992) have made a comparison review of all three methods for carbon fibers in epoxy.

The objective of this study is to measure the interfacial shear strength using the microdebond method for glass fibers treated with block copolymer silanes embedded in a matrix equal to the tail end of the block copolymer. Furthermore, to examine the influence of hydrolysis on the interfacial shear strength by exposing fibers with micro drop of polymer in boiling water for 100 hours prior to testing.

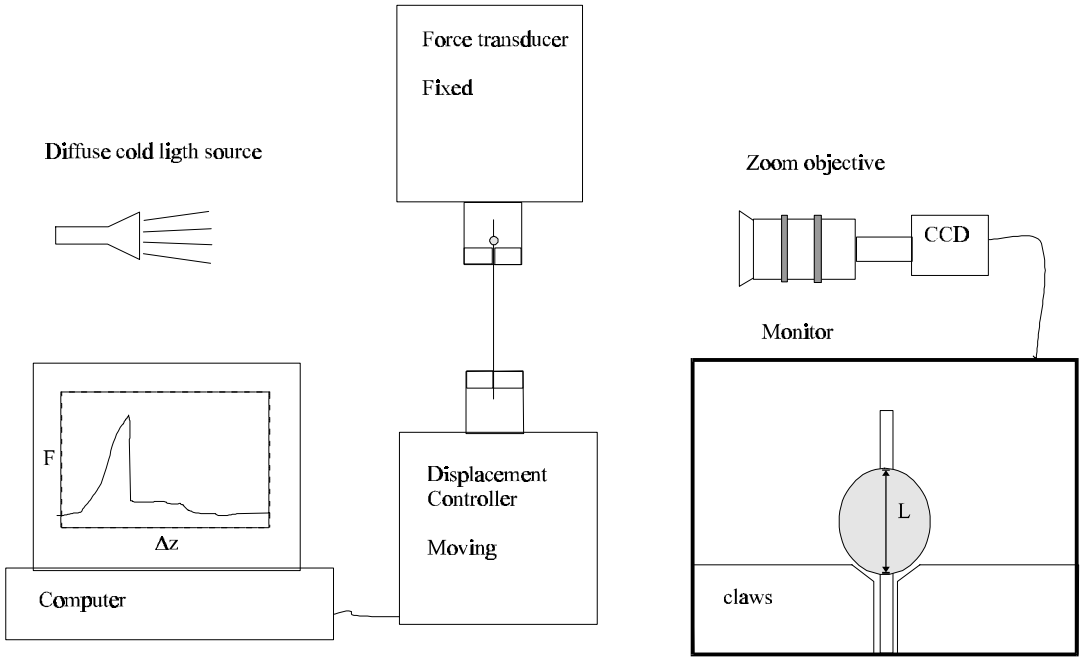

Figure 4.9. Principal sketch of the microdebond apparatus.

4.3.1 Experimental

Apparatus: The microdebond apparatus was built by modifying a dynamic mechanic spectrometer (RSA II from Rheometric Scientific Inc.). This rheometer was built of two identical displacement control/force transducer units enabling the instrument to make controlled speed displacements with a displacement precision of 50 nm. The force transducer used has a maximum load of 1000 g with a precession of 0.1 g. The glass fiber was mounted in a fiber fixture supplied with the rheometer. One end was fixed between two claws. The other end of the fiber was sliding in a 150 µm triangular slit in one of the metal claws. The polymer drop resting on top of the completely compressed claws was monitored from the side by CCD camera connected to a monitor. The embedded fiber length was measured directly on the monitor with a calibrated precession of 5 µm.
Fiber preparation: 50 µm diameter optical glass fibers (SOG 70 from Roblon Fiber Optics) coated with a paraffin size was extracted 1 hour in boiling xylene to remove most of the sizing. The fibers were then heated to 500°C for 3 hours in a ventilated oven to remove last traces of sizing. The glass fibers were then treated in 1% wt. solutions of block copolymer silanes in toluene for 1 hour at room temperature. A batch of fibers was treated in 1% wt. solution of n-propylsilane (98% ABCR). After silane treatment, the fibers were washed 3 times in pure toluene and three times in methanol to remove adsorbed silane. After washing, the fibers were dried at 110°C for 1 hour. The fibers were mounted individually on an aluminum frame by double-sided tape.
PDMS drops: a tow component curable polydimethylsiloxane elastomer (Sylgard 184 Silicon Elastomer from Dow Corning) is blended following the specifications. The blend is degassed using a rotational evaporator. Small drops are applied to the glass fibers by a syringe under an optical microscope. The drops are cured at 80°C for 3 hours. The embedded length of the PDMS drops varied from 200-900 µm.
PS drops: Standard Polystyrene for injection molding (Polystyrol 158K form BASF AG.) were dissolved in toluene (super pure, Romil) and precipitated in methanol (super pure, Romil) in a household blender to make a fine polystyrene powder. The powder was washed 3 times in methanol before drying under vacuum. The powder was heated to approx. 210°C in a glass petridish and polystyrene fibers were drawn from the melt using a pin. The average diameter of the polystyrene fibers varied between 50-200 µm. A small knot of polystyrene fiber was tied around the glass fibers under an optical microscope. The ends of the polystyrene fiber were cut using a pair of cutting nippers. The polystyrene knots were fixed on the glass fiber by approaching an electronics solder. The glass fibers were heated at 190°C for 20 minutes to form micro-drops of polystyrene. Figure 4.10 illustrates the effect of this heat treatment. The embedded length of the PS drops varied form 150-600 µm
Aging: after preparation, half the fibers were placed in boiling water (demineralized, Millipore) under reflux for 100 hours.

Procedure of testing: The fibers were placed so that the polymer droplets were resting above the upper set of claws. The embedded length (L) was measured on the monitor and the actual length was calculated by a calibration on the optical set-up. The lower claws were moved so that the polymer drop was resting on the upper claws. The micro-debonding was measured with a constant rate of displacement of 1.0 µm/s. The force/displacement curve was followed during the experiment and compared to the image of the micro drop to make sure the measured maximum force originated from debonding and not from fiber break. The apparent interfacial shear strength was calculated as a mean value of 10 separate successful fiber debondings for each surface treatment before and after exposure to boiling water for 100 hours.

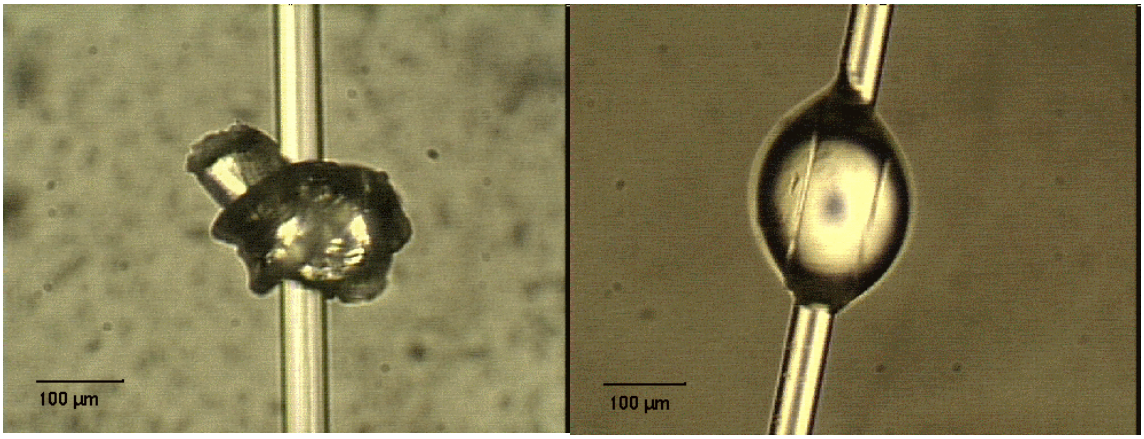

Figure 4.10. Optical micrograph a polystyrene fiber knot on a glass fiber before and after heat treatment 190°C, 20 min.

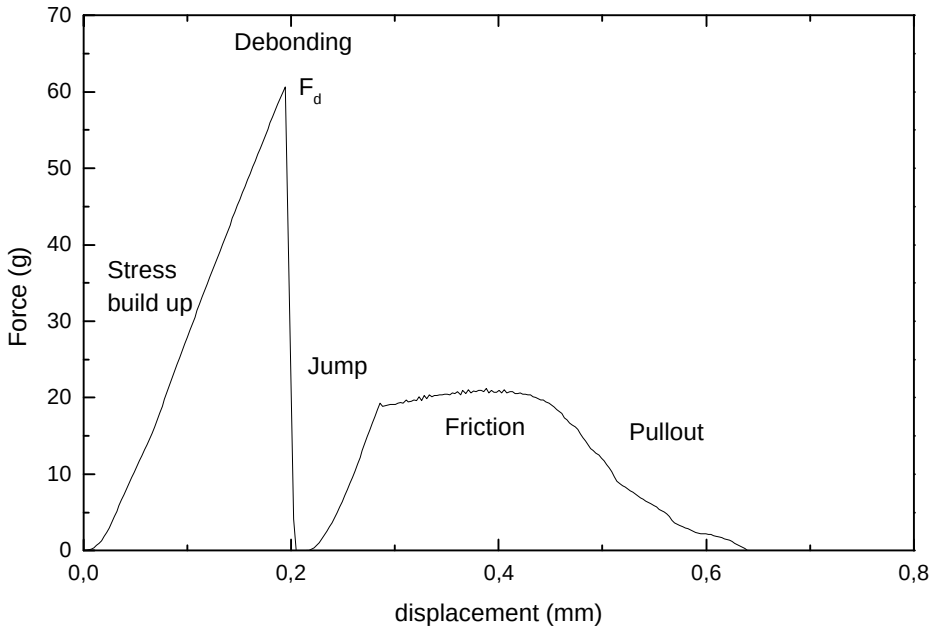

Figure 4.11. Example of a microdebond test for polystyrene. A glass fiber treated with sPB-PS 10 k embedded in a drop of PS with the length (L = 245 µm).

4.3.2 Results and discussion

A typical force/displacement curve for debonding a polystyrene drop from a glass fiber is shown in Figure 4.11. The curve is divided into separate regions. The first region shows a linear force-displacement relationship originating from elastic deformation of the polystyrene drop resulting in increasing stress at the fiber/matrix interface. At the maximum force here denoted as the debonding force (F_d) the stress at the interface has reached so high a value that debonding occurs. After debonding the force falls to zero before it again builds up to a value where the fiber is pulled inside the polystyrene drop. Observing the debonding on the monitor shows that the polystyrene drop jumps along the fiber at debonding. This jump is related to the release of stored elastic energy in the polystyrene accumulated during loading. The force reaches a constant plateau where the drop is pushed along the fiber resisted by friction between the fiber and matrix. This friction induced force decreases as the fiber is pulled out of the polystyrene drop.

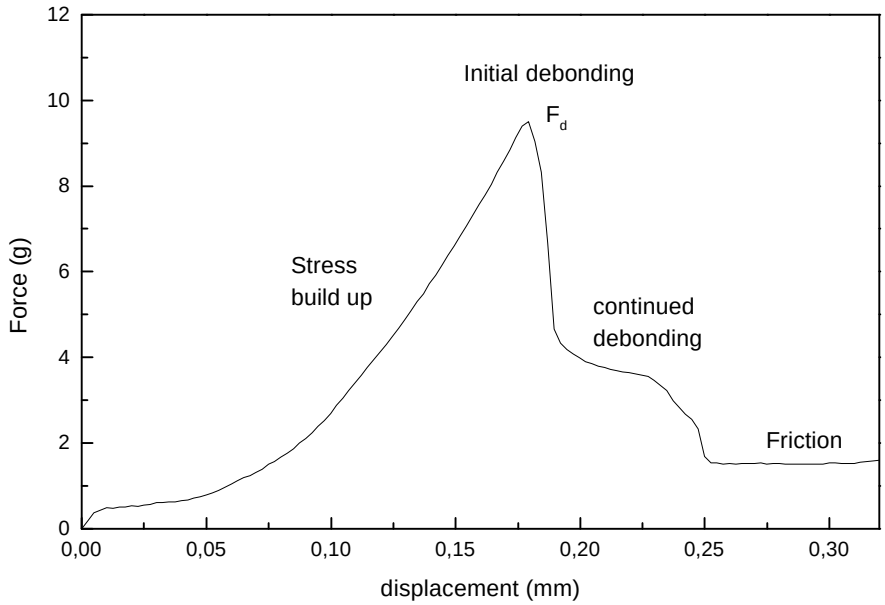

Figure 4.12. Example of a microdebond test for polydimethylsiloxane. A glass fiber treated with sPB-PDMS 10 k embedded in a drop of PDMS with the length (L = 535 µm).

The debonding of a PDMS elastomer drop from a glass fiber shows a sligthly different behavior (Figure 4.12). At the maximum force the PDMS drop starts to debond from the claw-end and the debonding front moves along the fiber as the displacement increased. The rate of debonding is sufficiently slow to observe the moving debonding along the fiber on the monitor. When the drop is completely debonded from the fiber the force reached a plateau as the fiber is pulled through the PDMS drop resisted by friction. This gradual debonding means that the apparent interfacial shear strength calculated using the total fiber-matrix contact area does not reflect the actual interfacial shear strength. The question is, does the same gradual debonding also occur for the much more ridged polystyrene drops but at a much higher rate. Photo-elastic and final element stress analyses on the microdebond geometry done by Herrera-Franco & Drzal (1992), showed that the assumption that the interfacial shear stress is uniformly distributed along the fiber is not true. All analyses showed that the stress profile along the fiber always has a maximum close to the support of the polymer drop. These analyses are in good agreement with the gradual debonding observed for PDMS but should also be considered in the interpretation of the polystyrene debonding experiments. Comparing values of interfacial shear strength on identical systems using different methods, generally show that the lowest values are found using the microdebond method. This could be explained by gradual debonding yielding lower values of interfacial shear strength.
Because of this uncertainty of the debonding mechanism the calculated values are apparent values of interfacial shear strength.

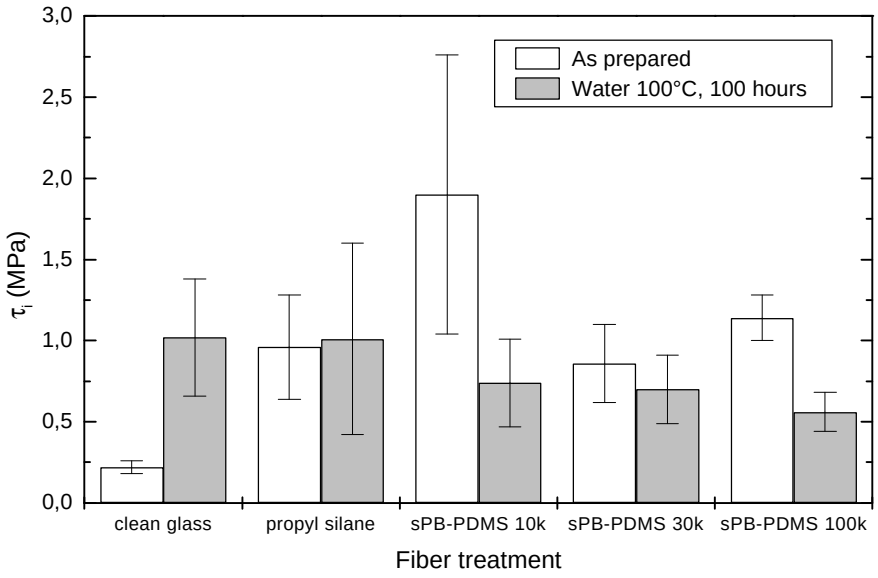

Figure 4.13. Apparent interfacial shear strengths (τ_i) for PDMS microdrops on glass fibers with different surface treatments. Measured before and after exposures to boiling water for 100 hours.

Comparing values of apparent interfacial shear strengths (as prepared) of PDMS drops on glass fibers with different surface treatments (Figure 4.13) shows a significant increase in the fiber/matrix adhesion by silane treatment. The observed effect of the molecular mass of the PDMS tail ends is comparable to the observation done by the JKR method. The lowest molecular mass (sPB-PDMS 10k) gives the highest values of interfacial shear strength, but considering the standard deviation on these measurements (Table 4.2) there are no significant differences between any of the silane treated samples. It is important to state that the hysteresis in the JKR experiments on PDMS/PDMS systems are only observed when the PDMS elastomers have been extracted to remove the PDMS chains that are not covalently bonded to the network. The PDMS elastomer drops in the microdebond experiments have not been extracted, which mean that the results cannot be directly compared.

The values of apparent interfacial shear strength after 100 hours in boiling water reveal a somewhat surprising behavior for the clean glass fibers. The clean glass fibers show a significant increase in apparent interfacial shear strength after exposure to boiling water for 100 hours. This is completely opposite of the expected from experience from other fiber/matrix systems. The general behavior for untreated glass fibers in both thermosetting and thermoplastic matrices is that the interfacial shear strength decreases, as a result of hydrothermal break down of the fiber/matrix interface. Investigation of the glass fiber/PDMS interface using an optical microscope reveals that the interface of the clean fibers/PDMS has become undulated and spreads the light in a diffuse manner as a result of boiling in water for 100 hours.

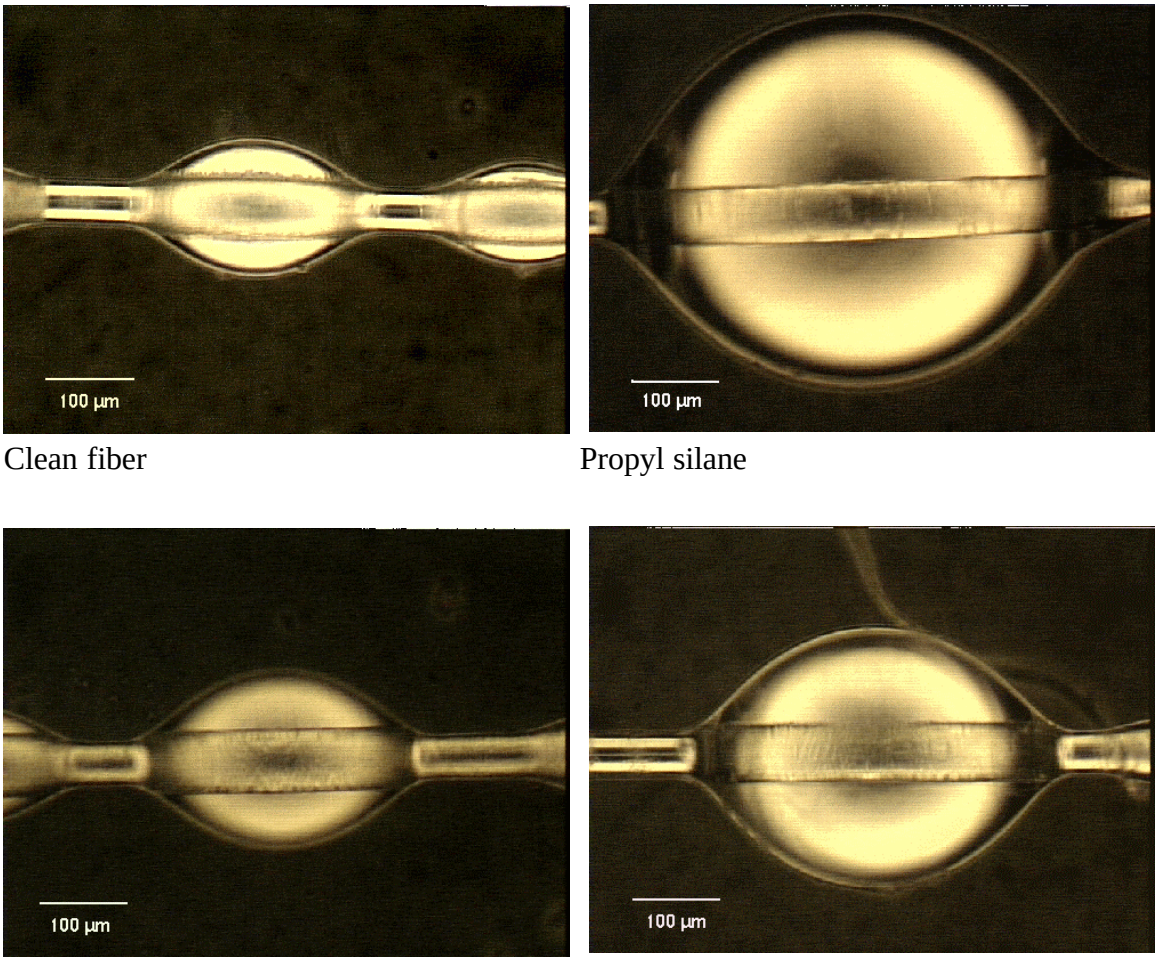

Clean fiber | Propyl silane

sPB-PDMS 30k | sPB-PDMS 100k

Figure 4.14. Optical micrographs of PDMS microdrops on glass fibers with different surface treatments after 100 hours in boiling water.

The optical micrographs of PDMS elastomer drops on glass fibers with different surface treatments after exposure to boiling water for 100 hours are shown in Figure 4.14. The optical micrographs show visual differences in the state of the PDMS/glass interface as a result of hydrothermal attack on interface region. The clean glass fiber sample shows a jagged region around the glass fiber indicating morphology changes at the interface due to corrosion of the glass fiber. Corrosion of glass fibers by ion exchange reaction of alkali and earth-alkali metal ions results in precipitation of alkali and earth-alkali salts at the interface. (Jones & Chandler 1985, Nagae & Otaska 1994 and Schutte 1994). This can explain the increase in apparent interfacial shear strength after exposure in boiling water for the untreated fibers.
Generally, the apparent interfacial shear strengths for PDMS elastomers are very low which is why the effect of a jagged interface region have such relative large effect on the results compared to the protective properties of the silane treatment.

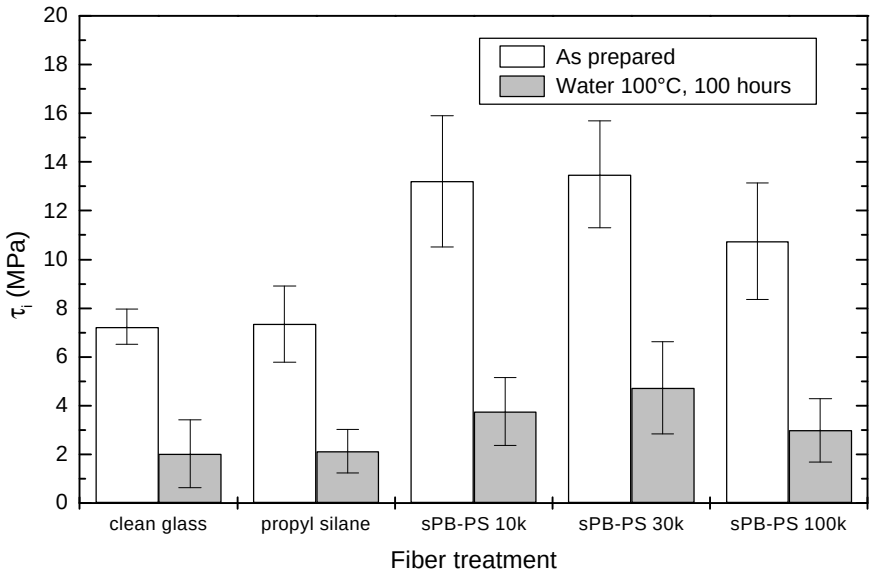

Figure 4.15. Apparent interfacial shear strength for Polystyrene microdrops on glass fibers with different surface treatments. Measured before and after exposures to boiling water for 100 hours.

The polystyrene system shows significantly higher apparent interfacial shear strengths than the PDMS system before boiling Figure 4.15. The measurements show no difference between the clean glass fibers and the fibers treated with n-propyl trimethoxysilane. A significant improvement in apparent interfacial strength is observed for fibers treated with polystyrene block copolymer silanes, but the results show no evidence of improved interface adhesion with increasing molecular mass of the polystyrene tail ends. As discussed before, this could be because the molecular mass of the PS tail end is not sufficiently large compared to the molecular mass between entanglements. Exposure to boiling water reduces the interfacial shear strength to around 30% of the dry strength. The block copolymer silane treated fibers show higher residual strengths compared to untreated and n-propylsilane treated fibers. It should be noted that 100 hours of exposure in boiling water is considerable longer than standard test used for determination of hydrothermal stability of silane coupling agents. The standard is 2 or 5 hours exposure in boiling water compared with non-exposed samples to prove hydrothermal stability of silane coupling agents (Plueddemann 1982). A 100 hours exposure is used here to get closer to the real long term stability, because in 2 hours exposure the diffusion of water through the matrix can be a limitation for the breakdown of the interface. The reduction of the apparent interfacial shear strength to 30% of the dry strength observed in these microdebond experiments shows, that the interface region is damaged by water. The block copolymer silane-coupling agents are not able to prevent water form attacking the fiber and interface region after prolonged exposure at 100°C.

Table 4.2. Apparent interfacial shear strengths (τ_i) for Polydimethylsiloxane (PDMS) and polystyrene (PS) micro-drops on glass fibers with various silane treatments.

Fiber treatment	Matrix polymer	As prepared τ_i (MPa)	100 h Boil, water τ_i (MPa)
Clean glass	PDMS	0,22 ± 0,04	1,0 ± 0,36
Propyl silane		0,96 ± 0,32	1,0 ± 0,59
sPB-PDMS 10k		1,9 ± 0,86	0,74 ± 0,27
sPB-PDMS 30k		0,9 ± 0,24	0,70 ± 0,21
sPB-PDMS 100k		1,1 ± 0,14	0,56 ± 0,12
Clean glass	PS	7,2 ± 0,72	2,0 ± 1,4
Propyl silane		7,4 ± 1,56	2,1 ± 0,9
sPB-PS 10k		13,2 ± 2,7	3,8 ± 1,4
sPB-PS 30k		13,5 ± 2,2	4,7 ± 1,9
sPB-PS 100k		10,8 ± 2,4	3,0 ± 1,3

Although the standard deviations on the apparent interfacial shear strength are large when only measuring 10 samples for each condition, the measurements show significant differences between surface treatments and environmental conditions.

The microdebond measurements appear to be a suitable tool for investigation of hydrothermal stability of different surface treatments. Further optimization of the hydrothermal stability of block copolymer silane coupling agents could be tested using this method. As an example, changing the solvent for the polystyrene based silanes from toluene to dimethyl formamide (DMF) to get better surface coverage according to the discussion of the AFM and contact angle measurements (chapter 3.6 & 7). Another method to achieve better hydrothermal stability of the block copolymer coupling agents would be to exchange relatively hydrophilic triethoxysilane group with a more hydrophobic silane group. Kirkland & Henderson (1994) have studied the hydrothermal stability of different C_{18} silane coupling agents for HPLC silica columns. They found that the optimum hydrothermal stability was achieved by using mono functional silanes with two bulky side-groups on the silicon atom like isopropyl or isobuthyl. They explained this by steric protection of the siloxane bond to the surface.

4.4 Summary on interface characterization

Two different methods have been used to investigate the influence of block copolymer silane coupling agents on the interface properties.
The JKR method has successfully been used to investigate the thermodynamical work of adhesion between PDMS elastomers and block copolymer silanes attached on oxidized silicon. The JKR measurements showed significant hysteresis when compressing an extracted PDMS elastomer network against oxidized silicon treated with block copolymers containing PDMS tail blocks. The hysteresis is analogous to the hysteresis observed by compressing bulk PDMS against bulk PDMS. The extent of the hysteresis measured by the strain energy release rate appears to be dependent on the local pressure applied during contact. But the origin of this enhanced interface adhesion is still not completely understood. The measurements showed no indications of increased adhesion by increasing molecular mass of the PDMS tail ends. A JKR apparatus have been build at Risø for further investigations.
A microdebond apparatus has been built using a dynamic mechanic spectrometer and methods have been developed to measure apparent interfacial shear strength for both thermosetting and thermoplastic matrixes on glass fibers. Microdebond experiment using an elastomer PDMS matrix revealed a gradual debonding for the glass fiber in agreement with the stress profile along the glass fiber calculated by Herrera-Franco and Drzal (1992). This observation can question the method of calculating interfacial shear strength from microdebond experiments. The microdebond experiments using a relative small number of samples (10 samples for each condition) showed significant differences in apparent interfacial shear strength as a function of surface treatment. The experiments also showed a reduction in apparent interfacial shear strength after exposure in boiling water for 100 hours. This show that despite the structural advantage block copolymer silanes are not capable of protecting the interfacial region form hydrolysis. Considering the structure of polybutadiene hydrosilylated with triethoxysilane on a glass surface, it is plausible that the structure contains a surplus of Si-OEt or Si-OH groups that are not covalent bonded either to the surface or to neighboring silanes. The existence of such groups will enhance the hydrophilic nature of the silane layer making penetrations of water molecules easy. All block copolymer silane coupling agents resulted in enhanced interfacial adhesion, but no difference were found by varying the molecular mass of the tail end.
No evidence was found for enhanced interfacial adhesion by increasing the molecular mass of grafted polymer chains above the molecular mass of entanglement for bulk. This could be because the molecular mass of the tail end is not sufficiently high to form real entanglement with the bulk phase. But this has to be tested by applying even higher molecular mass of the block copolymer tail end.

5 Hydrothermal aging of PPS and PA66 glass fiber filled composites

5.1 Introduction

This chapter is a brief description of a separate project that has been running parallel to the work on block copolymer silane coupling agents. The project is a collaboration between two industrial companies (Danfoss A/S and Grundfos A/S) and the Department of Condensed Matter Physics and Chemistry, Risø National Laboratory. The project has been established as an industrial project under the Danish Polymer Center, with the aim to show the status of the thermoplastic composite industry with respect to hydrolysis stability of “state of the art” glassfiber reinforced thermoplastic composites

The main goal of the project is to investigate the hydrothermal aging of short glass fiber filled polyphenylensulphide (PPS) and poly(hexamethylene aldipamide) (PA66) composites and through this work to achieve a better understanding of the aging mechanisms of glass fiber filled thermoplastics in hot water. The investigation is carried out by exposing injection-molded composites to water with different pH values at various temperatures. Mechanical properties of the exposed samples are measured as a function of exposure time, pH and temperature.

Hydrothermal stability of glass fiber has recently been reviewed by Shutte (1994). Kloos (1985) has examined the hydrothermal stability of glass fiber reinforced PPS in water at various temperatures. Valentin et al. (1987) have studied the stability of glass fiber PA66 at various temperatures and relative humidity levels. The main conclusion of these studies is that the break down of the interface region caused by hydrothermal attack is the main reason for reduction in mechanical properties in connection with exposure in hot water.

The outline of this chapter is to show selected results for this project to illustrate the main conclusions drawn from the investigation. The full description of the project is given in two technical reports in Danish: Jensen & Madsen (1998) and Larsen & Madsen (1998) given as appendices for this thesis.

5.1 Experimental

5.1.1 Materials

Polyphenylensulfide (PPS): The PPS composite materials used for this investigation are Ryton BR 4-220 NA and Ryton R-4XT from Philips Petroleum Chemicals. Both materials are linear PPS with 40 wt.% E-glass fibers. Ryton BR 4-220 NA is a recently developed material with improved hydrolysis stability compared to Ryton R-4XT. As a reference-material, unfilled linear PPS is used.

Polyamide 66 (PA66): The PA66 composite materials used for this investigation are Zytel 70G30 HSR3 309BK, Zytel 70G30 HSL2 and Zytel 122 from DuPont. The first two are black materials with 30 wt. % E glass fibers. Zytel HSR3 is optimized for hydrothermal stability. Zytel 122 is an unfilled, uncolored and hydrolysis stabilized.

All materials are injection molded according to specifications into a dumbbell tensile test specimen ASTM standard type IV.

5.1.2 Aging in water

The conditions for exposure of the composites are given in Table 5.1-2.

Table 5.1. Exposure conditions for PPS composites (Ryton BR 4-220 NA and R-4XT)

Medium	Temperature [C°]	Exposure time [h]
H_2O pH 7	90	0, 100, 300, 1.000, 3.000, 9.000
(phosphate-buffer system)	125	“
	140	“
H_2O pH 9	90	“
(Hydro-X buffer system)	125	“
	140	“
H_2O pH 12	90	“
(phosphate-buffer system)	125	“
	140	“
Air	140	“

Table 5.2. Exposure conditions for PA66 materials. (Zytel 70G30 HSR3 309BK, Zytel 70G30 HSL2 and Zytel 122.

Media	Temperature [C°]	Exposure time [h]
H_2O pH 7	70	0,300, 1.000, 3.000, 7.600
(phosphate-buffer system)	90	"
	110	"
H_2O pH 9,8 *	70	"
(Hydro-X buffer system)	90	"
	110	"
H_2O pH 12 *	70	"
(phosphate-buffer system)	90	"
	110	"

* Only Zytel 70G30 HSR3 309BK

5.1.3 Analyses

PPS materials:
Tensile tests were carried out on a Shenck tensile test machine with an Instron 2626/601 extensiometer. The speed of elongation was 1 mm/min in the strain interval from 0-0.3% and then 5 mm/min till break. The Young's modulus, tensile strength and elongation to break were measured for 5 test specimens for each condition.
Impact strength was measured using the Charpy method on a Zwick & Co impact test machine with a 5 kpcm pendulum hammer. The impact strength was calculated as a mean value of 10 test specimens.
Dynamical mechanical torsion tests were carried out on a RMS 800 dynamical mechanical spectrometer from Rheometric Scientific. The measurements were performed with increasing strain from 0.1-2 % at 40°C with a torsion frequency of 1 Hz. The shear modulus (G´) and the loss modulus (G´´) were measured as function of applied strain for three consecutive runs for each test specimen.
Scanning electron microscopy (SEM) of the fracture surfaces was preformed on selected test specimens to relate the modus of failure to the mechanical properties. Light microscopy and low vacuum SEM was performed on the surfaces of selected test specimens.
Various analytical methods were used to investigate the sizing on the glass fibers used in the two different PPS materials (see Jensen & Madsen 1998).

PA66 materials:
Tensile tests were carried out on an Instron tensile test machine. The speed of elongation was 1 mm/min in the strain interval from 0-0.5% and then 5 mm/min till break. The Young's modulus, tensile strength and strain were measured for 5 test specimens for each condition. The water content in the samples was normalized by keeping the samples in water at 40°C in the period from the end of exposure to the performance of tensile test. The tensile tests were preformed at 40°C at ambient humidity.
Dynamic mechanical torsion tests were carried out on a RMS 800 dynamical mechanical spectrometer from Rheometric Scientific. The measurements were performed with increasing strain form 0.1-2 % at 40°C with a torsion frequency of 1 Hz. The Shear modulus (G´) and the loss modulus (G´´) were measured as a function of applied strain for three consecutive runs for each test specimen.
The molecular mass distribution of the PA66 was measured using gel permeation chromatography (GPC) for selected test specimens. GPC analyses of PA66 were performed at 50°C using a three column system (Nucleosil 1000 –OH, 300 –OH, 100 –OH form Macheray-Nagel) connected to a Knaur Refractive index detector. The eluent was pure hexafluoroisopropanol (Fluorochem ltd.). The samples were dissolved in hexafluoroisopropanol and filtered before injection. The molecular mass distribution was found by calibration with a series of polyethylenglycols with known molecular mass.
Scaning electron microscopy (SEM) was performed on the fracture surfaces of selected test specimens to relate the modus of failure to the mechanical properties.

5.2 Results and Discussion

The results are divided with respect to the matrix material because of the slightly different aging mechanisms observed in the two systems. Furthermore, only the results for the two materials from each matrix system optimized with respect to hydrolysis are presented. Results from reference materials are only presented in order to clarify the breakdown mechanisms for the optimized materials.

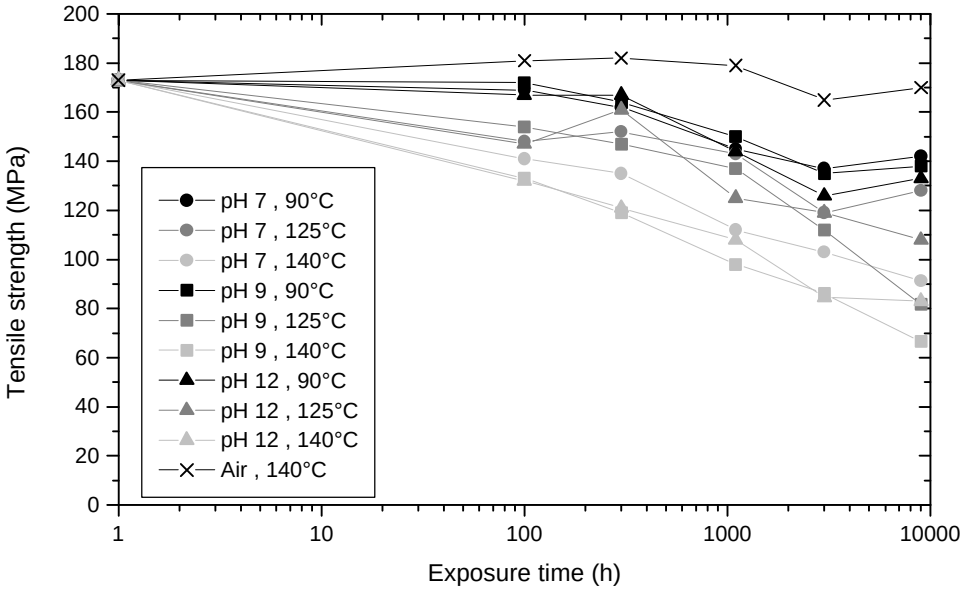

Figure 5.1 Tensile strength of Ryton BR4 220NA as a function of exposure time in different media.

5.2.1 PPS composites

All measured mechanical properties for the PPS composites decrease as a result of long time exposure in hot water. The object of interest is the rate of decrease of the mechanical properties, and the actual time dependence of the mechanical properties. The time dependence of the tensile strength of Ryton BR4 220NA is shown in Figure 5.1. For all temperatures and pH values tested an approximately linear dependence with the logarithm of the exposure time is found. This shows that the decrease in tensile strength is largest in the beginning of the exposure and the rate of decrease falls with the exposure time. This kind of hydrothermal break down behavior makes it possible to predict the tensile strength at a certain time within an acceptable uncertainty, because no sudden or catastrophic breakdown occurs. It is clear from Figure 5.1 that the rate of hydrothermal breakdown is related to the water temperature. The rate of hydrothermal breakdown increases with increasing water temperature. On the other hand, there is no obvious relation between the pH value of the water and the rate of breakdown. After 9000 hours (approx. 1 year) the tensile strength calculated as an average for all pH values are reduced to 80% at 90°C, 60% at 125°C and to 45% of the initial value at 140°C. Comparing the results from hydrothermal aging with the values from test species aged in air at 140°C, clearly shows that the reduction of tensile strength is related to the presence of water. After an exposure in air at 140°C in up to 9000 hours the tensile strength does not change within the uncertainty of the measurements.

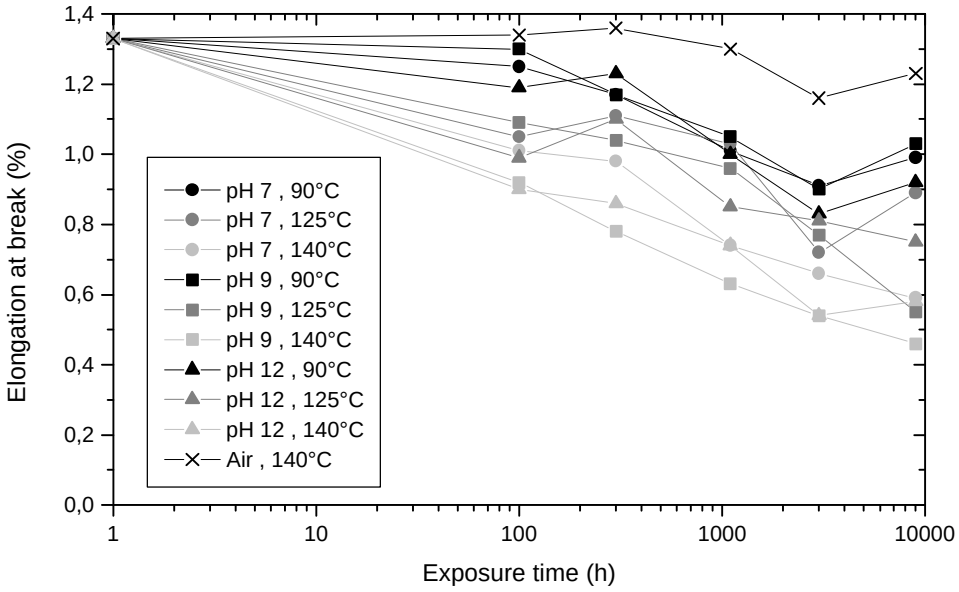

Figure 5.2. Elongation at break for Ryton BR4 220NA as a function of exposure time in different media.

The elongation at break as a function of exposure time (Figure 5.2) shows the same pattern as the tensile strength. The tensile strain after 9000 hours are reduced to 75% at 90°C, 55% at 125°C and 40% at 140°C of the initial value.

The pattern for the impact strength as a function of exposure time (Figure 5.3) is the same as for the tensile tests. The impact strength after 9000 hours is reduced to 75% at 90°C, 50% at 125°C and 40% at 140°C of the initial value.

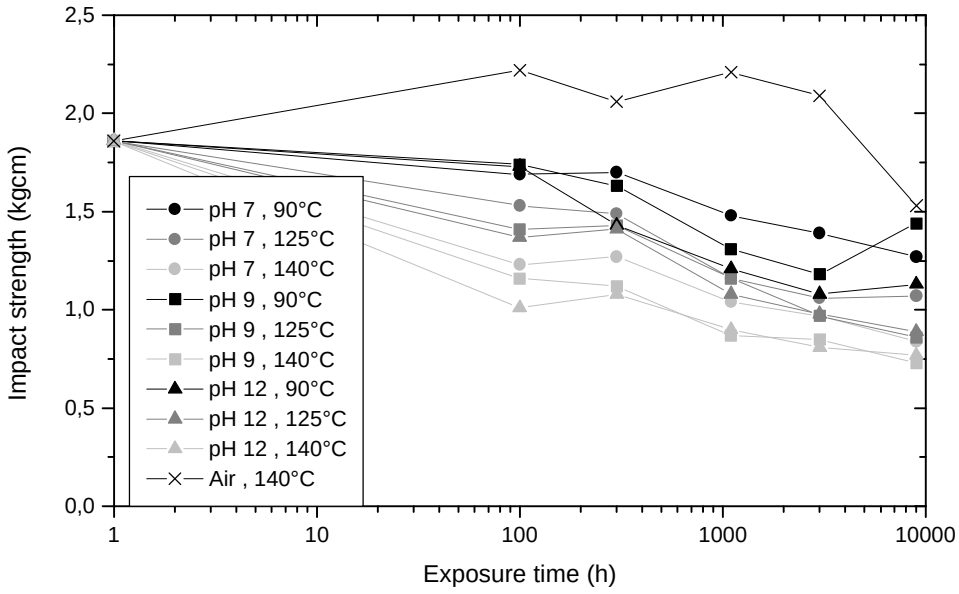

Figure 5.3. Impact strength for Ryton BR4 220NA as a function of exposure time in different media.

Examples of dynamic mechanical torsion tests are shown in Figure 5.4. The tests are performed by increasing the strain from 0.1 to 2 %. This applied strain is not sufficient to cause visible fracture in the material. The shear modulus (G') and the loss modulus (G'') are measured as a function of applied strain. The strain sweep is repeated three times for each sample. The pure PPS sample show an approximately linear shear modules strain relationship with no change in modulus as a function of strain. Repeating the strain sweep does not change the relationship at all. The unexposed glass fiber filled Ryton BR4 220NA show a clear nonlinear behavior, the shear modulus decreases with increasing strain. The curves also reveal difference between first and second strain sweep. The nonlinear behavior and the modulus difference ($\Delta G'$) is clearly related to the presence of glass fibers in the material. The irreversible modulus difference ($\Delta G'$) can originate from two processes in the material: Fiber-break or interfacial debonding between fibers and matrix. The modulus difference ($\Delta G'$) clearly increases as a result of exposure in water. It is assumed that the loss of shear modulus is a result of interfacial debonding resulting in decreased stress transfer from matrix to fibers. The debonding occur at the first strain sweep resulting in a decreased shear modulus in the consecutive strain sweeps.

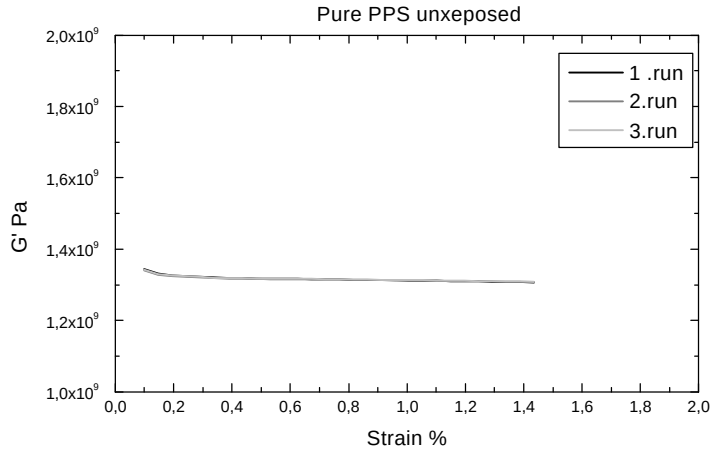

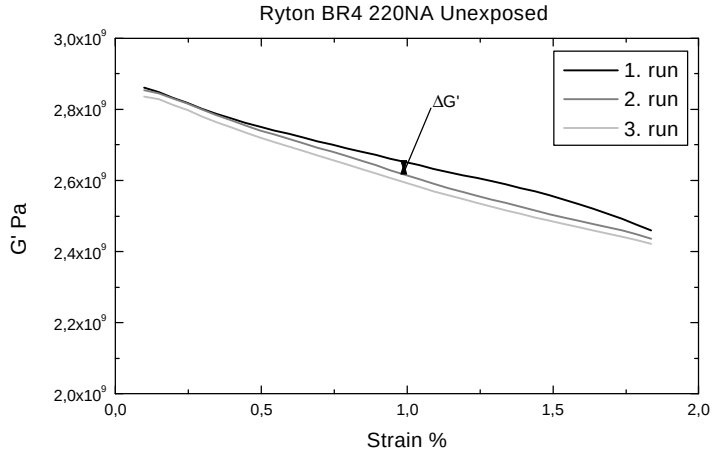

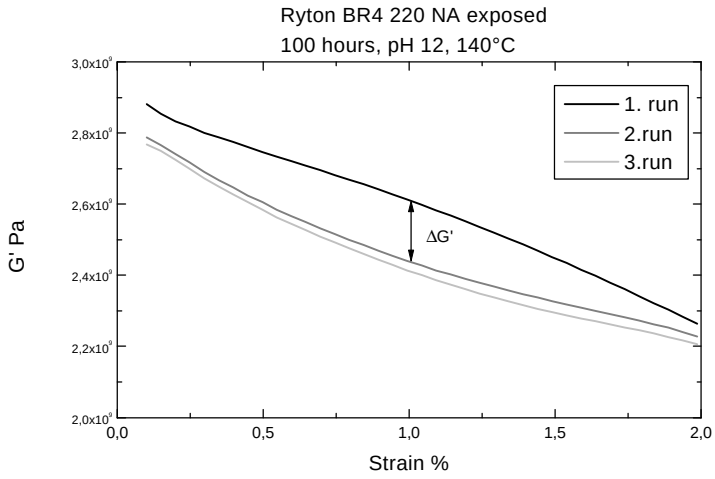

Figure 5.4. Examples of dynamic mechanical torsion tests.

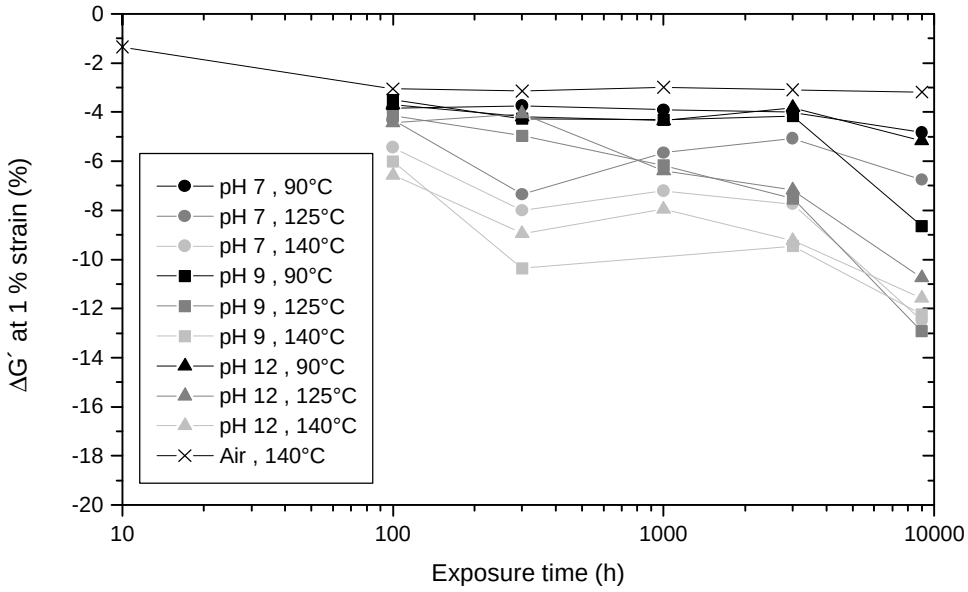

Figure 5.5. Difference in shear modulus (ΔG´) between 1. and 2. strain sweep measured at 1% strain for Ryton BR4 220NA as a function of exposure time in different media.

Plotting the difference in shear modulus (ΔG') measured at 1 % strain as a function of exposure time in water at different conditions (Figure 5.5) show the same pattern as for the tensile and the impact tests. The extent loss in shear modulus loss is primarily correlated to the water temperature.

The dynamical mechanical method measures both the real (G') and the imaginary (G'') parts of the shear modulus. The real part (G') is the modulus for the stress in phase with the applied strain and the imaginary part (G'') is the modulus for the stress 90° out of phase with the applied strain. The imaginary part of the modulus (G'') is often referred to as the viscous or loss modulus because it is related to the part of the mechanical energy that is dissipated in the material during testing. The ratio between the real and the imaginary part of the modulus is measured by measuring the phase shift (δ) between the applied strain and the measured stress. The ratio is determined as G''/G' = tan(δ). Tan(δ) is referred to as the energy dissipation factor. Tan(δ) measured at 1 % strain is plotted in Figure 5.6 as a function of exposure time.

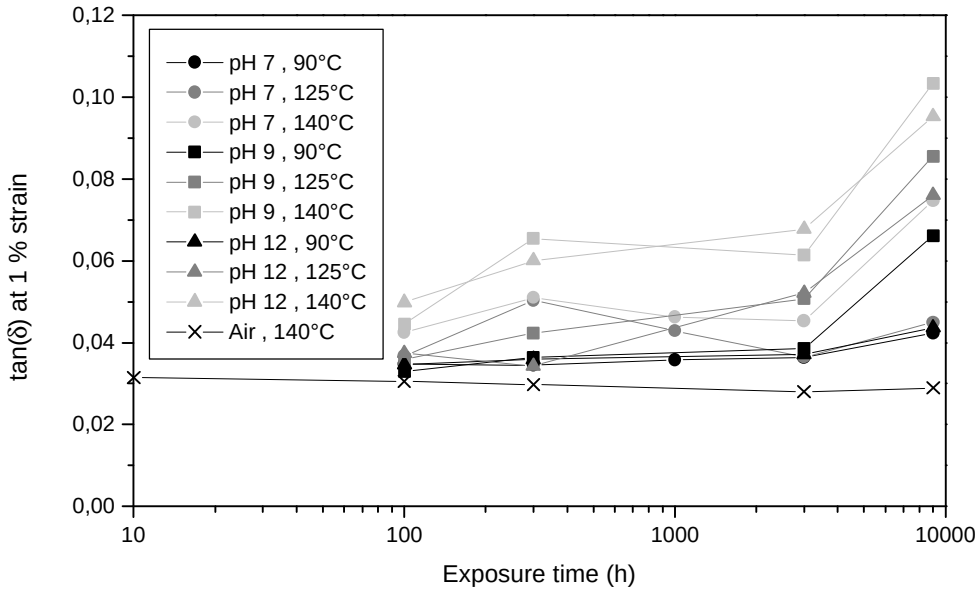

Figure 5.6. tan(δ) measured at 1% strain for Ryton BR4 220NA as a function of exposure time in different media.

The energy dissipation factor tan(δ) shows approximately the same pattern as all the other mechanical methods applied here.
Zorowski & Murayama (1972) put forward a simplified theory for the energy dissipation in polymer composites based on the following relationship (5.1):

$$\tan(d)_{comp} = \tan(d)_s + \tan(d)_{in} \qquad (5.1)$$

where $\tan(\delta)_{comp}$ is the measured energy dissipation for a polymer composite, $\tan(\delta)_{in}$ is the internal energy dissipation due to poor adhesion at the interface, which can be used for evaluating the interfacial adhesion, $\tan(\delta)_s$ is the ideal energy dissipation for a composite with perfect interfacial adhesion as defined by (5.2):

$$\tan(d)_s = \frac{\tan(d)_f G_f V_f + \tan(d)_m G_m V_m}{G_f V_f + G_m V_m} \qquad (5.2)$$

where G is the shear modulus and V is the volume fraction of the fiber and matrix. This theory has been applied by Gu et al. (1995) in investigations of different surface treated glass fibers in a epoxy matrix using vibrational damping. They found the highest $\tan(\delta)_{in}$ values for untreated

glass fibers as expected. Furthermore they found a monotone relationship between $\tan(\delta)_{in}$ and the transverse tensile strengths of the composites.
This theory (5.1) shows that the energy dissipation is closely related to the fiber/matrix adhesion. The increasing $\tan(\delta)$ values with exposure in water at high temperatures (Figure 5.6) can, in the light of this theory, be explained by interfacial break down resulting in higher energy dissipation at the interface region.

Scanning electron micrographs of the fracture surfaces from the tensile tests are shown in Figure 5.7. The fracture surface from a tensile test of an unexposed Ryton BR4 220NA composite shows a glass fiber still completely embedded in PPS matrix material. This indicates cohesive failure and not interfacial failure. The fibers appear to be fractured very close to the matrix fracture plane indicating a minimum of fiber pull out. Together, these observations indicate good fiber matrix adhesion.
The fracture surface of the composite aged in air at 140°C for 1000 hours also shows indication of cohesive failure. This sample also shows very limited fiber pullout on other micrographs.
The sample exposed in water at 140°C, pH 12 for 1000 hours shows apparently clean fibers indicating interfacial failure. The fiber fractures also appear to be away from the matrix fracture plane indicating some extent of fiber pullout during fracture.

By comparing the results form all the applied techniques, the hydrothermal aging of Ryton BR4 220NA is primarily found to be related to hydrothermal break down of the interface region between the glass fibers and the PPS matrix.

a) Unexposed

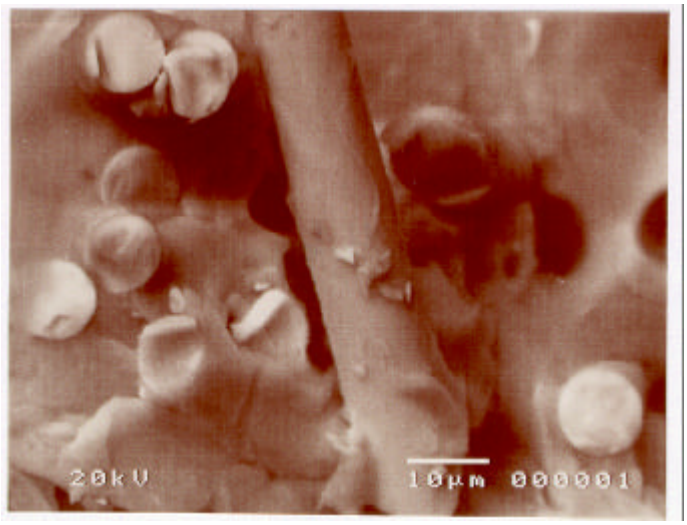

b) Exposed in Air at 140°C
for 1000 hours.

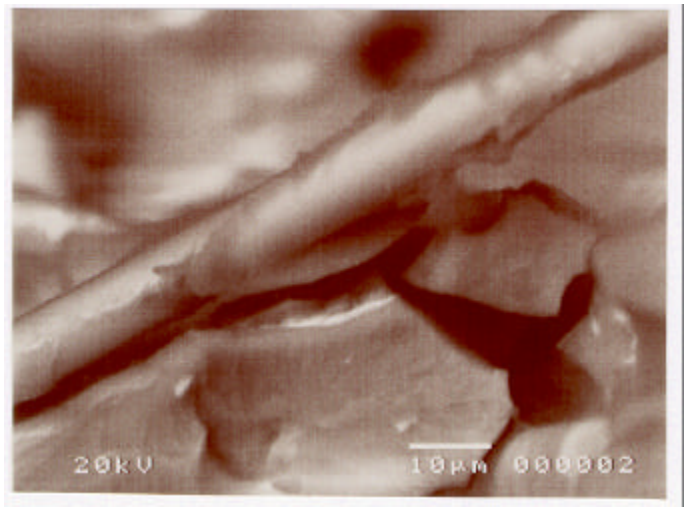

c) Exposed in Water, pH 12
at 140°C for 1000 hours.

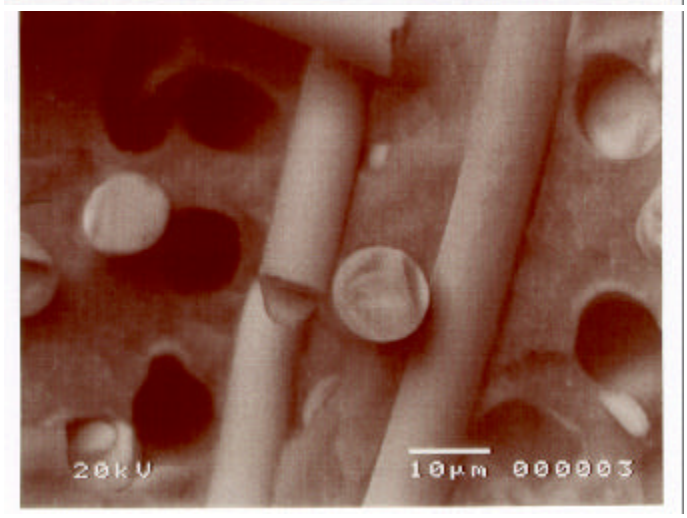

Figure 5.7. SEM micrographs of fracture surfaces from tensile tests of Ryton BR4-220 NA composites after different exposures.

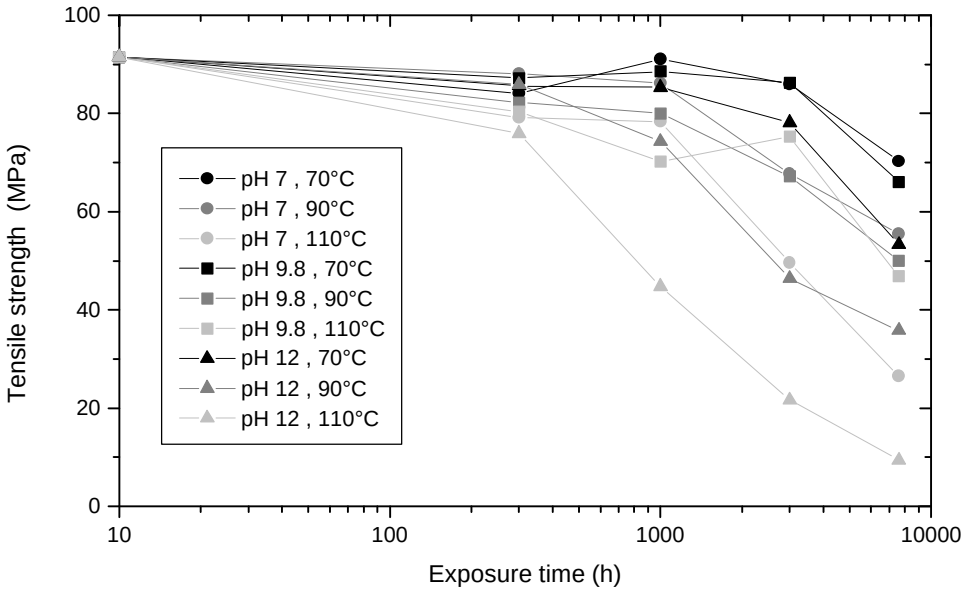

Figure 5.8. Tensile strength of Zytel 70G30 HSR3 309BK as a function of exposure time in water at various temperatures and pH values.

5.2.2 PA66 composites

The tensile strength of polyamide 66 glassfiber reinforced composite Zytel HSR3 (Figure 5.8) shows a different time dependence from that of the PPS composites. The tensile strength as a function of exposure time decreases at a slow rate until a certain time where the curve kinks and the tensile strength decreases more rapidly. The time at which the time curve kinks is dependent on both the temperature and the pH value of the water. This indicates that the mechanism for hydrothermal break down is different for the PA66 composites compared to PPS composites. The major difference between the two matrix polymers is that PA66 has a much higher water content in equilibrium with liquid water than PPS, and that PA66 is sensitive to hydrolysis in hot water.
As expected the decrease of tensile strength is a monotone function of the water temperature. The tensile strength as function of the pH value shows the largest reductions at pH 12 for all temperatures indicating that the hydrothermal break down of the PA66 composites is sensitive to the pH value of the water in contrast to observations for the PPS composites.

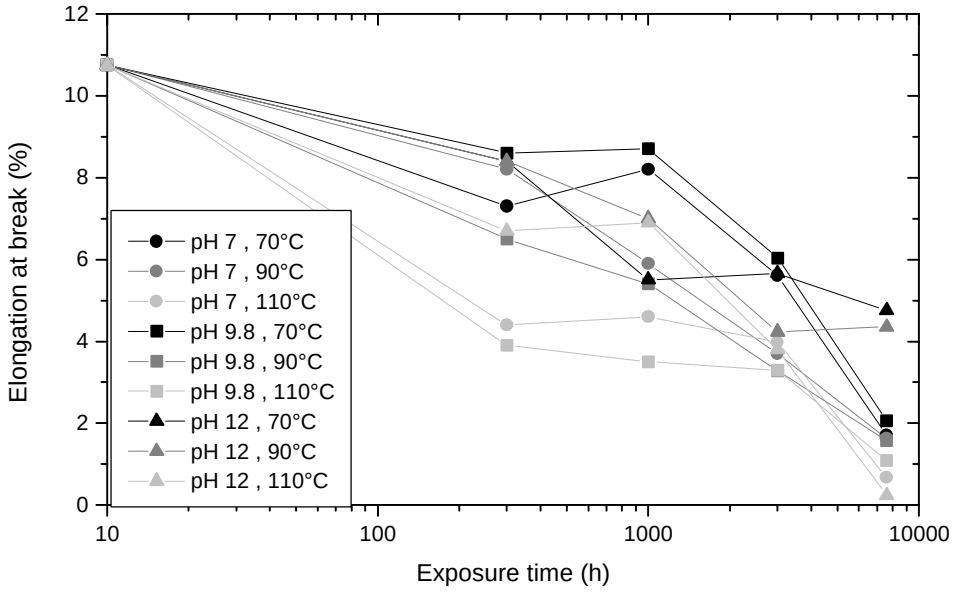

Figure 5.9. Tensile strain for Zytel 70G30 HSR3 309BK as a function of exposure time in water at various temperature and pH.

The time dependence of the elongation at break for the PA66 composites also shows a more severe reduction than for the PPS composites. After 7600 hours, the elongation at break has been reduced to critically low values except for the two samples exposed at 70 and 90°C at pH 12. The reduction of tensile strain is also dependent on the water temperature. The measured tensile properties and especially the elongation at break are extremely sensitive to the actual content of water in the samples at the time of testing. It is possible that the scattering of the tensile strength measurements is caused by insufficient time to normalize the water content at 40°C.

Scanning electron micrographs of the fracture surfaces of Zytel HSR3 unexposed and exposed in water at 110°C, pH 12 for 3000 hours are shown in Figure 5.10. The unexposed sample clearly shows cohesive failure while the exposed sample clearly shows interfacial failure. The pictures show that the interfacial adhesion is reduced to a minimum by hydrolysis of the interface region. This is in full agrement with the statement from the materials supplier (DuPont) concerning these materials:

"*Breakdown of the glass-nylon bonding is the single main cause of loss of properties with exposure to hot aqueous solutions.*"

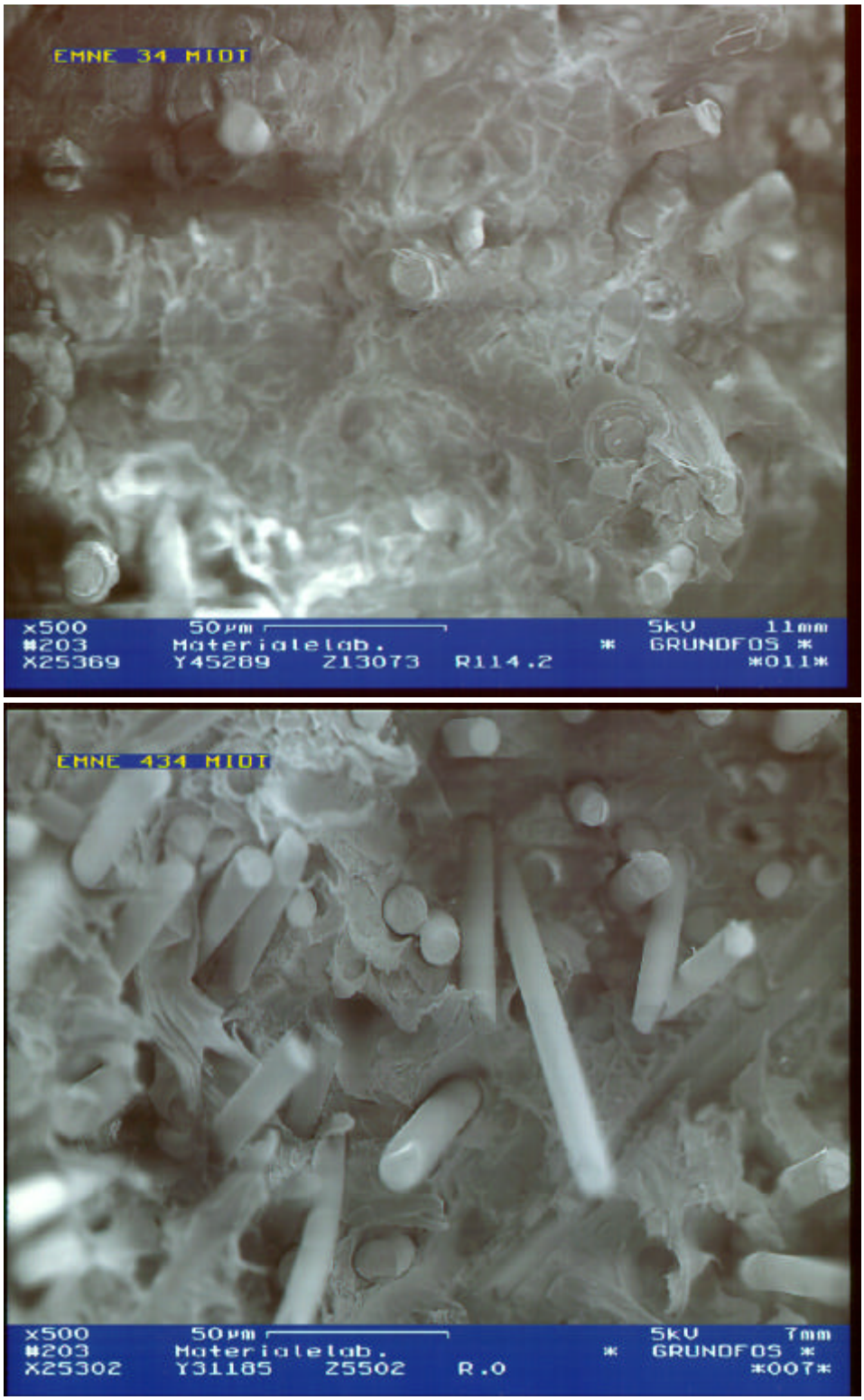

Figure 5.10. Scanning electron micrographs of the fracture surfaces of Zytel 70G30 HSR3 BK308 form tensile tests. *Upper*: Unexposed. *Lower*: Exposed in water at 110°C, pH 12 for 3000 hours.

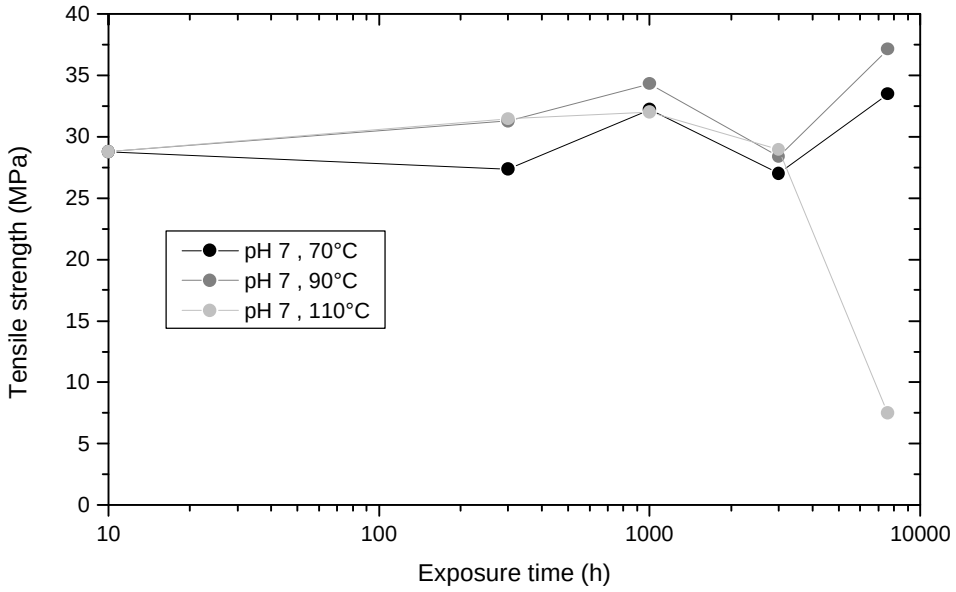

Figure 5.11. Tensile strength of Zytel 122 (PA66 without glass fibers) as a function of exposure time in water at various temperature and pH.

The tensile strength of the unfilled PA66 as a function of exposure time in water pH 7 at increasing temperature is shown in Figure 5.11. The figure shows that the tensile strength is not changed significantly with exposure time except when exposed at 110°C. The point for 7600 hours at 110° only represents one sample because the other four samples were so brittle that they broke during handling.

This observation increased the effort to determine the molecular mass distribution of these samples. The molecular mass distribution of these samples are interesting because they can reveal at what critical average molecular mass the PA66 matrix becomes brittle and looses mechenical strength. Efforts made at Grundfos A/S to determine the molecular mass distributions using high temperature GPC with meta-cresol as eluent gave no results. It was therefore chosen to explore the possibility to use hexafluoroisopropanol as eluent for ambient temperature GPC, because hexaflouroisopropanol is a good solvent for PA66 at room temperature.

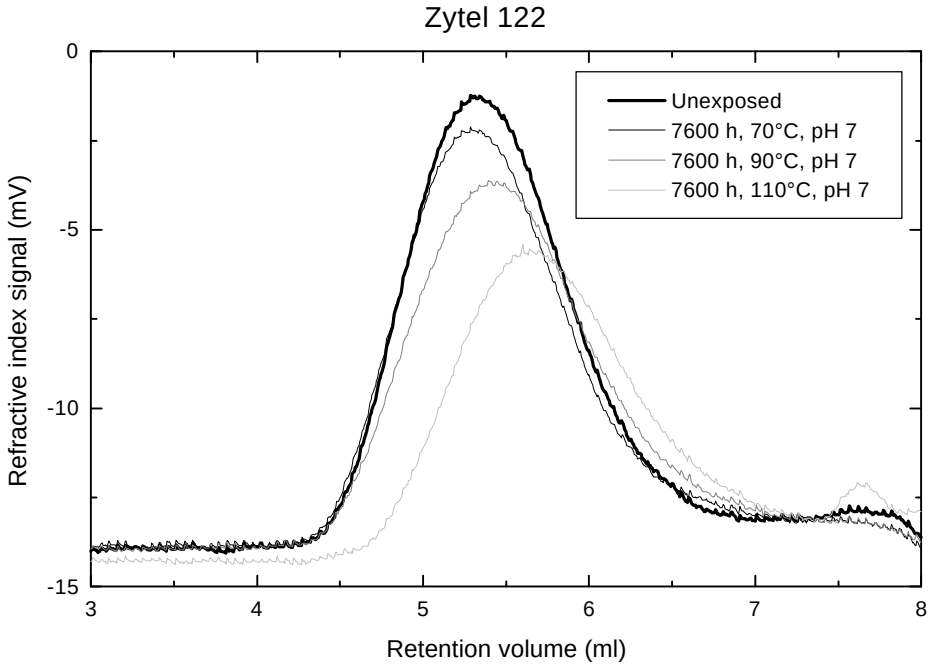

Figure 5.12. GPC analyses of Zytel 122 (PA66 without glass fibers) exposed in water for 7600 hours at different temperatures.

The gel permeation chromatograms of the pure PA66 dissolved in hexaflouroisopropanol are shown in Figure 5.12. The chromatogram should be interpreted as for all gel permeation chromatograms with pure size exclusion: higher retention volume corresponds to lower molecular mass. Figure 5.12 shows that the hydrolysis of PA66 is strongly dependent on the water temperature. By calibrating the chromatograms with a series of polyethylenglycols (PEG) with know molecular mass and polydispersity, it is possible to calculate average molecular masses for the PA66 samples expressed in PEG-units. The average molecular mass calculated from the peak positions with respect to PEG are shown in Table 5.3.

Table 5.3. Average peak molecular masses from GPC calculated by standard calibration with polyethylene glycol. Unexposed M_p = 21000 g/mol.

Zytel 122 exposed in water pH 7, 7600 h at	M_p g/mol.
70°C	21000
90°C	16000
110°C	9000

Comparing the calculated molecular masses with the tensile strengths in Figure 5.11, it is seen that a reduction of the molecular mass for 21000 to 16000 g/mol does not effect the mechanical properties, while a reduction from 16000 to 9000 g/mol has a tremendous effect on the mechanical properties. When the molecular mass is below a critical value the chain length in the amorphous regions between the crystallites is no longer sufficiently long to form entanglements. This results in loss of tensile strength and the material become very brittle.
This critical molecular mass is important for the interpretation of the tensile tests of the glass fiber reinforced samples, because the mechanical properties change so dramatically below this value.

The GPC analyses the glassfiber reinforced PA66 material exposed for 7600 hours in water at 110°C with various pH values are shown in Figure 5.13. The GPC analysis show an extensive reduction of the molecular mass as a result of the hydrothermal aging.

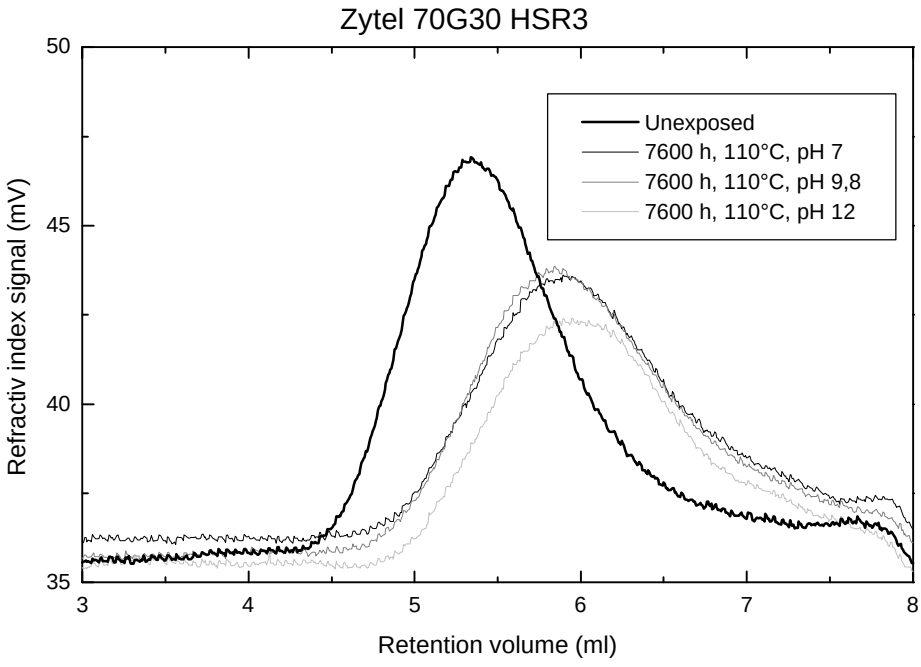

Figure 5.13. GPC analysis of Nylon 66 with 30% glass fibers as a function of the pH value of the water it has been exposed in.

Table 5.4. Average peak molecular masses from GPC calculated by standard calibration with polyethylene glycol. Unexposed M_p = 18000 g/mol.

Zytel HSR3 exposed in water 110°C, 7600 h	M_p g/mol.
pH 7	4300
pH 9,8	4900
pH 12	3700

The average molecular masses in Table 5.4 shows that the value after 7600 hours exposure at 110°C is below the critical value observed for the pure PA66 material. This observation is in good agreement with the very low tensile strain values for these materials (Figure 5.9). The effect of the pH value of the water does not appear to follow a trend, but the lowest molecular mass is observed for the highest pH value. The hydrolysis reaction of PA66 (1) is like most hydrolysis reactions both catalyzed by strong bases and acids.

(1) $\sim C\text{-}(CH_2)_4\text{-}CONH\text{-}(CH_2)_6\text{-}NH\sim + H_2O \rightarrow \sim C\text{-}(CH_2)_4\text{-}COOH + H_2N\text{-}(CH_2)_6\text{-}NH\sim$

So it should be expected that the largest reduction in molecular mass is found at the highest pH values as observed.

The time dependencies of the molecular masses for pure and reinforced PA66 are shown in Figure 5.14. The curve for the unfilled PA66 (Zytel 122) show that the molecular mass is unchanged up to 1000 hours exposure, after which it decreases rapidly. As mentioned in the experimental section, Zytel 122 is hydrolysis stabilized. The time dependence of the molecular mass change shows that Zytel 122 is hydrolysis stabilized, but that the hydrolysis stabilizer is either used up or washed out of the material after long exposure at 110°C. This shows that hydrolysis of the PA66 matrix in not only dependent on the rate of the hydrolysis reaction (1), but also dependent on the rate at which the hydrolysis stabilizer is removed from the matrix. The mechanism for removal of the hydrolyses stabilizer is unknown, because the chemical identity of such stabilizers is kept as internal know-how by the materials suppliers.

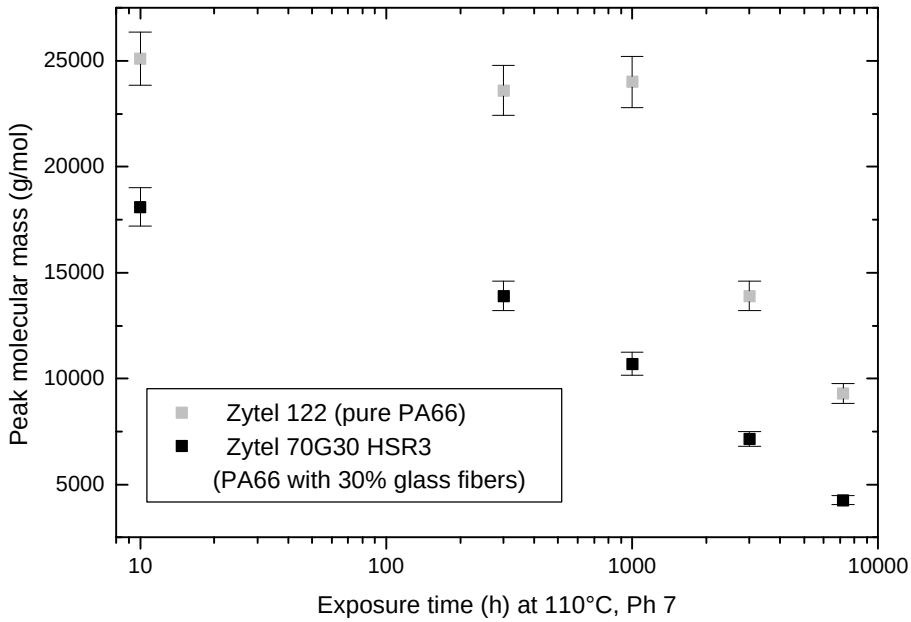

Figure 5.14. Average peak molecular masses from GPC analysis for PA66 materials as a function of exposure time in water at 110°C, pH 7. The time for the unexposed was set to 10 hours.

Figure 5.14. clearly illustrates that the used hydrolysis stabilizers can delay but not prevent hydrolysis of the matrix material.
The glass fiber reinforced material Zytel HSR3 show a much shorter, if any, time where the PA66 is stabilized against hydrolysis. The molecular mass of the reinforced matrix falls faster below the critical molecular mass then observed for the unfilled material. This can be illustrated with the observation that the last two samples are very easy to break by hand.

In conclusion, from the hydrothermal aging studies of PA66 composites the following should be stated:

The loss of mechanical properties for PA66 composites exposed in hot aqueous solution is caused by hydrolyses of the interfacial region and by hydrolyses of the matrix polymer.

5.4 Conclusions

These investigations have shown that hydrothermal aging is a severe problem for the use of glassfiber reinforced thermoplastic composites in hot water applications.

The investigated of glassfiber reinforced PPS composites show a single aging mechanism making long term prediction of the mechanical properties possible. Dynamic mechanical torsion tests and scanning electron micrographs show that the loss of mechanical properties are caused by hydrolysis of the interface between glassfibers and matrix.

The investigation of glassfiber reinforced PA66 composites showed a more complex aging mechanism making long term predictions of mechanical properties very difficult. As for the PPS composites, the loss of mechanical properties in PA66 composites is connected to hydrolysis of the interfacial region between glassfibers and matrix. Furthermore, gel permeation chromatography studies show severe reductions of molecular mass of the matrix polymer as a result of hydrolysis. This reduction of molecular mass was found to have catastrophic impact on the mechanical properties of unfilled PA66. The hydrothermal aging of PA66 composites are found to be a combination of hydrolysis of the interface region and the matrix polymer.

The general conclusion is that the hydrolysis of the interface region is still a major problem for “state of the art” glassfiber reinforced thermoplastic composites.

6 Conclusions

The work on hydrothermal aging of glassfiber reinforced PPS and PA66 composites in Chapter 5 illustrates that hydrothermal break down of the interfacial region is still a major problem in *state of the art* commercial composites. This clearly justifies the continued search for more efficient interface modifiers.
The primary objective of the present work has been to investigate new types of diblock copolymer silane coupling agents and to find analytical methods to investigate coupling agents in general.

The synthesis method chosen to achieve these new types of diblock copolymer silane coupling agents proved to be successful. Polybutadiene-polystyrene (PB-PS) and polybutadiene-polydimethylsiloxane (PB-PDMS) diblock copolymers were synthesized by living anionic polymerization in tetrahydrofuran. Six different diblock copolymers have been synthesized varying the molecular mass of the PS and PDMS blocks of 10, 30 and 100 kg/mol. These molecular masses were chosen because they are below, around and above the critical molecular mass of entanglement for the two bulk systems. This was done to investigate the effect of entanglement formation on interfacial adhesion.
The six diblock copolymers were hydrosilylated with triethoxysilane in toluene using a hexachloroplatinum acid catalyst. This hydrosilylation was found to be preferential anti-Markovnikov addition on the pendant double bonds in the 1,2 polymerized butadiene units.

A number of surface analytical methods have been used to investigate coupling agents on inorganic surfaces. Wet chemical methods have been found useful in quick identification of coupling agents. Especially one of these methods, the reaction of ninhydrine with primary amine groups, has been developed to quantitatively determine the amount of aminosilane on filler surfaces.
Investigations of different sampling techniques for Fourier transformed infrared spectroscopy (FTIR) showed that diffuse reflectance FTIR (DRIFT) is a suitable method to investigate coupling agents on filler surfaces. Analyses of glass fillers treated with various amounts of γ-methacryloxy propyltrimethoxysilane have showed the ability for quantitative determination of silane coupling agents on filler surfaces using DRIFT.
X-ray photoelectron spectroscopy (XPS) was found to be a powerful tool for chemical investigation of silane coupling agents on oxidized silicon wafers. By using chemical oxidized silicon wafers it is possible to compare the average layer thickness of different silane overlayers on the surface by looking at the reduction of the Si (2p) signal originating from the underlying silicon wafer. This method revealed a basic difference between PDMS and PS block copolymer silanes. When applied to oxidized silicon wafers, toluene solutions of PDMS block copolymer silanes show increase of the average layer thickness with increased molecular mass of the PDMS

chain, while the PS block copolymer silanes does not. This observation was confirmed by ellipsometry. The difference in adsorption behavior has been explained by the difference in surface tension of PDMS and PS with respect to the surface tension of toluene. PDMS has a lower surface tension than toluene while the surface tension of PS is higher. This makes PS adsorb on the high surface tension SiO_2 from a toluene solution, while PDMS does not. As a result PS block copolymer silanes forms a pancake like structure on the surface while the PDMS block copolymer silanes form mushroom like structures on the surface. If this assumption is true, it would give higher surface coverage of PS silanes to use a solvent with higher surface tension than PS like dimethyl formamide.
Tapping mode atomic force microscopy (AFM) has been used to investigate the lateral structure of the block copolymer silane coupling agents. The investigations showed that the polystyrene block copolymer silane coupling agents form an island structure on the surface of oxidized silicon wafers. The island structure is explained by segregation of the PS end blocks. Whether this segregation is a result of the surface treatment and subsequent washing or a result of long time exposure is still inconclusive. The island structure is only observed for the PS block copolymer and not for the PDMS block copolymers. This observation is supported by contact angle hysteresis measurements. The PS block copolymer treated samples show significant contact angle hysteresis with water while the PDMS block copolymer treated samples did not.

In order to determine the influence of block copolymer silane coupling agents on the interfacial adhesion, two different methods have been applied: the Johnson, Kendall, Robterts (JKR) method and a single fiber microdebond method.
JKR measurement showed that silicon wafers treated with PDMS block copolymer silanes exhibit enhanced adhesion to crosslinked PDMS. This enhanced adhesion is explained by the interdiffusion of the surface attached PDMS chains into the PDMS network. The extent of the enhanced adhesion appeared to increase with the local pressure applied during contact. The extent of the adhesion was not found to increase with the molecular mass of the surface attached PDMS chains. It was expected that the adhesion would increase significantly due to entanglement effects. By comparing with results for other systems, it is possible that the molecular mass of the longest PDMS chain is not sufficiently high to show entanglement effects.

The single glass fiber microdebond method is a method to measure apparent interfacial shear strengths. That the measured interfacial shear strengths are apparent was realized from an observation of gradual debonding between glass fibers on crosslinked PDMS. The measurements of apparent interfacial shear strengths showed that the block copolymer silane coupling agents improve the interfacial adhesion between glass fibers and a polymer equal to the end block. But, no significant increase of the adhesion was observed by increasing the molecular mass of the end block. This could, as mentioned earlier, be because none of the synthesized block copolymer have sufficiently long end blocks to cause entanglement effects. Boiling the micro composites in water for 100 hours significantly decreased the apparent interfacial shear strengths. This shows

that despite the structural advantage of block copolymer silanes, they are not capable of offering complete protection of the interfacial region from hydrolysis. This could be because the triethoxysilane groups used have a surplus of ethoxy groups that are not participating in covalent bonding. The existence of such groups will enhance, rather than protect, the siloxane bond to the glass from hydrolysis.

The main conclusion is that silane modified block copolymers show promising results as coupling agents for thermoplastic/inorganic composites. But the block copolymer systems need to be optimized on a number of areas like: methods of applying them to inorganic surfaces, molecular mass of the end blocks and chemical nature of the silane groups.

7 Suggestions for future work

On the basis of the present work a number of questions remains unanswered. In order to answer these questions the following is suggestions for future work on block copolymer silane coupling agents.

In order to clarify the influence of the solvent on the adsorption behavior of block copolymer silane coupling agents, it would be very informative to investigate the structure of hydrosilylated polybutadiene-polystyrene block copolymers when applied from a high surface tension solvent. The suggestion is to use dimethylformamide to conduct these experiments.

To investigate if the formation of entanglements is a possible way to significantly improve interfacial adhesion, it is suggested to synthesize polystyrene block copolymer coupling agent with higher molecular mass of the polystyrene end. Using the synthesis methods presented in Chapter 2, it should be straight forward to synthesize a block copolymer coupling agent with a molecular mass of the polystyrene end of around 200 kg/mol.

To investigate the influence of chemical structure of the silane group on the hydrothermal stability, it would be interesting to exchange the triethoxysilane group with a monoethoxysilane group. According to the work by Kirkland and Henderson (1994) using a di(t-butyl)ethoxysilane could improve the hydrothermal stability of the block copolymer silanes.

Finally it is suggested that these block copolymer silane are tested in real composite systems to compare them with existing coupling systems.

8 References

Ahn D. & Shull K.R.(1996):
JKR Studies of Acrylic Elastomer Adhesion to Glassy Polymer Substrates.
Macromolecules, vol. 29 pp. 4381-4390.

Bjorksten J. and Yaeger L. (1952):
Vinyl Silane Sizing for Glass.
Modern Plastics Vol 29. pp. 124 and 188.

Blümel J. (1995):
Reactions of Ethoxysilanes with Silica: A Solid-State NMR Study.
Journal of American Chemical Society, Vol. 117, p. 2112-2113.

Boroumand F., van der Bergh H. & Moser J.E. (1994):
Quantitative Diffuse Reflectance and Diffuse reflectance Infrared Spectroscopy of Surface-Derivatizied Silica Powders.
Analytical Chemistry Vol. 66(14) pp. 2260-2266.

Brown H.R. (1993)
Effect of Chain Pull out on Adhesion of Elastomers
Macromolecules, vol. 26(7) pp. 1666-1670.

Buchwalter L.P. & Lacombe R.H. (1992):
Adhesion of polyimide to fluorine-contaminated SiO_2 surface. Effect of aminopropyltriethoxysilane on the adhesion. pp. 401-409.
Mittal K.L.(ed), Silanes and other coupling agents. VSP. The Netherlands

Buchvalter L.P., Oh T.S. & Kim J. (1992):
Adhesion of polyamides to ceramics: Effects of aminopropyltriethoxysilane and temperature and humidity exposure on adhesion. pp. 411-421.
Mittal K.L.(Ed), Silanes and other coupling agents. VSP. The Netherlands

Cameron G.G., Quresshi M.Y. (1981):
Grafting of Polybutadiene Functionalized with Chlorosilane Groups.
Makromol. Chem., Rapid Commun., Vol. 2, pp. 287-291.

Chaudhury M.K & Whitesides G.M. (1991):
Direct measurements of interfacial interactions between semispherical lenses and flat sheets of poly(dimethylsiloxane) and their chemical derivatives.
Langmuir, vol. 7(5), pp.1013-1025.

Chaudhury M.K & Whitesides G.M. (1992):
Correlation between surface free energy and surface constitution.
Science, vol. 225, pp. 1230-1232.

Chaudhury M.K & Owen M.J. (1993):
Adhesion hysteresis and friction.
Langmuir, vol. 9(1), pp. 29-31.

Choi G.Y., Kim S. & Ulman A. (1997):
Adhesion Hysteresis Studies of Extracted Poly(dimethylsiloxane) Using Contact Mechanisms.
Langmuir, vol. 13, pp. 6333-6338.

Chua P.S., Dai S.R. & Piggott M.R. (1992):
Mechenical properties of the glass fibre-polyester interphase.
Part I Effects due to silanes.
Journal of Materials Science, vol. 27, pp. 913-918.

Cosgrove T., Heath T.G. & Ryan K. (1994):
Terminally attached polystyrene chains on modified silicas.
Langmuir Vol. 10(10) pp. 3500-3506.
Creton C., Brown H.R. & Shull K.R. (1994):
Molecular Weight Effects in Chain Pullout.
Macromolecules, vol. 27, pp. 3174-3183.
Crivello J. V. & Daoshen B. (1993):
Regioselective Hydrosilations. IV. The Synthesis and Polymerization of Monomers Containing Epoxy and Alkoxysilane Groups.
Journal of Polymer Science: Part A: Polymer Chemistry, Vol. 31. pp. 3121-3132.
Debois L.H. & Zegarski B.R. (1993):
Reaction of Alkoxysilane Coupling Agents with Dehydroxylatet Silica Surfaces.
Journal of American Chemical Society, Vol. 115, p. 1190-1191.
Deruelle M. Leger L. & Tirrell M. (1995):
Adhesion at the Solid-Elastomer Interface: Influence of the Interfacial Chains.
Macromolecules vol. 28 pp. 7419-7428.
Durig J.R. & Sullivan J.F. (1987):
Infrared and Raman Spectroscopy, Deternination of Chemical Compositions and Molecular Structure-Part A Physical Methods of Chemistry, 2. edition.
(Ed. Rossiter B.W & Hamilto J.F.), John Wiley and Sons, New York.
Falsafi A. (1998):
Poster presented at the conference: Unifying Principles for Engineering Soft Materials.
Risø National Laboratories, Denmark June 22-25 1998.
Feller J.F., Chabert B., Guyot A., Spitz R., Wagner H.D. & Gerard J.F. (1996):
Silane grafted isotactic polypropylene as a coupling agent on glass. Consequence on the interfacial adhesion.
Journal of Adhesion, vol 58, pp. 299-313.
Feller J.F., Guyot A., Spitz R., Chabert B., & Gerard J.F. (1995):
Coupling agents for polypropylene/glass fiber composites: Synthesis of functionalized isotactic polypropylene and crystallization.
Composite Interfaces vol. 3(2), pp. 121-134.
Ferry J.D. (1980):
Viscoelastic properties of polymers, Third edition
John Wiley & Sons Inc. New York.
Fleer G.J., Cohen Stuart M.A., Scheutjens J.M.H.M, Cosgrove T.,Vincent B.(1993):
Polymers at interfaces.
Chapman & Hall, London, U.K.
Flory P.J. (1940):
Molecular Size Distribution in Ethylene Oxide Polymers.
Journal of the Anerican Chemical Society, vol. 62, pp. 1561-1565.
Gaur U. & Miller B.(1989):
Microbond Method for Determination of the Shear Strength of a Fiber/Resin Interface: Evaluation of Experimental Parameters.
Composite Science and Technology, vol. 34, pp. 35-51.
Gonon L., Chabert B., Bernard A., van Hoyweghen D. & Gérard J.F. (1997):
New coupling agents as Adhesion Promoters at the Poly(Phenylene Sulfide)/Glass Interface – Studies with Micro and Macro Composites.
Journal of Adhesion, vol. 61, pp.271-292.

Gu W., Lu G.-Q., Wu H.F., Kampe S.L., Lichtenstein P.R & Dwight D.W (1995):
Nondestructive Characterization of Fiber-Matrix Adhesion in Composites by Vibrational Damping.
Materials Research Society Symposium Proceedings, vol. 385, pp. 33-39.

Guo X., Farwaha R. & Rempel G.L. (1990):
Catalytic Hydrosilylation of Diene-Based Polymers.
1. Hydrosilylation of Polybutadiene
Macromolecules, Vol. 23, pp. 5047-5054.

Guo X.& Rempel G.L. (1992):
Catalytic Hydrosilylation of Diene-Based Polymers.
2. Hydrosilylation of Styren-Butadiene Copolymer and Nitrile-Butadiene Copolymer
Macromolecules, Vol. 25, pp. 883-886.

Hammouch S.O., Beinert G.J., Zilliox J.G. & Hertz J.E. (1995):
Synthesis and Characterisation of Monofunctional polydimethyl siloxanes with a narrow molecular weight distribution.
Polymer, Vol. 36(2) pp. 421-426.

Herrera-Franco P.J. & Drzal L.T. (1992):
Comparison of methods for the measurement of fiber/matrix adhesion in composites.
Composites, vol. 23(1), pp. 2-27.

Hölle H.J. & Lehnen B.R. (1975):
Preperation and Characterization of Polydimethylsiloxanes with Narrow Molecular Weight distribution.
European Polymer Journal, Vol 11, pp. 663-667.

Iraqi A., Seth S., Vincent C.A., Cole-Hamilton D.J., Watkinson M.D., Graham I.M. & Jeffrey D. (1992):
Catalytic Hydrosilanation of Polybutadien as a Route to Functional Polymers.
Journal of Materials Chemistry, Vol. 2(10), pp.1057-1064.

Jones R.L & Chandler H.D. (1985):
Strength Loss in E-Glass Fibers after Exposure to Hydrochloric, Hydrobromic and Hydroiodic Acids.
Journal of Materials Science, Vol. 20, pp. 3320-3324.

Karim A., Tsukruk V.V., Douglas J.F., Satija S.K., Fetters L.J. Reneker D.H. &
Foster M.D. (1995):
Self-Organization of Polymer Brush Layers in a Poor Solvent
Journal de Physic II France Vol. 5 pp. 1441-1456.

Kirkland J.J. & Henderson J.W. (1994):
Reversed-Phased HPLC Selectivity and Retention Characteristics of Conformationally Different Bonded Alkyl Stationary Phases.
Journal of Chromatographic Science, vol. 32 pp. 473-480.

Kloos K.H. Müller K & Krollmann N. (1985):
Thermishe Grenzbelastbarkeit II. Vorharben Nr. 69
Forschungshefte nr. 121. Forshungskuratorium Maschinenbau e.v. (FKM).

Koenig J.L. (1985):
FTIR Studies of Interfaces
In Silanes, Surfaces and Interfaces. Proceedings of the Silanes, Surfaces, and Interfaces Symposium, Snowmass, Colorado, June 19-21, 1985.
Edd. Leyden D.E. Gordon & Breach Science Publishers.

Landry C.J.T., Coltrain B.K., Teegarden D.M., Long T.E & Long V.K. (1996):
Use of Organic Copolymers as Compatibilizers for Organic-Inorganic Composites.
Macromolecules, vol. 29, pp. 4712-4721.
Laumer P.J. (1987):
Infrared analysis of Organosilicon compounds: Spectra-structure correlations
In. Silicon Compounds, Petrarch System Silanes & Silicones. P 69-72.
Li J.-X. (1994):
Analysis of the Pullout of single Fibers from Low-Density Polyethylene.
Journal of Applied Polymer Science, vol. 53, pp. 225-237.
Ligoure C. (1996):
Adhesion between a Polymer Brush and an Elastomer: A Self-Consistent Mean Field Model.
Macromolecules, vol. 29, pp. 5459-5468.
Lund C.J., Murphy P.D. & Plat M.V. (1992)
Oligomerization of an aminosilane coupling agent and its effects on the adhesion of thin polyinide films to silica. pp. 423-437.
Mittal K.L.(ed), Silanes and other coupling agents. VSP. The Netherlands
Mangipudi V., Tirrell M. & Pocius A.V. (1994):
Direct measurement of molecular level adhesion between poly(ethylene terephthalate) and polyethylene films: determination of surface and interfacial energies.
Journal of Adhesion Science and Technology, vol. 8(11), pp. 1251-1270.
Mangipudi V.,Huang E., Tirrell M. & Pocius A.V. (1996):
Measurement of interfacial Adhesion Between Glassy Polymers Using the JKR Method.
Macromolecular Symposia, vol. 102, pp. 131-143.
Marciniec B. (1992):
Comprehensive Handbook on Hydrosilation.
Pergamon Press, Oxford New York.
Marciniec B., Lawandowski M., Pietraszuk C. & Foltynowicz Z. (1997):
Functionalization of 1,2-polybutadiene by ruthenium complex catalysed coupling with vinylsilanes.
Polymer Vol. 38, pp. 5169-5172.
Mark J.P. (1996):
Physical properties of polymers Handbook
American Institute of Physics Press.
Matsuoka S. (1992):
Relaxation Phenomena in Polymers.
Hanser Publishers, Munich.
McAlea K.P. & Besio G.J. (1988):
Adhesion between polybutylene terephthalate and E-glass Measured with a microdebond technique.
Polymer Composites, vol. 9(4), pp. 285-290.
McConnell R.G. (1975):
Polypropylene/Acrylic Acid Graft Copolymers.
U.S. Patent no. 3,483,276.
McGrath M.P., Sall E.D. & Tremont S.J. (1995):
Functionalization of Polymers by Metal-Mediated Processes.
Chemical Review, Vol. 95, pp. 381-398.

Morton M., Bostick E.E., Livigni R.A. & Fetters L.J. (1963a):
Homogeneous Anionic Polymrization IV. Kinetics of Butadiene and Isoprene Polymerization with Butyllithium.
Journal of Polymer Science: Part A, Vol. 1, pp. 1735-1747.
Morton M.,Fetters L.J. & Bostick E.E. (1963b):
Mechanisms of Homgeneous Anionic Polymrization Alkyllithium Initiators.
Journal of Polymer Science: Part C, No. 1, pp. 311-323.
Morton M. (1983):
Anionic Polymerization Principle and Practice
Academic Press inc. New York.
Moulder J.F., Stickle W.F., Sobol P.E., Bomben K.D. & Chastain J (1992):
Handbook of X-ray Photoelectron Spectroscopy.
Perkin-Elmer Corporation, Physical Electronics Div. USA.
Nagae S. & Otsuka Y. (1994):
Effect of sizing agents on corrosion of glass fibers in water.
Journal of Materials Science Letters, vol. 13, p. 1482-1483.
Ndoni S., Papadakis C.M., Bates F.S. & Almdal K. (1995):
Laboratory-scale setup for anionic polymerization under inert atmosphere
Rev. Sci. Instrum., Vol.66(2). pp. 1090-1095.
Pape P.G. & Plueddemann E.P. (1986):
History of Silane Coupling Agents in Polymer Composites.
History of Polymeric Composites, Proceeding of the Symposium held during the 192nd ACS Meeting. Anaheim Ca. USA 10-12 September 1986
VNU Science Press, Utrecht, The Netherlands.
Paul J.T. (1969):
Glass Fiber Reinforced Crystalline Polypropylene Composition and Laminate.
U.S. Patent No. 3,437,550.
Perutz S., Kramer E.J., Baney J. & Hui C.-Y. (1997):
Adhesion Between Hydrolyzed Surfaces of Poly(dimethylsiloxane) Networks
Macromolecules, vol. 30, pp. 7964-7969.
Petit P.H. (1969):
A simplified method of determination the inplane shear stress-strain response of unidirectional composites.
ASTM STP 460, American Society for testing and Materials.
Plank D.A. (1974):
Grafted Polyolefins as Stabilizer Components in Polyolefins.
U.S. Patent no. 3,849,516.
Plueddemann E.P. (1960):
Methods of Treating Glass with Epoxy-silanes.
U.S. Patent No. 2,946,701 (to Dow Corning)
Plueddemann E.P., Clark H., Nelson L., & Hoffman K. (1962):
New Silane Coupling Agents for Reinforced Plastics.
Modern Plastics.Vol 39, pp.135.
Plueddemann E.P. (1963):
Treated Siliceous Article.
U.S. Patent No. 3,079,361 (to Dow Corning)

Plueddemann E.P. (1974):
Cationic Unsaturated Amine-Functional Silane Coupling Agents.
U.S. Patent No. 3,819,675 (to Dow Corning)
Plueddemann E.P. (1982):
Silane Coupling Agents.
Plenum Press, New York.
Plueddemann E.P. (1988):
Present Status and Research in Silane Coupling.
Interfaces in Polymer, Ceramic and Metal Matrix Composites
Elsevier Science Publications Co., Inc. pp 17-33.
Porro T.J. & Pattacini S.C. (1992):
Quantitative FT-IR diffuse reflectance analysis of vinyl silanes on an aluminum hydroxide substrate.
In Silanes and Other Coupling Agents Ed. K.L. Mittal pp.289-294. VSP.
Qian L.L., Bruce F.A., Kellar J.J. & Winter R.M. (1995):
An instrument for testing interfacial shear strength in polymer matrix composites.
Measurement Science and Technology, vol.6, pp. 1009-1015.
Rosen B.W. (1972):
A simple procedure for experimental determination of the longitudinal shear modulus of unidirectional composite materials.
Journal of Composite materials vol. 6, pp.552-554.
Rossiter B.W. & Hamilton J.F. (1987):
Physical Methods of Chemistry Volume IIIA
Determination of chemical composition and Molecular Structure-Part A
John Wiley and Sons, Inc.
Salehi-Mobarakeh H., Brisson J.& Ait-Kadi A. (1997):
Interfacial polycondensation of nylon-6,6 at the glass fibre surface and its effect on fibre-matrix adhesion.
Journal of Materials Science, vol. 32, pp 1297-1304.
Sarin K.V., Kent S.B.H., Tam J.P. & Merrifeild R.B. (1981):
Quantitative Monitoring of Solid-Phase Peptide Synthesis by the Ninhydrin Reaction.
Analytical Biochemistry, Vol. 117, pp. 147-157.
Schutte C.L. (1994):
Environmental durability of glass-fiber composites
Materials Science and Engineering, R13, no. 7 pp. 265-324.
Sellinger A., Laine R.M., Chu V. & Viney C. (1994):
Palladium- and Platinum-Catalyzed Coupling Reactions of Allyloxy Aromatics with Hydridosilanes and Hydridosiloxanes: Novel Liquid Crystalline/ Organosilane Materials
Journal of Polymer Science: Part A: Polymer Chemistry, Vol. 32. pp. 3069-3089.
Shull K.R., Ahn D.& Mowery C.L. (1997):
Finite-Size Correction to the JKR Technique for Measuring Adhesion: Soft Spherical Caps Adhering to Flat, Rigid Surfaces.
Langmuir, vol. 13, pp. 1799-1804.
Silberzan P., Perutz S. Kramer E.J. & Chaudhury M.K. (1994):
Study of the Self-Adhesion Hysteresis of a Siloxane Elastomer using the JKR Method.
Langmuir, vol. 10 pp. 2466-2470.

Speier J.L. (1979):
Homogeneous Catalysis of Hydrosilation by Transition Metals.
Advances in Organometallic Chemistry, Vol. 17, pp. 407-447.
Stamouli A., Pelletier E. Koutsos V. van der Vegte E. & Hadziioannou G. (1996):
An Atomic Force Microscopy Study on the transsitions form Mushrooms to Octopus Surface "Micelles" by Changing the Solvent Quality.
Stein J., Grade H., Williams E.A., Codella P.J. & Smith J.F. (1993):
Network Structure and Properties of Platinum-Catalyzed Addition Cure Release Coatings.
Journal of Applied Polymer Science, Vol. 47. pp. 2257-2267.
Steinkamp R.A. & Grail T.J. (1975):
Polymers with Improved Properties and Process Therefor.
U.S. Patent no. 3,862,265.
Steinman R.(1951):
Fibrous Glass Laminates
U.S. Patent No. 2,563,228 (to Owens-Corning Fiberglass)
Strålin A. & Hjertberg T. (1993):
Adhesion between Hydrated Aluminium and Ethylene Copolymers Contaning Methoxy Silane Groups.
Journal of Adhesion, vol. 41, pp. 51-80.
Szwarc M. (1968):
Carbanions Living Polymers and Electron Transfer Processes
Interscience Publishers, John Wiley and sons.
Tirrell M.(1996):
Measurement of Interfacial Energy at Solid Polymer Surfaces.
Langmuir, vol. 12, pp. 4548-4551.
Tripathi D. & Jones F.R. (1998):
Single fibre fragmentation test for assessing adhesion in fibre reinforced composites.
Journal of Materials Science, vol 33(1), pp.1-16.
Tsukruk V.V. & Reneker D.H. (1995):
Scanning Probe Microscopy of the Organic and Polymeric Films:
From Self-Assembled Monolayers to Composite Multilayers.
Polymer. Vol. 36(9), p. 1791-1808.
Valentin D. Paray F. & Guetta B. (1987):
The hygrothermal behavior of glass fibre reinforced Pa66 composites: a study of the effect of water absorption on their mechanical properties.
Journal of Materials Science, vol. 22, pp. 46-56.
Walrath D.E. & Adams D.F. (1983):
Analysis of the stress state in an Iosipescu shear test specimen
Composite Materials Research group, DME, University of Wyoming
Wiedemann G., Wustmann B. Frenzel H. & Keusch S. (1978):
Zur Chemischen Analytik von Haftmitteln bei Glasseidenerzeugnissen für Verbundwerkstoffe.
Faserforchung und Textiltechnik, Vol. 29(11/12), pp. 681-685.
Whitney J.M., Daniels I.M. & Pipes R.B. (1982):
Experimental mechanics of fiber reinforced composite materials
Monograph 4, Society for experimental stress analysis.

Wu S. (1982):
Polymer interface and adhesion
Marcel Dekker Inc. New York.
Yamamoto M. & Ohata M. (1996):
New molecular silane coupling agents synthesized by living anionic polymerization; grafting of these polymers onto inorganic particles and metals.
Progress in Organic Coatings, vol. 27, pp. 277-285.
Ying J.Y., Benziger J.B.& Navrotsky A. (1993):
Structural Evolution of Alkoxide Silica Gels to Glass.
Journal of American Ceramic Society. Vol. 76(10) pp. 2571-82.
Yue C.Y. & Quek M.Y. (1994):
The interfacial properties of fibrous composites.
Journal of Materials Science, vol. 29, pp. 2487-2490.
Zhao W., Krausch G., Rafailovich M.H. & Sololov J. (1994):
Lateral Structure of a Grafted Polymer Layer in a Poor Solvent
Macromolecules, vol. 27, pp. 2933-2935.

List of abbreviations

AFM	Atomic force microscopy
ATR	Attenuated total reflectance (an infrared sepctroscopy method)
BHT	Butylated hydroxytoluene (2,6-Di-tert.-butyl-4-methyl-phenol)
D_3	Hexamethylcyclotrisiloxane
DMF	N,N-dimethylformamide
DRIFT	Diffuse reflectance infrared spectroscopy
DTGS	Deuterated triglycine sulfate
FTIR	Fourier transformed infrared spectroscopy
GPC	Gel permeation chromatography
HPLC	High performance liquid chromatography
IMFP	Inelastic mean free path
JKR	Adhesion measurement method of Johnson, Kendall & Roberts
LDPE	Low density polyethylene
MCT	Mercury-cadmium telluride
MPS	Methacryloxy propyltrimethoxysilane
NMR	Nuclear magnetic resonance
n-PTMS	n-propyltrimethoxysilane
PA66	Poly(hexamethylene adipamide)
PAS	Photoacoustic infrared spectroscopy
PB	Polybutadiene
PB-PDMS	Diblock copolymer of polybutadiene and poly(dimethylsiloxane)
PB-PS	Diblock copolymer of polybutadiene and polystyrene
PBT	Poly(butylene terephthalate)
PDMS	Poly(dimethylsiloxane)
PEG	Polyethylenglycol
PPS	Polyphenylensulphide
PS	Polystyrene
SEM	Scanning electron microscopy
sPB-PDMS	Diblock copolymer of polybutadiene and poly(dimethylsiloxane) hydrosilylated with triethoxysilane
sPB-PS	Diblock copolymer of polybutadiene and polystyrene hydrosilylated with triethoxysilane
TGS	Triglycine sulfate
THF	Tetrahydrofuran
UV	Ultra violet
XPS	X-ray photoelectron spectroscopy
γ-APS	γ-aminopropyltrimethoxysilane

List of symbols

$[I]$	Initiator concentration
$[M]$	Monomer concentration
a	Contact radius in the JKR-method
A	Frequency factor
$\cos(D)$	phase change measured by ellipsometry
d	Fiber diameter
DP	Degree of polymerization
E	Elastic modulus
E_a	Activation energy
E_b	Binding energy
E_k	Kinetic energy
F_d	Debonding force
G	Strain energy release rate
G	Shear modulus
G’	Real part of the dynamic shear modulus
G’’	Complex part of the dynamic shear modulus
$h\nu$	Photon energy
K	Compression modulus
k_p	Propagation rate constant
L	Embedded fiber length
l_c	Critical fiber length
M_c	Critical molecular mass of entanglements
M_e	Average molecular mass between entanglements
M_n	Number average molecular mass
M_w	Weight average molecular mass
P	Applied load
Q	Polydispersity
R	Radius of curvature
R_g	Radius of gyration in theta solvent
R_{km}	Kubelka-Munk corrected infrared reflectance
R_{ob}	Observed infrared reflectance
T	Absolute temperature
t	Time
$\tan(\delta)$	Energy dissipation factor (tangents of the phase shift δ)
$\tan(y)$	Amplitude change measured by ellipsometry
U	Molecular inhomogeneity
W_a	Work of adhesion
W_c	Work of cohesion

List of symbols (continued)

Δ	General abbreviation for difference
d	Solubility parameter
δ	Phase shift between applied strain and measured stress
g	Surface tension
g_c	Critical wetting surface tension
l	Inelastic mean free path
ν	Poisson's ratio
q	Angle (contact angle)
q_a	Advancing contact angle
q_r	receding contact angle
s	Stress
σ_f	Tensile strength of a fiber
τ_i	Interfacial shear strength

Bibliographic Data Sheet **Risø-R-1113(EN)**

Title and authors

Modification and Characterization of the interface in polymer/inorganic composites

Nils Berg Madsen

ISBN	ISSN
87-550-2540-4 87-550-2541-2 (Internet)	0106-2840

Department or group	Date
Condensed Matter Physics and Chemistry Department	March 1999

Groups own reg. number(s)	Project/contract No(s)

Pages	Tables	Illustrations	References
150	22	75	99

Abstract (max. 2000 characters)

New types of diblock copolymer silane coupling agents have been investigated as interface modifiers in polymer/inorganic composites. Diblock copolymers composed of polybutadiene-polystyrene (PB-PS) and polybutadiene-polydimethylsiloxane (PB-PDMS) have been synthesized with varying molecular mass of the PS and PDMS blocks by living anionic polymerization. These polymers have been catalyticly hydrosilylated with triethoxysilane to form diblock copolymer silane coupling agents. The investigation has involved a number of surface analytical techniques such as wet chemical analysis, Fourier transformed infrared spectroscopy with different sampling techniques, X-ray photoelectron spectroscopy, ellipsometry, atomic force microscopy and contact angle measurements. Investigations of the interfacial adhesion have been done by JKR-measurements and single fiber microdebond experiments. The investigations showed that the synthesized diblock copolymer silanes perform well as adhesion promoters between SiO_2 and a polymer matrix equal to end block of the silane. The measurements showed no increase in interfacial adhesion by increasing the molecular mass of the end block up to 100 kg/mol.
This work also included a study of hydrothermal stability of *state of the art* glassfiber reinforced polyphenylensulfide (PPS) and Poly(Hexamethylene adipamide) (PA66) composites. The materials were exposed in water at different temperature and pH values up to more than one year. Measurement of various mechanical properties in combination with electron microscopy showed the primary mechanism for reduction of mechanical properties was hydrolysis of the interfacial region. Furthermore gel permeation chromatography showed extensive reduction of the molecular mass of PA66 as a result of exposure in hot water. Hydrolysis of the interface region is still the main problem in thermoplastic glassfiber composites. Diblock copolymer silanes show potential as coupling agents for such systems but they must be optimized for hydrolytic stability. This work presents the tools for such an optimization.

Descriptors INIS/EDB

Available on request from Information Service Department, Risø National Laboratory,
(Afdelingen for Informationsservice, Forskningscenter Risø), P.O.Box 49, DK-4000 Roskilde, Denmark.
Telephone +45 46 77 40 04, Telefax +45 46 77 40 13